CHEMICAL REVIEWS

REVIEW

pubs.acs.org/CR

Nucleation and Growth of Nanoparticles in the Atmosphere

Renyi Zhang,*[,†,‡,§] Alexei Khalizov,[†] Lin Wang,[‡] Min Hu,[§] and Wen Xu[†]

[†]Department of Atmospheric Sciences and Department of Chemistry, Center for Atmospheric Chemistry and Environment, Texas A&M University, College Station, Texas 77843, United States

[‡]Department of Environmental Science & Engineering and Institute of Global Environment Change Research, Fudan University, Shanghai 200433, China

[§]State Key Laboratory of Environmental Simulation and Pollution Control, College of Environmental Sciences and Engineering, Peking University, Beijing, 100871, China

CONTENTS

Received: May 17, 2011
Published: November 01, 2011

1. INTRODUCTION

This review intends to critically assess recent findings related to nucleation and growth of atmospheric nanoparticles, with an emphasis on the understanding of these processes at a fundamental molecular level. Aerosols (small particles suspended in air) can be directly emitted into the atmosphere from primary sources or be formed in the atmosphere through nucleation of gas-phase species. Aerosol nucleation events produce a large fraction of atmospheric aerosols. New particle formation occurs in two distinct stages,[1] i.e., nucleation to form a critical nucleus and subsequent growth of the critical nucleus to a larger size (>2−3 nm) that competes with capture and removal of the freshly nucleated nanoparticles by coagulation with pre-existing aerosols. Nucleation is generally defined as creation of molecular embryos or clusters prior to formation of a new phase during the transformation of vapor →liquid→ solid. This process is characterized by a decrease in both enthalpy and entropy of the nucleating system (i.e., $\Delta H < 0$ and $\Delta S < 0$). Hence, although thermodynamically favorable according to the first law of thermodynamics, (i.e., exothermic) nucleation is hindered in entropy according to the second law of thermodynamics. A free energy barrier, ΔG ($\Delta G = \Delta H - T\Delta S > 0$), is often involved and needs to be surmounted before transformation to the new phase becomes spontaneous. Another major limitation in the nucleation and growth of atmospheric nanoparticles lies in significantly elevated equilibrium vapor pressures above small clusters and nanoparticles, also known as the Kelvin (curvature) effect, which considerably restricts growth of freshly nucleated nanoparticles.

Formation of molecular clusters occurs through random collisions and rearrangements of atoms or molecules of the existing phase (Figure 1a). Growth of a cluster can be represented as a reversible, stepwise kinetic process. After reaching a critical size (the critical cluster or nucleus), further growth of the cluster becomes spontaneous. At each step, formation and decomposition of a cluster can be described by fundamental kinetic rate theories. A cluster can form *homogeneously* within the original phase or *heterogeneously* on various irregularities, such as pre-existing small particles or ions, which assist in surmounting the free energy barrier associated with formation of an interface between the small cluster of the new phase and the original phase (Figure 1b). The lifetime of clusters is extremely short, but since a very large number of clusters form and dissociate at any time, a few can reach the critical size and continue to grow spontaneously to form larger particles. Atmospheric nucleation of aerosols from vapors[1,2] is, in principle, analogous to that of freezing of liquids,[3] crystallization of supersaturated solutions,[4] and formation of vapor bubbles inside the bulk liquid;[5] all proceed by the same basic mechanism. The common feature of the nucleation process is that there exists a dividing surface[6,7] at the critical nucleus that separates the properties of the original and new phases. From an energetic perspective, the free energy of cluster formation, ΔG, increases with cluster size prior to but decreases after the critical nucleus, reaching a maximal value at the critical size, $i = i^*$. Hence, the critical nucleus can be identified if the free energy surface leading to cluster growth is available[6]

$$(\partial \Delta G/\partial i)_{i=i^*} = 0. \tag{1.1}$$

The properties of the critical nucleus are central to nucleation theory. The rate at which nucleation occurs is related to the chemical makeup of the critical nucleus and the gaseous concentrations of the nucleating species and is an important variable in simulations of aerosol formation in atmospheric models.[1]

Nucleation from the vapor phase is *homomolecular* when a single type of a gas is involved in formation of a critical nucleus and *heteromolecular* when several types of gases are involved in formation of a critical nucleus. In the absence of existing heterogeneities, homomolecular nucleation requires an extremely high supersaturation. For instance, homogeneous nucleation of pure water vapor requires a supersaturation of a few hundred percent. Since such a condition is hardly realized in the atmosphere, homomolecular nucleation of water vapor, leading to formation of cloud droplets, is always heterogeneous in nature, taking place on pre-existing water-soluble seeds, i.e., cloud condensation nuclei (CCN). In fact, clouds would have never formed in the Earth's atmosphere in the absence of CCN.

Homogeneous nucleation of atmospheric nanoparticles, the focus area of this review, is always heteromolecular, involving two (binary), three (ternary), or possibly more mutually interacting

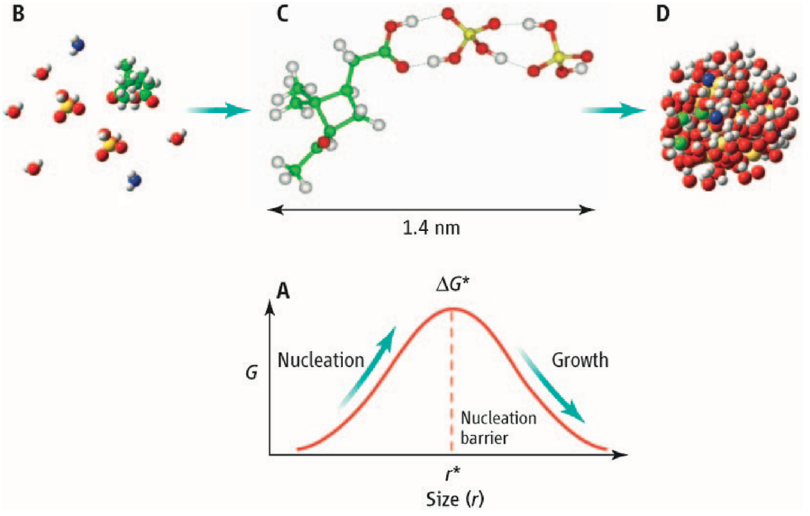

Figure 1. Schematic representation of the transformation from the molecular complex through the critical nucleus to 2−3 nm nanoparticle (top) and associated free energy variation (bottom). (Reprinted with permission from ref 1. Copyright 2010 American Association for the Advancement of Science.)

vapors (multicomponent). The abundance, volatility, and reactivity likely determine the potential of a chemical species as a nucleation precursor. Atmospheric aerosol formation is closely linked with the gas-phase chemistry because the abundances required for nucleation to occur are achieved through a gradual increase in the concentration of the nucleating vapors produced from photo-oxidation of atmospheric gases, such as sulfur dioxide and volatile organic compounds (VOCs), including many saturated, unsaturated, or aromatic hydrocarbons,

$$SO_2 + OH \xrightarrow{O_2, H_2O} H_2SO_4 \quad (1.2)$$

$$VOCs + OH \xrightarrow{O_2} \text{oxidized organics} \quad (1.3)$$

The most common nucleating species is sulfuric acid because of its low vapor pressure at typical atmospheric temperatures, which is further reduced in the presence of water due to the large mixing enthalpy of these two substances.[8−10] The presence of gaseous H_2SO_4 in concentrations exceeding 10^5 molecules cm^{-3} has been shown as a necessary condition to observe new particle formation in the atmosphere.[11,12] In addition to sulfuric acid, a number of other nucleating precursors, including atmospheric ions, ammonia, amines, organic acids, and iodine oxides, have been proposed to be involved in formation of the critical nucleus under different ambient environments. The size and chemical make up of atmospheric critical nuclei are not well-known presently, because of the lack of existing analytical methods to directly probe the critical nucleus. Indirect measurements and theoretical calculations suggest that the critical nucleus has a diameter on the order of 1 nm and consists of a relatively small number of molecules held together by noncovalent van der Waals (vdW) interactions. Since the molecules of known nucleating vapors possess a significant dipole moment and/or contain a hydrogen atom connected with an electronegative atom (nitrogen or oxygen), electrostatic, polarization, and hydrogen-bonding interactions have been recognized to play a significant role in formation of the smallest clusters. As clusters grow, proton transfer from an acid moiety (e.g., H_2SO_4) to a base moiety (e.g., H_2O or NH_3) becomes possible because the resulting ion pair is stabilized by interactions with surrounding polar molecules (e.g., H_2O) within the cluster. Formation of an ion pair can significantly increase the nucleation rate by reducing the free energy of the critical nucleus. However, current understanding of the role of proton transfer and other possible chemical processes in the nucleation of atmospheric clusters is still inadequate.

Aerosol nucleation events, which are reflected as episodes with very high concentrations (up to 10^4 particle cm^{-3} or higher) of nanoparticles generated in a short period of time, are frequently observed in the free troposphere and under remote, urban, forested, and marine environments of the lower troposphere. Thermodynamically stable larger clusters and small nanoparticles formed during a nucleation event need to grow quickly so that they are not scavenged by coagulation through collisions with existing larger particles. The surface of pre-existing particles also acts as a condensation sink for nucleating vapors, reducing their concentration and inhibiting nucleation. Whereas condensation of low-volatility vapors and reversible partitioning of semivolatile vapors are commonly recognized as the major contributors to growth of aerosols, the role of heterogeneous chemical reactions between gas-phase chemical compounds and particles is not well understood and is a subject of intensive research.[13] When reaching a size of about 50−100 nm, aerosols become efficient light scatterers and CCN.[14] Overall, during the atmospheric lifetime, the size of particles may vary over 5 orders of magnitude, from a lower limit of about 1 nm corresponding to stable molecular clusters to an upper limit of about 1 mm for cloud droplets. Growth of nanoparticles driven by condensation, partitioning, heterogeneous chemical reactions, and coagulation is another focus area of this review.

Atmospheric aerosols have profound impacts on the Earth−atmosphere system, influencing the weather, climate, atmospheric chemistry and air quality, ecosystem, and public health.[15] Those particles cool the atmosphere by directly scattering a fraction of the incoming solar radiation back to space, an effect commonly referred to as direct climate forcing. By acting as CCN and ice nuclei (IN), aerosols play an important role in controlling cloud formation, development, and precipitation, impacting the albedo, frequency of occurrence, and lifetime of clouds on local, regional, and global scales,[16−21] which is often referred to as indirect climate forcing. Presently, the aerosol direct and indirect effects represent the largest uncertainty in climate predictions.[22] Also, chemical reactions occurring on the surface or in the bulk of aerosols[23,24] may alter the properties of aerosols and the gaseous composition of the atmosphere. For example, heterogeneous reactions on particle surfaces convert inactive chlorine species into photochemically active forms in the middle atmosphere (between 20 and 50 km altitudes), leading to depletion of stratospheric ozone,[25−35] which acts as a UV shield. In the lower atmosphere (below 20 km), particle-phase reactions can modulate formation of tropospheric ozone,[36−41] which is a key criteria air pollutant. On the regional and local scales, fine particulate matter (i.e., aerosols smaller than 2.5 μm or $PM_{2.5}$) represents a major contributor to air pollution.[42] Elevated concentrations of $PM_{2.5}$ cause degradation in visibility, exacerbate accumulation of pollutants in the planetary boundary layer (PBL), and adversely affect human health.[43] Increasing evidence has implicated aerosols not only in aggravation of existing health symptoms but also in the development of serious chronic diseases.[44] When inhaled, aerosols can amplify the adverse effect of gaseous pollutants, such as ozone,[45] and the smallest particles cause the most severe health impacts[46] because they have higher probability than larger particles to deposit in the pulmonary region and penetrate into the bloodstream.[47,48]

Several previous review articles have provided a detailed account of different aspects of new particle formation in the atmosphere, including field measurements of atmospheric aerosols and nucleation events,[49−51] coastal new particle formation,[52] the relation between laboratory, field, and modeling nucleation studies,[53,54] and the role of different types of nucleation processes in the atmosphere.[55] Over the past few years, there has been substantial research progress in the area of atmospheric aerosol nucleation, including development of novel detection methods for atmospheric nanoparticles and clusters, as summarized in a recent review by Bzdek and Johnston.[56] Advances in analytical instruments have led to a number of laboratory and field studies that produced exciting yet often contradictory results regarding the compositions of the critical nucleus and the role of sulfuric acid and other species in the nucleation and growth of nanoparticles.[57−61] In the present review, we first provide the background information on theoretical and experimental approaches toward investigation of homogeneous vapor nucleation

and then introduce recent advances in nucleation and growth of atmospheric nanoparticles. Throughout this review, we strive to present the various nucleation aspects from a fundamental chemical prospective. Since there is a vast body of literature in the area of atmospheric aerosol nucleation, we do not attempt to be inclusive to cover all available publications on this subject. Instead, we choose in this review to focus on the studies that make the most important advances in this field.

In section 2, we introduce the nucleation theories and illustrate how the predicted nucleation rates are related with results of laboratory experiments for a number of simple nucleating systems. Nucleation of atmospheric aerosols, including ambient measurements, laboratory experiments, and theoretical studies, is described in section 3. Results of laboratory experiments and ambient measurements of nanoparticle growth are presented in section 4, and section 5 provides the numerical approaches developed to connect measured aerosol nucleation and growth rates. Section 6 contains the concluding remarks and describes future research needs. A glossary of acronyms is provided at the end of the review.

2. OVERVIEW OF VAPOR NUCLEATION

2.1. Nucleation Theories and Computational Approaches

In the absence of heterogeneities, formation of a new phase occurs through random fluctuations in the vapor density, generating clusters that can grow or decay by gaining or losing a monomer molecule. Growth of the cluster can be represented by a reversible, stepwise kinetic process in a single or multicomponent system

$$\ldots C_{i-1} \underset{k_i^-}{\overset{+A_{i-1},\,k_{i-1}^+}{\rightleftharpoons}} C_i^* \underset{k_{i+1}^-}{\overset{+A_i,\,k_i^+}{\rightleftharpoons}} C_{i+1} \ldots \tag{2.1}$$

where A_{i-1} denotes a monomer species to be added to the cluster C_{i-1} at the $(i-1)$th step and k_i^- and k_i^+ represent the cluster decomposition and association rate constants, respectively. A complete nucleation theory can be established to describe the evolution of the population of clusters, i.e., the rates and mechanism by which these clusters grow and decay. As reflected by equation 1.1, the free energy of the nucleating system reaches a maximum (i.e., the nucleation barrier) when the critical nucleus forms. In addition, a multicomponent system may exhibit multiple nucleation barriers, leading to further complication in the identification of the critical nucleus on the basis of the free energy surface of the cluster growth.

Kinetically, at the critical nucleus, the rate to form the $(i+1)$th cluster is equal to that of decomposition of the critical nucleus to form the $(i-1)$th cluster, i.e.

$$k_i^-[C_i^*] = k_i^+[A_i][C_i^*] \tag{2.2}$$

where $[A_i]$ and $[C_i]$ are the number concentrations of the associating monomer and the cluster of size i, respectively. Furthermore, since the molecular flux between adjacent clusters achieves the minimum at the critical nucleus (commonly referred to as a bottleneck[7]), another practical approach to locate the critical nucleus is to variationally minimize the molecular flux as a function of the cluster site

$$dF_i/di = 0 \tag{2.3}$$

where F_i is the number of clusters growing from a size i to a size $i+1$ per second. The rate of nucleation, J, is defined as the rate of growth of the critical nucleus

$$J = k_i^+[C_i*] \tag{2.4}$$

The association and decomposition rate constants can be calculated employing the kinetic rate theories, such as transition state theory (TST).[62] For each cluster, the association rate is related to the dissociation rate by detailed balance[63−70]

$$\frac{k_{i-1}^+}{k_i^-} = \frac{Q_{C_i^*}}{Q_{C_{i-1}} Q_{A_{i-1}}} \exp\left(\frac{D_{C_i^*}}{kT}\right) \tag{2.5}$$

where $Q_{C_i}{}^*$ is the partition function of the critical nucleus, $Q_{C_{i-1}}$ and $Q_{A_{i-1}}$ are the partition functions of the respective $(i-1)$th cluster and monomer, k is the Boltzmann constant, T is the temperature, and $D_{C_i}{}^*$ is the binding energy of the critical nucleus relative to monomer and $(i-1)$th cluster. The decomposition rate constant of each cluster can be calculated according to the following expression[63−70]

$$k_i^- = \frac{kT}{h} \frac{Q_{C_i^*}^{\ddagger}}{Q_{C_i^*}} \exp\left(-\frac{\Delta E}{kT}\right) \tag{2.6}$$

where $Q_{C_i*}{}^{\ddagger}$ is the partition function of the transition state, h is the Planck constant, and ΔE is the transition state energy relative to the critical nucleus. In the case that the association reaction proceeds without an activation barrier (a loose transition state), the location of the transition state can be determined variationally by minimizing the decomposition reaction rate constant using canonical variational transition state theory (CVTST).[71] The partition functions required for eqs 2.5 and 2.6 can be evaluated by treating the rotational and translational motion classically and treating vibrational modes quantum mechanically. Vibrational frequencies, moments of inertia, and reaction energies can be taken from quantum chemical calculations.[72] An example of such an approach is the dynamical nucleation theory (DNT) of Kathmann et al.,[73−75] which uses CVTST to locate transition states and calculate evaporation rate constants k_i^- for each stage of the nucleation process.

Depending on the assumptions and approximations made, three major types of theoretical approaches have been established to characterize the nucleation process. Phenomenological theories, e.g., classical nucleation theory, attempt to obtain the free energy of formation of the critical nucleus from macroscopic parameters, such as the surface tension and the bulk liquid density. Some kinetic theories derive the cluster distribution and hence the nucleation rate by calculating rate constants for association and decomposition of clusters, avoiding explicit evaluation of cluster formation energies from macroscopic parameters. Molecular-scale approaches, including molecular dynamics, Monte Carlo simulations, and density functional theory, apply first principles to calculate the cluster structure and free energy of cluster formation.

2.1.1. Classical Nucleation Theory. The classical nucleation theory (CNT) was formulated by Becker and Döring[76] and Frenkel[77] on the basis of the kinetic theory of nucleation established by the work of Volmer and Weber[78] and Farkas.[79] CNT includes the thermodynamic and kinetic components by evaluating the free energy change of formation of a nascent phase cluster and calculating the nucleation rate. The phenomenological approach to CNT describes the nucleation process in terms of the change in Gibbs free energy of the system upon transfer of i molecules from the vapor phase to an i-mer cluster of radius r

$$\Delta G = -ikT \ln S + 4\pi r^2 \sigma \tag{2.7}$$

where $S = p_A/p_A{}^S$ is the saturation ratio, p_A is the vapor pressure of substance A in the gas phase, $p_A{}^S$ is the vapor pressure of

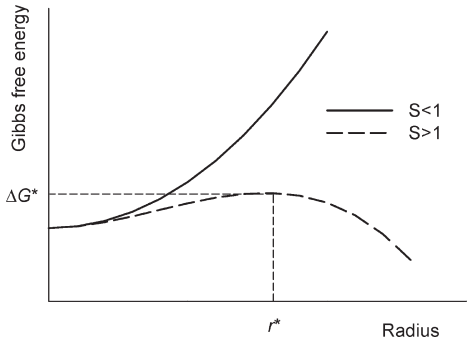

Figure 2. Gibbs free energy change for formation of a droplet of radius r from unsaturated ($S < 1$) and supersaturated ($S > 1$) vapor; ΔG^* corresponds to a critical nucleus of radius r^*.

substance A over a flat surface of the corresponding liquid, and σ is the surface tension. Although the cluster may consist of only a few molecules, it is assumed to have sharp boundaries and the same physical and chemical properties as the bulk phase (capillarity approximation). For a spherical cluster, the number of molecules i can be explicitly related to its radius $i = (4/3)\pi r^3/v_l$, where v_l is the volume of a single molecule in liquid. Equation 2.7 is one of the forms of the Kelvin equation, which expresses the elevation in the saturation vapor pressure above a curved surface, such as the interface between a small liquid droplet and surrounding air.

The free energy change of the cluster formation given by the right-hand side of eq 2.7 consists of two terms. The first term represents the energy decrease upon the transition from vapor to liquid and may be either negative or positive, depending on the vapor saturation ratio. The second term, which is related to the excess of the free energy at the liquid/vapor interface, is always positive. When vapor is subsaturated ($S < 1$), the free energy of cluster formation is always positive and condensation is prohibited (Figure 2). If the system is supersaturated ($S > 1$), the free energy term is negative, favoring condensation of vapor molecules and growth of the embryonic droplet. For very small particles, the increase in the free energy due to formation of the new surface area dominates over the free energy decrease from bulk phase formation, resulting in an energy barrier to nucleation. For droplets with size greater than the critical radius r^*, the condensation term dominates, leading to a decrease in ΔG as shown in Figure 2. The free energy of cluster formation ΔG reaches a maximum at r^*, and the location of the critical nucleus can be determined by differentiation of eq 2.7 with respect to r

$$r^* = \frac{2\sigma v_l}{kT \ln S} \tag{2.8}$$

The corresponding number of molecules i^* at the critical size and free energy barrier height ΔG^* are given in the following relations

$$i^* = \frac{32\pi\sigma^3 v_l^2}{3(kT \ln S)^3} \tag{2.9}$$

$$\Delta G^* = \frac{4\pi}{3}\sigma r^{*2} = \frac{16\pi}{3}\frac{\sigma^3 v_l^2}{(kT \ln S)^2} \tag{2.10}$$

The critical nucleus at the top of the ΔG curve is in a metastable equilibrium with the vapor. If a single molecule is removed from the critical nucleus, the free energy decreases and the cluster decomposes. If a molecule is added to the critical nucleus, the free energy also decreases and the cluster continues to grow spontaneously. The nucleation rate J can be defined as the number of clusters that grow past the critical size per unit volume per unit time

$$J = J_0 \exp\left(-\frac{\Delta G^*}{kT}\right) \tag{2.11}$$

where J_0 is the pre-exponential factor typically determined from gas−kinetic considerations. The nucleation rate has a negative exponential dependence on the height of the free energy barrier. An increasing saturation ratio decreases the critical nucleus size and the height of the free energy barrier, resulting in a faster nucleation rate (eqs 2.10 and 2.11).

Classical nucleation theory can be applied to nucleation of multicomponent vapors. When several molecular species participate in nucleation, the chemical composition of the critical nucleus, which is usually different from the vapor composition, becomes an additional degree of freedom. CNT of binary homogeneous nucleation is first introduced by Flood[80] and further developed by Reiss.[81] The free energy change, $\Delta G^*(i_1, i_2)$, associated with formation of a critical nucleus from binary vapor depends on the concentrations of molecules of both components, i_1 and i_2. The critical nucleus is located at the saddlepoint on the $\Delta G^*(i_1, i_2)$ surface and corresponds to the smallest cluster for which growth by addition of another molecule of vapor of either component is a spontaneous process.

An alternative kinetic formulation of the classical nucleation theory can be obtained for cluster formation and dissociation corresponding to reaction 2.1

$$\frac{d[C_i]}{dt} = k_{i-1}^+[C_{i-1}][A_{i-1}] - k_i^-[C_i] - k_i^+[C_i][A_i] + k_{i+1}^-[C_{i+1}] \tag{2.12}$$

In the steady state, the concentrations of clusters of different sizes are independent of time and the net rate, at which clusters C_i become C_{i+1}, is constant for all i. This simplification reduces the problem of calculating the nucleation rate to the derivation of the association and decomposition rate constants.[82] Whereas the association rate constant k_i^+ can be calculated from first principles, usually assuming that it is the gas−kinetic collision rate, the decomposition rate k_i^- requires evaluation of the cluster stability, typically from the free energy change of cluster formation, based on the properties of bulk solutions.[83] For this reason, not only the resulting nucleation rate derived by the kinetic approach takes a general form given by eq 2.11 but also it is exactly equivalent to the nucleation rate obtained within the framework of the phenomenological approach.

The advantage of CNT lies in its simplicity. The CNT approach provides closed analytical expressions for the critical saturation and nucleation rate based on the free energy of critical nucleus formation derived from measurable bulk properties, readily available for many substances. Although CNT allows estimation of critical supersaturations reasonably well, it fails frequently, by many orders of magnitude, in reproducing measured nucleation rates for a broad range of substances and experimental conditions. Specifically, the nucleation rates are underestimated at low temperatures and overestimated at high temperatures,[84] and critical supersaturations are significantly underestimated for strongly associated vapors, such as organic carboxylic acids.[85] One of the major reasons for the poor

dx.doi.org/10.1021/cr2001756 |Chem. Rev. 2012, 112, 1957–2011

quantitative performance of CNT is the assumption that the critical nucleus can be approximated by a spherical droplet with a well-defined, sharp boundary and physical properties that are identical to those in the bulk phase. However, macroscopic values of the surface tension and molecular volume may not be directly applicable to clusters consisting of a small number of molecules. In fact, molecular dynamics and density functional theory calculations indicate that surface tension decreases as the clusters become smaller.[86,87] As follows from eqs 2.10 and 2.11, the nucleation rate, $J \propto \exp(\sigma^3 v_1^2)$, is extremely sensitive to the absolute values of surface tension and molecular volume, so that even small uncertainties in σ and v_1 change the nucleation rate by many orders of magnitude. While treatment of larger ($i > 10$) clusters can be made using the standard capillarity approximation, the capillarity approximation fails for the smallest clusters ($i < 10$).[88−90]

Alternatively, the agreement between CNT and experimental nucleation rates can be improved by deriving Gibbs free energies for small clusters from accurate ab initio quantum chemical calcualtions.[91]

In addition to the capillarity approximation, CNT contains other inconsistencies and assumptions. As follows from eq 2.7, the change in Gibbs free energy does not equal zero for a cluster composed of a single monomer molecule ($i = 1$), which is physically unrelistical. Several groups have proposed corrections to ensure that $\Delta G = 0$ for $i = 1$, thus making CNT self-consistent,[92−94] although questions arise on the validity of such ad hoc adjustments. Also, an assumption of the steady-state population of subcritical clusters throughout the entire nucleation process and the concentration of monomers being much higher than the concentration of subcritical clusters may be invalid under a broad range of nucleation conditions. In the case of fast nucleation, a large fraction of the nucleation flux is due to cluster−cluster collisions, leading to underestimation of the nucleation rate by phenomenological CNT in comparison to the kinetic approach.[95]

The relatively small size of nucleating clusters allows treating the molecular interactions explicitly. A number of theoretical and computational approaches have been developed that rely on molecular simulations to calculate cluster properties, which are then used to determine nucleation rates. In these approaches, condensation rate constants are often approximated by gas-phase collision rates of vapor molecules with growing clusters as in CNT, whereas the cluster distribution functions, partition functions, and Helmholtz free energies are computed from molecular simulations. The simulations may employ quantum mechanical electronic structure calculations to develop a harmonic model of molecular interactions together with the rigid-rotor harmonic oscillator approximation to determine free energies or use analytic empirical or semiempirical interaction potentials and calculate the full anharmonic free energy through statistical mechanical sampling. Using ab initio electronic structure calculations has the general benefit that chemical bonds in the clusters can be formed or broken and that the accuracy of the energies can be systematically improved. However, these benefits come at a high computational cost, making statistical mechanical sampling of the nuclear configuration space impractical. The use of analytic interaction potentials not only allows performing statistical mechanical sampling but also avoids the rigid-rotor harmonic oscillator approximation. Overall, an accurate prediction of nucleation rates requires precise representations of the molecular interactions combined with a theoretical formalism connecting interaction energies to rate constants and appropriate statistical mechanical sampling to obtain accurate free energies or, equivalently, equilibrium constants.[96]

2.1.2. Kinetic Theories. There are a number of kinetic theories that obtain the cluster distributions and hence the nucleation rate by calculating rate constants for formation and decomposition of clusters using methods that avoid explicit evaluation of cluster formation energies and surface tension.[74,97] The method of Ruckenstein and co-workers is based on calculation of the decomposition and association rates independently by solving the Smoluchowski or Fokker−Planck equation governing the motion of a single molecule in a potential well around the cluster.[98,99] In the original version of this method, the cluster is assumed to have sharp boundaries and uniform density equal to that of the bulk liquid that significantly simplifies calculation of the effective potential field, allowing derivation of an analytical expression for the effective potential. The parameters in the interaction potential are fit to obtain the correct density of the liquid and the proper surface tension for large spherical clusters, ensuring that this theory reduces to CNT for large clusters. In later developments, the density uniformity assumption is eliminated by using density functional theory (DFT) methods. The more realistic density profile allows for a more accurate calculation of the potential field created by the cluster, its rate of evaporation, and the nucleation rate.[100]

The dynamical nucleation theory (DNT) of Kathmann and co-workers[74,75,101] applies a gas-phase perspective to vapor nucleation, treating it as a multistep binary collision process between nucleating molecules and clusters. Calculation of the nucleation rate involves explicit consideration of interacting molecules to obtain kinetic parameters followed by solving the kinetic equations for cluster evolution. The interaction energies may come from either analytic potentials or high-level ab initio electronic structure calculations. In DNT, the dynamical bottleneck in phase space is explicitly evaluated for each stage of the kinetic process. This bottleneck is characterized by a dividing surface in the phase space that separates reactant states from product states, allowing an unambiguous definition of a cluster, which is consistent with the detailed balance and the decomposition and association rate constants. Most approaches, including CNT, approximate the association rate constant using a gas−kinetic model and then obtain an estimate of the decomposition rate from detailed balance. On the contrary, the emphasis of DNT is evaluation of the decomposition rate constant (eq 2.6). The association rate constant is then obtained from the ratio of the decomposition and association rate constants and differences in Helmholtz free energy between adjacent-sized clusters using a detailed balance (eq 2.5). Use of CVTST for calculation of decomposition rate constants eliminates the ambiguity in determining the size of the relevant regions of the configuration space by varying the dividing surface to minimize the reactive flux and also provides a systematically improvable framework for rate constant calculations, in which corrections to approximations in the theory can be included. The DNT shows a good agreement with the experiment for the nucleation of pure water[73,74] and has been extended to include multicomponent systems.[102]

2.1.3. Molecular Dynamics and Monte Carlo Methods. Molecular level approaches, such as molecular dynamics (MD) and Monte Carlo (MC) simulations, apply first principles to calculate the structure and free energy of cluster formation.[103,104] The MC method is stochastic and simulates the evolution of an

ensemble of molecules by sampling random molecular configurations, i.e., one molecule at a time, and accepting or rejecting configurations according to certain criteria. On the contrary, the classical MD method uses Newton's laws to explicitly simulate the trajectories of all molecules undergoing a phase transition. The trajectories are determined by imposed initial positions and momenta of molecules and by the intermolecular potential. The presence of a cluster of the new phase is identified on the basis of the molecular density, bond number per molecule, chemical potential of molecules in the new phase, or other properties.[105,106] Such information is used to calculate the association and decomposition rate coefficients, which are utilized to determine nucleation rates. Direct MD simulations involve the preparation and evolution in time of a metastable system until nucleation occurs.[107,108] Since there is no analytical solution to the many body problem, calculations by the molecular dynamics or even by stochastic Monte Carlo are computationally expensive because of the necessity of solving the interaction among numerous molecules. This limitation places a constraint on the number of molecules that can be treated, the size of the spatial domain, and integration times. Since fluctuations leading to nucleation are seldom events on the simulation time scale, direct simulation of nucleation is highly impractical. A viable alternative to direct simulation is provided by biased sampling methods, such as umbrella sampling,[109] first introduced into the field of nucleation by Frenkel and co-workers[110] and widely used afterward.[111,112] The umbrella sampling methods force the metastable system to cross the free-energy barrier reversibly along a reaction coordinate in a tractable amount of time by means of a biasing potential.

The classical MC and MD methods require knowledge of a realistic intermolecular potential. The Lennard−Jones (LJ) potential function represents the most widely used one and has been successfully applied to simple atoms and their mixtures, such as Ar and He.[113] However, the LJ potential is inappropriate for molecules of associative vapors, such as water, sulfuric acid, and other plausible atmospheric nucleating species. Other more advanced potentials, such as transferable intermolecular potentials (TIP), have been developed and proven successful, yielding reasonable agreement with measured liquid water properties directly related to stochastic molecular-scale fluctuations associated with the phase transition.[114−116] Although use of these potentials for the vapor−liquid transition yields the correct temperature dependence of the nucleation rates, predictions of the absolute nucleation rates still fail by several orders of magnitude.[117]

In the first-principle MD, no model potential needs to be specified because the electronic structure of the molecular system is treated explicitly by density functional theory or quantum chemistry, whereas the motion of atomic nuclei is treated according to classical mechanics.[118,119] This approach is capable of explicit treatment of nuclear quantum effects, including proton transfer and corresponding changes caused in the hydrogen-bond network of the cluster. However, application of the hybrid method is computationally expensive and currently limited to investigation of dynamics that occurs on a tens to hundreds picosecond time scale.

2.1.4. Density Functional Theory. The basic assumption of density functional theory applied to the problem of nucleation is that the nucleating vapor can be considered as an inhomogeneous fluid.[120−123] The interface between the nucleus of the new phase and the initial phase has a finite width and is characterized by a density profile, but unlike in CNT the density at the center of a cluster is not constrained to be equal to the bulk liquid density. Also, the density profile at the interface is not required to match that at a planar interface but only constrained to approach the bulk vapor density at large distances from the cluster. In contrast to the molecular dynamics approach, which explicitly evaluates interactions between each molecule in the system, DFT considers the interaction between a given individual molecule and the mean potential field produced by the rest of the other molecules. Thus, DFT is macroscopic, using an average density distribution instead of atomic coordinates for nucleating monomer entities, but considers effects that are characteristic of the molecular-level scale. The fundamental variable in DFT is the molecular density field as a function of spatial coordinates, whereas all other variables, including the free energy, are functions of the density. This theory derives the properties of the critical nucleus from the free energy of the nonuniform system, which is a unique functional of the average density and whose minima determine the thermodynamically stable states at a given temperature.[124] At a given supersaturation, this functional has a saddle point in the function space where it is defined. The solution yields the density profile of the critical nucleus and the free energy or work of formation from the unstable vapor. The DFT approach is computationally efficient, allowing treatment of more complex systems relevant to atmospheric nucleation. With the use of a proper interaction potential, it can be successfully applied to associative molecules,[125] producing the proper temperature dependence of the water nucleation rate.[126] The generalization of DFT to multicomponent systems has been developed[127,128] and applied to binary nucleation.[129] Whereas most DFT work has centered on evaluation of the barrier to nucleation using the classical pre-exponential J_0 to estimate nucleation rates, several efforts exist to develop a more complete theory that calculates J_0 as well.[130,131]

2.1.5. Nucleation Theorem. The nucleation theorem introduced by Kashchiev,[132] unlike other nucleation theories, makes no a priori prediction of the nucleation rate and is derived directly from the first principle (i.e., eq 1.1). The nucleation theorem provides the molecular information on the composition of the critical nucleus when used in conjunction with experimental measurements. By differentiating eq 2.7, one can show that for a critical nucleus of size i^* in a single-component system

$$\frac{\mathrm{d}(G/kT)}{\mathrm{d}\ln S} = -n^* + \frac{\mathrm{d}(4\pi r^2\sigma)}{\mathrm{d}\ln S} = -i^* + \Delta \qquad (2.13)$$

where Δ is the number of vapor molecules displaced by the cluster. Since the concentration of the nucleating vapor is typically very low, Δ is close to zero and can be neglected. It can be shown from eq 2.11 that the slope of the logarithm of the nucleation rate versus the logarithm of the saturation ratio of the nucleating vapor A_i is related to the number of molecules in the critical nucleus

$$\left[\frac{\partial \ln J}{\partial \ln S_{A_i}}\right]_{T,A_j} = i + \delta \qquad (2.14)$$

where $\delta = 2$ for unary vapor nucleation[132] and $\delta = 0-1$ for binary vapor nucleation.[133] Since experimental nucleation rates are often measured at a constant temperature, the saturation vapor pressure is constant, making it possible to replace S_A in eq 2.14 with the monomer vapor pressure, p_A, or concentration, [A]. The

nucleation theorem is a thermodynamic result relating the sensitivity of the nucleation barrier height to the change in the logarithm of the nucleating vapor concentration. It has been shown that the nucleation theorem exhibits a general relation independent of the specific nucleation model assumptions and applies to a critical nucleus of any size.[133] Furthermore, the validity of the nucleation theorem has been confirmed on the basis of statistical mechanical[134] and kinetic[135] arguments, and it has been extended to multicomponent systems.[133,136−139]

2.2. Nucleation Experiments

In experimental studies, a number of methods and analytical instruments have been developed to measure a broad range of nucleation rates, spanning more than 20 orders of magnitude, i.e., from 10^{-4} to 10^{17} cm^{-3} s^{-1}. The main differences between the experimental methods are related to the way of achieving a supersaturated state. In nucleation studies involving a single-component system, the supersaturated state is typically obtained by cooling the vapor phase using either adiabatic expansion or a temperature gradient. In multicomponent systems, the preferred approaches are turbulent mixing of vapors followed by fast cooling or in-situ generation of one of the nucleating vapors chemically or photochemically. Some experimental methods are static (i.e., operate in cycles), while others operate continuously. Early studies using diffusion and expansion cloud chambers focus on measurements of the critical supersaturation needed to observe the onset of nucleation, corresponding to a detectable nucleation rate of unity (J = 1 cm^{-3} s^{-1}).[140] Implementation of various particle detection techniques in later studies allows one to count the number of nucleated particles and hence calculate their formation rate.[84]

2.2.1. Adiabatic Expansion Approaches. Several experimental approaches rely on vapor cooling by rapid adiabatic expansion to produce supersaturation and initiate nucleation. In a fast expansion cloud chamber (or a nucleation pulse chamber), nucleation starts when a piston is moved to produce an adiabatic expansion in a mixture of the nucleating vapor and a carrier gas.[141,142] The vapor originates from a liquid pool resting at the bottom of the chamber. Following a short period of time, on the order of milliseconds, nucleation is terminated by means of a small recompression using the same or an additional piston while the vapor phase remains supersaturated, allowing particles to grow to a detectable size. Depending on the specific chamber design, nucleation rates in the range from 10^{2} to 10^{10} cm^{-3} s^{-1} can be determined from the number of particles in the resulting droplet cloud. This method has been used to measure nucleation rates in a large number of single-vapor systems,[143] including water,[142,144] *n*-alcohols (methanol through hexanol),[145,146] toluene,[147] *n*-nonane,[148,149] argon,[150,151] and nitrogen,[152] and also in binary vapor systems, such as water−ethanol mixtures.[153]

Another expansion-based method of measurements of nucleation rates is the shock tube, consisting of two sections separated by a diaphragm. The driver section is filled with a high-pressure vapor−carrier gas mixture, whereas the driven section is maintained at low pressure.[154−156] Rupturing of the diaphragm produces an adiabatic expansion from the driver to the driven section, causing the vapor to become supersaturated and initiating nucleation. The nucleation pulse is terminated after about 0.1 ms by recompression, which is caused by the reflected expansion shock wave. The number of nucleated particles and their growth rates are determined from the light scattering intensity. Using this approach, nucleation rates up to 10^{17} cm^{-3} s^{-1} can be obtained.[157]

The supersonic nozzle method utilizes adiabatic expansion of a flowing nucleating vapor−carrier gas mixture to achieve high supersaturation.[158] Nucleation and condensational growth of clusters occur as the flow passes out of the throat region of the nozzle. The latent heat of condensation raises the local pressure, allowing detection of the location of the condensation onset. Nucleation rates are determined by combining the results from pressure trace measurements with those of the cluster size and number density from small angle neutron scattering,[159] small-angle X-ray scattering,[160] or tunable diode laser absorption spectroscopy.[161] In the supersonic nozzle, nucleation occurs under highly supersaturated conditions with rates in excess of 10^{16} cm^{-3} s^{-1}, which is several orders of magnitude faster than the rates measured in other expansion devices. The maximum nucleation rate obtained by this approach is 10^{18} cm^{-3} s^{-1},[62] and both single and binary vapor systems can be studied.[163]

Cryogenic versions of the expansion chamber,[152] shock tube,[164,165] and supersonic nozzle[166,167] have been developed to study nucleation of inert gases, argon and nitrogen. To reach temperatures low enough to observe condensation, the expansion starts near the boiling point of liquid nitrogen. Under these cryogenic conditions, elimination of contamination and controlling of heat transfer are extremely challenging, resulting in substantial scatter reported among the experimental data. Generally, the common limitation of all expansion methods is that they are not applicable to systems with a long time lag, in which nonsteady state nucleation takes place during most of the duration of the nucleation pulse (as in sulfuric acid−water). The expansion chamber provides the most accurate and reproducible data, although uncertainties may increase when large expansions are used or when the nucleating vapor is strongly associating. The shock tube and supersonic nozzle measurements are less accurate in comparison with other methods because pressure pulses cannot always be accurately reproduced but provide an option to measure high nucleation rates.

2.2.2. Diffusion Chamber. In contrast to expansion chambers, which produce short nucleation pulses, diffusion chambers operate continuously. In an upward diffusion chamber,[140] the supersaturation is achieved by establishing a temperature gradient between two parallel plates. The bottom plate is warm and covered with liquid, whereas the top plate is cool. As the vapor from the warm bottom plate diffuses toward the top cool plate, its temperature and partial pressure decrease almost linearly with the distance. Since the saturation vapor pressure varies exponentially with temperature, a maximum saturation ratio occurs between the two plates. The supersaturated vapor nucleates liquid droplets that grow and settle down toward the bottom plate to be detected and counted with a laser beam. The temperatures of the top and bottom plates are adjusted to achieve a desirable nucleation rate, typically in the range from 10^{-4} to 10^{3} cm^{-3} s^{-1}. Although the upward diffusion chamber has been used to measure critical supersaturations and nucleation rates of both individual and mixed vapors,[143] this method yields the most reliable results for single-component systems but provides rather inaccurate nucleation data for multicomponent systems because the maximum saturation ratios of different components generally occur at different heights. Also, continuous evaporation and condensation of vapors in a multicomponent system alter the compositions of liquid at the bottom, enriching it with less volatile components, which leads to further changes in the vapor composition.

2.2.3. Laminar Flow Chamber. Another approach that utilizes the thermodynamic and transport properties of gas to achieve supersaturated state is the laminar flow diffusion chamber, also known as the laminar flow tube reactor.[168−171] In the flow chamber, the carrier gas is saturated with the nucleating vapor in the hot saturator section and then abruptly cooled in the condenser section, where the vapor becomes supersaturated and nucleates to form the condensed phase. The nucleation zone is confined to a relatively small volume. Freshly nucleated particles rapidly leave the nucleation zone and continue to grow in the supersaturated environment of the carrier gas until they are large enough to be detected optically. Nucleation rates in the range from 10^2 to 10^8 cm^{-3} s^{-1} can be measured in this way. The laminar flow diffusion chamber is mostly suitable for vapors of high molecular weights, such as dibutylphthalate.[168,172,173] In the case of low molecular weight vapors, such as water, closeness of molecular and thermal diffusivities results in a lack of a sharply defined nucleation zone and significant condensation losses of vapor to the wall, complicating measurements of the nucleation rate.[174] Both static and laminar flow diffusion chambers require a transport model to calculate the temperature and saturation ratio profiles, which are then related to the measured nucleation rates.[140,175−177]

2.2.4. Turbulent Mixing Chamber. In the investigation of atmospherically important binary or ternary nucleation, various flow chambers consisting of a turbulent mixing section followed by a laminar nucleation section have been developed.[57,58,178−182] In the flow chambers, two or more gas flows carrying the nucleating vapors are rapidly mixed in the turbulent section that is maintained at a similar or elevated temperature relative to the laminar section. In the isothermal case, the system becomes supersaturated and nucleation occurs immediately after mixing.[179] If the mixing section is heated, the supersaturated state is achieved only when the gas mixture enters the colder laminar section, where nucleation and growth of particles take place.[57,58,181] In some designs, a chilled carrier gas is admixed to hot nucleating vapors at the entrance of the laminar section to quickly reduce the gas temperature.[178,180,182] The nucleating vapors are delivered to the mixing chamber from saturators, such as silica gel impregnated with the material of interest,[178] or the headspace above the liquid,[57,58,179,181] or by nebulizing liquid into the heated zone where it rapidly evaporates.[180,182] Alternatively, the nucleating vapor can be chemically produced in the mixing region from different precursors through a dark or photoinitiated process, such as the reaction of gas-phase sulfur trioxide with water vapor (eq 2.15)[183] or oxidation of sulfur dioxide by the hydroxyl radical in the presence of molecular oxygen and water vapor[184]

$$SO_3 + H_2O \rightarrow H_2SO \quad (2.15)$$

$$H_2O + h\nu(184\text{nm}) \rightarrow O(^1D) + OH \quad (2.16)$$

$$O(^1D) + H_2O \rightarrow 2OH \quad (2.17)$$

$$SO_2 + OH + M \rightarrow HOSO_2 + M \quad (2.18)$$

$$HOSO_2 + O_2 \rightarrow SO_3 + HO_2 \quad (2.19)$$

When the concentration of nucleated particles is not excessively high, particle growth by condensation does not deplete the vapor and the nucleation zone may extend from the mixing point to the end of the laminar section, where nucleated particles are detected. One of the major limitations of the flow chambers is that the nucleating vapors can be efficiently removed by diffusion to the chamber wall. For instance, at atmospherically relevant relative humidities and temperatures, molecules of sulfuric acid vapor are lost on almost every collision with the surface. In such a case, the concentration profile of the nucleating vapor along the chamber is typically constructed from a single-position measurement either in the upstream[57,58] or in the downstream[181] of the nucleation zone, assuming that the wall loss in a laminar flow is a diffusion-limited, first-order process. As shown by eqs 2.10 and 2.11, the nucleation rate varies exponentially with the vapor saturation ratio; hence, even a small decrease in the vapor concentration effectively terminates the nucleation process. In such a case, the length of the nucleation zone, required for accurate calculation of nucleation rates, can be determined by measuring the number concentration of nucleated particles along the chamber.[181,182]

2.2.5. Continuous Generation of Nucleating Vapors from Chemical Reaction sources. In the flow chambers described above, nucleation in multicomponent vapors occurs immediately after cooling and/or turbulent mixing, when the laminar flow is not yet fully developed, resulting in wall losses of both the vapor and the newly formed clusters that are difficult to be accounted for. Recently, a laminar flow chamber with continuous formation of the nucleating vapors has been introduced for studying binary and ternary nucleation of atmospherically important sulfuric acid, which is subject to particularly severe wall loss.[185,186] In this approach, sulfuric acid is chemically produced from SO_2 along the whole length of the flow chamber through ozonolysis of alkenes[185] or photolysis of ozone.[186] Both processes form the hydroxyl radical, which converts sulfur dioxide to sulfuric acid in the presence of molecular oxygen and water vapor

$$O_3 + h\nu(254\text{nm}) \rightarrow O(^1D) + O_2 \quad (2.20)$$

$$O_3 + \text{alkene} \rightarrow OH + \text{otherproducts} \quad (2.21)$$

Continuous generation of condensable molecules (e.g., H_2SO_4) in the gas phase by chemical reactions leads to nucleation of new clusters or condensation on existing clusters and particles, promoting their growth to detectable sizes, thus increasing the accuracy of nucleation rate measurements. Continuous in-situ photochemical sources of nucleating vapors have also been used to study atmospheric new particles formation in various smog chambers.[187,188]

2.2.6. Comparison between Experimental Results and Nucleation Theories. Homogeneous nucleation has been experimentally investigated for a large number of substances, including inert gases, metal vapors, and vapors of various inorganic and organic compounds.[143] For all vapors, the nucleation rate J is a steep function of supersaturation S as illustrated in Figure 3. Because of this strong dependence, large disparities are often observed between theoretically predicted and experimentally measured nucleation rates. In all nucleating systems, the critical supersaturation decreases with increasing temperature whereas J increases with temperature at a constant S. Application of the nucleation theorem to experimental nucleation rates obtained as a function of supersaturation at different temperatures shows that the critical nucleus becomes smaller at higher supersaturations and at lower temperatures. Whereas the experimental nucleation rates often exhibit a dependence on

dx.doi.org/10.1021/cr2001756 |*Chem. Rev.* 2012, 112, 1957–2011

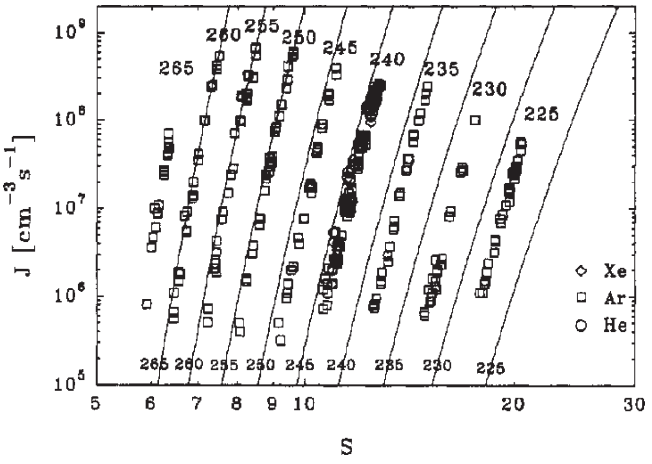

Figure 3. Experimental nucleation rates (symbols) for supersaturated *n*-butanol vapor compared to predictions of the classical nucleation theory (solid lines) in the 225−265 K temperature range. (Reprinted with permission from ref 189. Copyright 1994 American Chemical Society.)

supersaturation suggested by CNT, the temperature dependences of experimental and theoretical nucleation rates frequently differ from each other. The theoretical nucleation rates are typically underestimated at low temperatures but overestimated at high temperatures, with the errors of several orders of magnitude.

McGraw examined experimentally measured homogeneous nucleation thresholds for a number of vapors by a correlation approach employing dimensionless corresponding states, focusing on the influence of the molecular structure and degree of intermolecular association on nucleation.[190] Several vapors, such as argon and halogenated hydrocarbons, obey the corresponding states correlation between measured critical supersaturation and reduced temperature derived for simple molecules. Nonpolar molecules (*n*-alkanes and aromatics) nucleate at higher critical supersaturations than expected from the corresponding states correlation. Increasing the chain length of the molecules within a group and higher polarity (acetonitrile, benzonitrile, and nitrobenzene) increases the stability of the supersaturated vapor. However, some polar molecules (water and *n*-alcohols) nucleate at lower critical supersaturations because of a tendency toward association in the liquid phase through hydrogen bonding.

At present, theoretical models have yet to quantitatively describe nucleation of all substances under a broad range of temperature and saturation conditions. Theoretical assumptions and experimental uncertainties both contribute to the large discrepancies between theoretical and experimental results. In this situation, inert gases, such as argon, play the role of a test system for which experimental, theoretical, and simulation studies are combined to obtain better insight into the nucleation phenomenon and performance of different theories. Argon is a simple fluid whose behavior at the molecular level is adequately described by the Lennard−Jones (LJ) interaction potential, and equilibrium properties have been extensively studied experimentally and theoretically. However, experimental measurements of Ar nucleation are extremely challenging because of the necessity to use cryogenic temperatures, under which conditions leaks, contamination, and heat transfer are difficult to control. Given these challenges, it is not surprising that the results of early measurements of argon nucleation are extremely scattered and frequently inconsistent with each other.[164,165,191] More recent experiments[150,151,166,167] indicate that CNT consistently underpredicts the nucleation rates of argon by about 11−13 orders of magnitude, because of overestimations in both the size and the excess internal energy of the clusters. However, given the experimental uncertainties, the temperature dependence of the nucleation rate produced by CNT well matches the experimental data. Measurements of nucleation for the diatomic molecular nitrogen[152] show that CNT underpredicts the experimental results by 9−19 orders of magnitude and with an unrealistically stronger temperature dependence. The Reguera−Reiss theory,[192] on the basis of the combination of the "extended modified liquid drop" model and dynamical nucleation theory, predicts the correct temperature dependence at low temperatures and yields a smaller absolute deviation of 7−13 orders of magnitude. An empirical correction function to CNT, describing the experimental results for nitrogen,[152] is remarkably close to the ones for argon[151] and water.[193]

Often classical nucleation theory fails to agree with experimental measurements even at a single temperature, such as in the case of *n*-nonane, for which CNT-derived nucleation rates differ by 4 orders of magnitude from the experimental results.[84] A study of another four *n*-alkanes confirms that large temperature-dependent correction factors are needed for quantitative agreement between measured and predicted nucleation rates.[194] Similarly, the experimental results for dibutyl phthalate deviate by up to 6 orders of magnitude from those predicted by the model.[172,173] For alcohols, the deviations of CNT predictions from experimental values are over 5 orders of magnitude.[146] To assess the scatter produced by different methods, nucleation of *n*-pentanol has been thoroughly studied by several research groups. Although a good agreement with CNT is observed at 273 K,[195] for a broader temperature range (260−290 K) the experimental results are scattered 3 orders of magnitude above[196] the CNT predictions but other measurements are 3 orders of magnitude below.[197] Measurements of other hydrogen-bonded organic materials, such as a glycols, also exhibit strong disagreement in the temperature dependence of the nucleation rate from those predicted by CNT.[198]

The most noticeable deviations from classical nucleation theory have been observed for nucleation of metal vapors, such as lithium,[199] sodium,[200] cesium,[201] zinc,[202] silver,[202] and mercury.[203,204] For metals, even critical supersaturations, which are typically reproduced rather well for other substances, appear many orders of magnitude above (alkali metals) or below (zinc and mercury) those predicted by CNT, resulting in significant differences between measured and predicted nucleation rates. The unique properties of metals, such as high electrical and thermal conductivities and low vapor pressure, are attributed to the presence of delocalized electrons, which dominate metal cluster properties. Therefore, it is not obvious whether nucleation theories applicable to clusters composed of discrete molecules can describe metal clusters. For instance, because of efficient clustering, monomer metal atoms do not represent the major fraction of the vapor phase, contradicting a common assumption in classical nucleation theory.[205] When metal vapors form clusters, certain sizes are more tightly bound than others.[206] As the stability of clusters varies nonuniformly with size, a proper theoretical treatment of metal nucleation must explicitly account for this effect. Furthermore, an important difference between metals and molecular liquids is that in the former a size-dependent metal−nonmetal transition takes place, which may

significantly change cluster physical properties, including density and surface tension.[207] A possible cause for the extremely large deviations between experimental and CNT supersaturations in the case of mercury may be explainable because small mercury clusters are insulators, with much smaller effective surface tensions than those measured for bulk mercury.[203]

Nucleation of water droplets corresponds perhaps to the most studied single-component system. A large number of data has been collected for homogeneous nucleation of water vapor, after the first systematic studies of Allen and Kassner[208] and Heist and Reiss.[209] The great interest toward water is explained by large-scale application of steam turbines for power generation, where formation of the liquid phase in low-pressure turbines has been an important subject of theoretical and experimental studies.[210] For water, CNT successfully predicts the experimental nucleation rates within 1 order of magnitude for the temperature range of about 220−260 K and a relatively narrow range of supersaturations.[142,144,157,174] However, at a temperature of 220 K, classical theory underestimates the experimental results by up to 2 orders of magnitude. For a broader range of temperatures and supersaturations, the failure of CNT becomes more evident. Perhaps this is not surprising since McGraw and Laaksonen suggest that a theory based on the classical capillarity approach does not allow prediction of the correct temperature dependence.[211] Also, it is questionable whether all experimental measurements are actually made with pure water. As nucleation is highly sensitive to even small concentrations of contaminants,[174] early studies may suffer from an impurity deficiency, likely representing results for binary or multicomponent nucleation.

In the presence of several components, calculation of the cluster properties becomes more difficult because surface activities, nonideal mixing, and an inhomogeneous distribution of the components within the cluster need to be considered. Binary systems can be classified according to their nonideality as a function of vapor composition. The lines of the constant isothermal nucleation rate as a function of varying gas-phase activities (supersaturations) of the two species are straight for ideal solutions but bend in nonideal systems toward or away from the origin as illustrated in Figure 4. An example of a nearly ideal system is the mixtures of ethanol-*n*-hexanol[136] and ethanol−*n*-propanol vapors,[158] for which the isothermal onset vapor pressure of the mixture varies nearly linearly between the onset pressures for the pure components. On the other hand, strong deviations from binary CNT are observed for the water−*n*-alcohol and *n*-nonane−*n*-alcohol mixtures. Water and *n*-alcohol vapors show a mutual enhancement,[137,153,158,163,212] which persists even when the two chemical species exhibit a miscibility gap for bulk mixtures. As a result, the lines of the constant nucleation rate versus activity for these mixtures bend toward the origin. The observed trend is consistent with the surface enrichment of nucleating clusters by alcohol molecules. Alcohols have lower surface tension than water and greatly reduce the surface free energy of the critical nucleus, thus lowering the barrier of nucleation. This concept is supported by molecular dynamics simulations of ethanol−water clusters.[213] Another deviating system, the mixture of *n*-nonane and *n*-alcohols, only reluctantly conucleates,[214] revealing an opposite mixing behavior to that measured for the mutually enhancing water−alcohol systems. The poor mutual affinity is observed in all alcohols investigated,[214] decreasing with the length of the alcohol organic chain because small alcohols tend to demix with alkanes and exhibit a macroscopic miscibility gap for the *n*-nonane-methanol mixture.

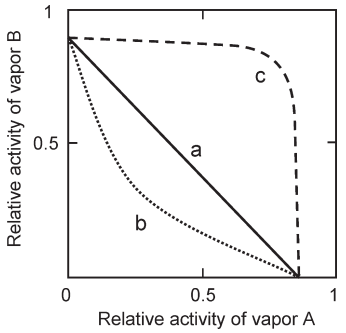

Figure 4. Onset activities corresponding to a constant reference nucleation rate for different types of mixed vapor systems: (a) ideal mixture, (b) mutual nucleation enhancement, (c) independent nucleation (no conucleation).

The activity plot of these mixtures becomes progressively more angular with decreasing chain length of the alcohol. In the extreme case of a water−*n*-nonane mixture, the plot is an almost perfect right angle because water and *n*-nonane vapors nucleate independently of each other.[215]

The enhanced tendency of nucleation may also result from the large mixing enthalpies, as is the case in the water−acid mixtures. Gaseous sulfuric acid and water are two well-recognized nucleation precursors in the atmosphere because of the very low vapor pressure above H_2SO_4−H_2O binary solutions.[9,10,29] Sulfuric acid forms stable hydrates in the vapor phase[216,217] due to the strongly negative free energy of hydrate formation.[8,218] Furthermore, when clusters composed of sulfuric acid and water molecules grow in size, formation of an ion pair upon proton transfer from H_2SO_4 to H_2O leads to additional cluster stabilization. Binary and multicomponent nucleation involving sulfuric acid, water, and other chemical species that serve as a major source of new particles in the Earth atmosphere will be discussed in details in section 3. Several previous review papers have presented in-depth descriptions of other theoretical and experimental aspects of general vapor nucleation.[7,55,74,75,123,143,210,219,220]

3. NUCLEATION OF NANOPARTICLES IN THE ATMOSPHERE

3.1. Atmospheric Measurements

New particle formation represents a global phenomenon that has been observed in a variety of environments ranging from urban centers[221,222] to remote areas, including forests,[223,224] grasslands,[225] coastal sites,[226,227] and the atmospheres of the sub-Arctic[228] and Antarctica.[229,230] Most frequently new particles form in regional events that extend hundreds of kilometers over the continental boundary layer. Localized events of formation of high concentrations of nanoparticles, such as those in urban and industrial plumes[231,232] and in coastal marine locations,[227] have also been observed. Studies of atmospheric aerosol formation typically involve measurements of the number concentration and size distribution of nucleation mode particles. Simultaneous measurements of nucleating precursor gases, chemical analysis of nanoparticles, and, more recently, measurements of atmospheric molecular clusters provide insights into aerosol nucleation and growth processes. Numerous field studies of aerosol nucleation and growth have been conducted since the 1990s, when new instruments capable of measuring size distributions of nanoparticles as small as ∼3 nm[233−235] and

detecting gas-phase precursors[236] have been developed. A range of measurement platforms, including ground sites, ships, and aircraft, have been used in local and regional field campaigns to study nucleation events at different altitudes, from the ground (or sea) level to the free troposphere.[50] Whereas most investigations are based on intensive short-term measurements, there are a growing number of studies reporting results of continuous long-term monitoring.[223,227,237] Kulmala et al. presented an extensive review that summarizes the findings of more than 100 campaigns before 2004.[50] Subsequent reviews by Curtius,[53] Holmes,[51] and Kulmala and Kerminen[54] not only provided an update on most recent field studies but also discussed the findings of atmospheric measurements in relation to the current laboratory and modeling work on atmospheric nucleation. Additionally, other recent reviews focused on specific aspects of atmospheric new particle formation, such as ion-mediated nucleation (IMN),[238−240] coastal new particle formation,[52,241] and the highlights of the major scientific findings of the European Integrated project on Aerosol Cloud Climate and Air Quality interactions (EUCAARI).[242]

3.1.1. Concentrations and Size Distributions of Atmospheric Nanoparticles. The concentration of atmospheric nanoparticles is typically measured by condensation particle counters (CPC), in which nanoparticles grow by condensation of supersaturated alcohol or water vapors to micrometer-size droplets and are then optically detected and counted.[243] The detection threshold of early CPCs is limited to particles larger than about 20 nm.[244] In 1991, Stolzenburg and McMurry developed an ultrafine condensation particle counter (UCPC) that detects nanoparticles as small as 2.5 nm.[233] Furthermore, the vapor supersaturation in the UCPC can be optimized to produce size-dependent particle growth, resulting in the dependence of the scattered optical signal on the initial nanoparticle size.[245] Particle number size distributions in the 3−10 nm range can be inferred from measured pulse height distributions using pulse height analysis (PHA).[246] Particle size distributions in a broader size range are usually obtained with a differential mobility particle sizer (DMPS)[247] or a scanning mobility particle sizer (SMPS).[248] Both instruments consist of a differential mobility analyzer (DMA),[249] which selects the size of charged particles on the basis of the electrical mobility diameter and a CPC or an electrometer to count mobility-classified particles. DMAs are available in various designs, including two common models that have been specifically developed for measurement of the size distributions of nanoparticles in the range of 3−50 nm.[234,235] Important design features of these DMAs include high particle penetration and high sizing resolution.

Since the minimum detectable size in most field measurements is typically 3 nm, new particle formation events are often defined by an abrupt appearance and rapid growth of 3 nm particles.[50] A typical new particle formation event on a summer day in Beijing is illustrated in Figure 5, showing the particle number size distribution, the total concentration of 3−20 nm particles, and the concentration of gas-phase sulfuric acid measured by chemical ionization mass spectrometry (CIMS) as a function of time.[250] New particle formation occurs following the traffic rush hour in the morning, and particles continue to grow throughout the course of the day, reaching the CCN size range (50−100 nm). The concentration of nucleation mode particles increases rapidly following a sharp rise in the concentration of sulfuric acid.[250,251] On the contrary, the concentration of nanoparticles emitted directly by traffic does not correlate with

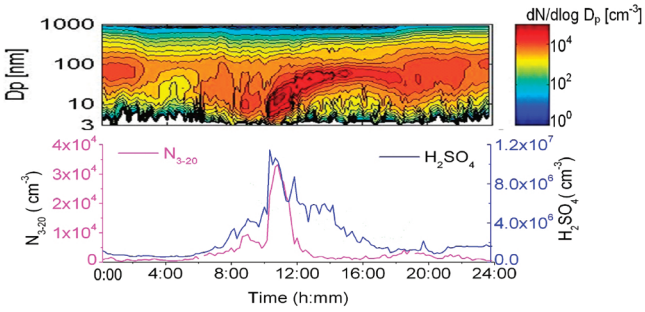

Figure 5. Particle number size distributions, particle number concentrations (3−20 nm), and sulfuric acid concentrations observed on Aug 12, 2008 (Local Time) in Beijing during the CAREBeijing-2008 campaign. A new particle formation event occurred between about 8 a.m. and noon. (Reprinted from ref 250. Copyright 2010)

gaseous sulfuric acid and their temporal profile is different from the typical "banana" shape characteristic of new particle formation events.[252] Because of the time required for clusters to grow to a detectable size, there is a lag between the maxima in the concentration profiles of sulfuric acid and nanoparticles. In clean environments this lag can be considerable, reaching 1−2 h.[253] A linear correlation between the average sulfuric acid concentration and the average new particle formation rate ($R^2 = 0.85$) indicates that sulfuric acid plays a dominant role in the nucleation events.[250] As demonstrated in a large number of investigations,[50] atmospheric new particle formation requires the presence of gas-phase sulfuric acid in concentrations in excess of 10^5 molecules cm^{-3}, indicating its central role in atmospheric aerosol nucleation. Gas-phase sulfuric acid in the atmosphere is produced via oxidation of sulfur dioxide[254,255] by the short-lived hydroxyl radical from ozone photolysis (eqs 2.17−2.20) and is rapidly lost to surfaces of pre-existing aerosols. Because of its short atmospheric lifetime (less than 1 min), H_2SO_4 concentration closely follows the diurnal solar cycle.[251] Since the surfaces of atmospheric aerosols correspond to the major sink for gas-phase sulfuric acid, an increase in atmospheric pollution does not always result in more frequent nucleation events because of sulfuric acid loss to particles. New particle formation is typically completely suppressed when the aerosol surface area exceeds 100 μm^2 cm^{-3}.[256]

There are significant differences in new particle formation among measurements conducted at various geographical locations, altitudes, and the overall degree and type of ambient pollution, suggesting that more than one atmospheric mechanisms may be responsible for aerosol nucleation. Typical formation rates of 3 nm particles measured in regional nucleation events in the boundary layer are in the range of 0.01−10 cm^{-3} s^{-1}, but much higher rates are often measured in urban areas (100 cm^{-3} s^{-1}), coastal zones (10^4−10^5 cm^{-3} s^{-1}), and SO_2-laden industrial plumes.[50] Particle growth rates vary from 0.1 nm h^{-1} in clean polar areas to 200 nm h^{-1} in coastal areas, with typical values between 1 and 20 nm h^{-1} for most locations. For most continental measurements, the data indicate two distinct types of nucleation, in the free troposphere in cloud outflows and near the ground level.[11] Measurements of gaseous sulfuric acid concentrations and new particle formation rates in the free troposphere are consistent with binary sulfuric acid−water nucleation. In the PBL, however, nucleation occurs at much lower sulfuric acid concentrations than predicted by the binary homogeneous nucleation theory because other gases, such as

ammonia, amines, or organic vapors, may also be involved in aerosol nucleation. In most locations, the measured growth rates of nucleated particles cannot usually be explained by condensation of sulfuric acid, water, and ammonia. Organic compounds with very low saturation vapor pressures or that are capable of reacting heterogeneously with nanoparticles to form low-volatility products are likely candidates for growth of nanoparticles,[257−259] as described in section 4.

The lowest part of the atmosphere, the PBL, is turbulent, and its composition is directly influenced by surface emission sources of anthropogenic and biogenic nucleation precursors. Nucleation events often start at the ground layer, i.e., near the source, and then evolve with the mixed layer.[258,260] Urban PBL is a significant source of sulfur dioxide, ammonia, and anthropogenic volatile organic compounds.[261,262] In remote areas, the canopy of boreal[258] and eucalyptus[259] forests produces enormous amounts of volatile organic compounds (e.g., monoterpenes),[263] whose photochemical oxidation products can contribute to both nucleation and growth of nanoparticles.[257,13,57,58,259,264] Although concentrations of nucleation mode particles above open oceans are generally low, massive bursts of new particles have been observed in coastal areas, with peak concentrations exceeding 10^6 particle cm^{-3}.[226] Coastal nucleation events are observed almost on a daily basis during the occurrence of low tide in the presence of sunlight, when the shore biota produce increased biogenic emissions due to dehydration and exposure to ultraviolet radiation.[265,266] Iodine oxides derived photochemically from these emissions are thought to be mainly responsible for the coastal nucleation.[267−269]

The free troposphere is much cleaner than PBL. Also, the free troposphere is usually nonturbulent or only intermittently turbulent, which further restricts mixing and transport of pollutants.[270] For this reason, observed new particle formation events in the free troposphere, tropopause, and lower stratosphere are often dynamically induced.[271,272] One of the dynamical processes that can trigger aerosol formation in the upper troposphere is the stratosphere−troposphere exchange.[273−275] Also, new particle formation in the free troposphere can occur in connection with convection and vertical motion,[276−278] which bring higher concentrations of water vapor and aerosol precursors from lower to higher altitudes, where nucleation is favored by low temperatures, enhanced photochemical production, and less aerosol surfaces ($\sim$10 μm^2 cm^{-3}).[279] The concentration of gas-phase sulfuric acid is moderately enhanced in cloud outflow regions, with typical values of 10^7 molecules cm^{-3}.[280] It has been suggested that deep convective systems may contribute to a substantial portion of the background aerosol in the upper troposphere at midlatitudes.[277] Recent aircraft studies have shown that despite low concentrations of nucleating vapors, new particle formation is quite active in the free troposphere over the continental United States even in the absence of folding events or convection, with average ultrafine particle concentrations exceeding 100 particle cm^{-3} in certain regions.[275] On the other hand, measurements over the Gulf of Bothnia in southern Finland show no evidence of nucleation mode particles in the free troposphere over the frozen sea.[260]

Most of the reported new particle formation events have been observed during the daytime, suggesting that the nucleating vapors have a photochemical origin. However, there is growing, albeit scattered, evidence of nighttime new particle formation. The first reported observations of nighttime nucleation events, near and in orographic clouds, were made in Northern England[281] and later in Germany.[282] These events are tentatively explained by ternary nucleation of unidentified gaseous substances outgassing from the evaporating particles at high relative humidity. Three-year measurements of aerosol size distributions from commercial aircraft show the presence of ultrafine particles at night in 20% of aerosol samples in the subtropical and midlatitude tropopause regions.[271] High concentrations of 4−9 nm ultrafine particles were measured in nighttime observations in the upper troposphere.[283] Continuous measurements of aerosol size distributions in Amazonia show the highest concentrations of nucleation mode aerosols during the nighttime. Nighttime new particle formation represents 5 out of 24 observed nucleation events at Appledore Island.[284] Nocturnal formation of clusters and nanoparticles is observed with a high frequency (30%) in a native Australian Eucalypt forest.[283,285] In some of these cases, nucleation may be driven by nighttime H_2SO_4[236,286] originated from nonphotochemically produced OH, such as in the dark reaction of ozone with alkenes.[66,287] However, other mechanisms for formation of nucleating precursors are possible. For instance, Mauldin et al.[288] measured significant nighttime concentrations of H_2SO_4, methanesulfonic acid, and ultrafine particles in the boundary layer over the Pacific in the absence of OH. Since nighttime nucleation contributes to global aerosols and CCN, future studies are required to understand the nighttime nucleation mechanisms and include them in global models.

3.1.2. Chemical Composition of Atmospheric Nanoparticles. Identification of the gaseous precursors responsible for nucleation and growth of atmospheric nanoparticles requires detailed analysis of the particle chemical compositions. Combined measurements of number concentrations, size distributions, and chemical compositions of nanoparticles represent a key approach to better understanding of the underlying mechanisms of new particle formation in the atmosphere. Because of the infinitesimally small mass of individual nanoparticles ($\sim 10^{-19}$ g for a 5 nm diameter particle), most of the early studies on aerosol chemical compositions were performed off-line using nanoparticles collected in cascade impactors or on filters to accumulate a sufficient sample mass for detailed chemical analysis by standard analytical techniques. Using the traditional methods, it has been shown that organic compounds, such as the organic acids from photochemical oxidation of terpenes[289] and alkylamines,[290] are important components in the ultrafine particles produced during nucleation events above forests. Also, since sulfuric acid is recognized as a key species in formation of nanoparticles in the atmosphere, measurements of sulfuric acid in the gas phase[253] and in aerosol particles[290] have been routinely carried out.

The off-line approaches have several drawbacks, including low temporal resolution and detection artifacts. The low temporal resolution of the off-line methods stems from the necessity to obtain sufficient material for identification and quantification of individual chemical components. Samples are collected for a period of hours to weeks, precluding the capture of real-time changes in the particle composition during nucleation events. Also, because the mass of a particle scales with the cube of its diameter, the retrieved compositions of the impactor and filter samples are dominated by larger particles, making it impossible to distinguish between the chemical species contributing to particle nucleation and subsequent growth. For example, using a cascade low-pressure impactor, Makela et al.[290] suggested that dimethylaminium ions are clearly present in the particle phase but cannot unravel at which stage the alkylamine is

involved, i.e., during nucleation or subsequent growth. Another deficiency of the off-line methods is sampling artifacts, including the gain or loss of species and possible chemical reactions during collection and analysis that can alter the sample composition. For instance, large mass concentrations of aldehydes measured in aerosol samples above boreal forest during nucleation events[258] are inconsistent with relatively high saturation vapor pressures of these compounds, which hinder their accumulation in nanoparticles.

Over the past decade, a large number of online and semionline approaches for chemical analysis of aerosols have been developed on the basis of mass spectrometry. In single-particle methods, aerosol is introduced into the high vacuum of the mass spectrometer through an aerodynamic lens inlet and particles are then evaporated and ionized with a laser beam[291−295] or by thermal heating and electron impact.[296] Because of the small mass of a single-aerosol particle and short interaction time, evaporation and ionization methods often result in significant molecular fragmentation, often down to atomic ions. Semionline methods, on the contrary, apply soft evaporation and ionization methods, because sufficient particle mass can be accumulated over a seconds-to-minutes-long sampling period. In these semionline methods, aerosol particles are deposited by aerodynamic impaction on a metal collector, which is then heated at a predetermined rate to evaporate the particle components according to their volatilities.[297−301] A major limitation for both types of instruments, however, is the use of the aerodynamic separation/collection of particles that limits the smallest detectable size to about 50 nm. Individual particles in this size range contain hundreds of thousands molecules, whereas the critical nucleus contains a few tens of molecules or less.

Recent advances in measurement technology have led to two novel instruments, the thermal desorption chemical ionization mass spectrometer (TDCIMS)[13,58,302−304] and the nano aerosol mass spectrometer (NAMS).[305,306] Both methods are capable of characterizing the chemical composition of nanoparticles as small as 4−7 nm in diameter. In the TDCIMS,[13,58,302−304] aerosol is drawn through a unipolar particle charger, size selected with a DMA, and collected by electrostatic deposition on a metal wire. After a sufficient particle mass is accumulated, the sample is evaporated and analyzed by an atmospheric pressure CIMS.[302−304] A slightly different version of this method, the thermal desorption-ion drift-chemical ionization mass spectrometer (TD-ID-CIMS), utilizes a drift tube operating at a 1−10 Torr pressure for chemical ionization.[58,307] These semidirect approaches utilize soft chemical ionization to obtain molecular composition of averaged nanoparticles in a 4−20 nm mobility size range. Deployment of TDCIMS in Atlanta during nucleation events provided the first direct in-situ measurements of the chemical composition of size-classified 6−15 nm atmospheric nanoparticles consisting mainly of ammonium sulfate.[308] Measurements in Tecamac, Mexico provided direct evidence for an important role of organic species in growth of nanoparticles.[309] Very recently, using the combined TDCIMS and ultrafine hygroscopicity TDMA techniques, it has been shown that aminium−carboxylate salts contribute significantly to nanoparticle mass.[60] As illustrated in Figure 6, alkylaminium ions (positive, Figure 6c) and carboxylate ions (negative, Figure 6d) are clearly evident in the mass spectra obtained for nanopaticles collected during new particle formation events in Hyytiälä, Finland (particle size distribution measured by a SMPS, Figure 6a).

In the NAMS method,[305,306] individual charged particles of a 7−30 nm mass normalized diameter are sampled through an inlet consisting of an aerodynamic lens and a quadrupole ion guide, captured, and focused into the center of a digital ion trap and then ablated with a high-energy laser pulse to reach the complete ionization limit. Positively charged atomic ions produced by laser ionization are analyzed by a time-of-flight mass spectrometer. Atomic compositions obtained by the NAMS help to constrain the molecular composition of nanoparticles. For instance, measurements of 21 nm mass normalized (18 nm mobility) diameter nanoparticles at a coastal site in Lewes, DE, showed only a small change in the particle composition during nucleation events compared with non-nucleation events. The N mole fraction increases 15% on nucleation events, whereas the C mole fraction decreases 25%, suggesting an enhanced inorganic component to aerosols during nucleation. The relatively small differences in the particle composition with and without the occurrence of nucleaion suggest that changes in the particle hygroscopicity and volatility observed in many studies during new particle formation events may be linked to subtle changes in the particle composition or characteristics of the organic content.[310]The NAMS and TDCIMS methods are complementary analytical techniques, as NAMS permits single-particle analysis and detects the elemental composition of both nonvolatile and semivolatile components, whereas TDCIMS yields molecular information, but only for semivolatile components in averaged nanoparticles samples.

The smallest nanoparticles that can be detected by current state-of-art mass spectrometry techniques contain several hundreds to several thousands molecules. On the contrary, commercially available aerosol sizing and counting instruments can detect 3 nm or even smaller particles, containing about 100 molecules. For this reason, particle size- and concentration-based aerosol measurements are widely used to indirectly infer the identities of particle chemical constituents and corroborate the findings of mass spectrometry studies. These indirect measurements include particle nucleation rates, growth rates, solubility, hygroscopicity, and volatility. For instance, measurements of nanoparticle growth rates indicate a clear annual cycle with the highest value in summer and the lowest in winter, showing a correlation between photochemistry and growth of nucleation mode particles, i.e., the contribution of organic vapors from biogenic sources.[311] An estimate of the composition of the critical nucleus can be performed according to the nucleation theorem (eq 2.14) from the logarithm of the slope of the measured nucleation rate versus the logarithm of the concentration of the nucleating vapor.[132,133,139] Field measurements have revealed a weak dependence of the nucleation rate on the concentration of gas-phase sulfuric acid, implying that only 1−2 H_2SO_4 molecules are present in the critical nucleus.[253,261] Using similar analysis, the involvement of organic vapors in atmospheric nucleation has been suggested to explain the variation in the nucleation rate prefactor between measurements at different sites,[264] although the exact identities of the organic species remain largely unidentified. On the basis of differing solubility of organic and inorganic nanoparticle constituents in *n*-butanol, which is the working fluid of the PHA CPC detector,[245] O'Dowd et al.[257] concluded that newly formed particles in Hyytiälä, Finland act similarly as organics (e.g., pinic or *cis*-pinonic acid) rather than electrolytes (e.g., sulfuric acid or ammonium sulfate).

The hygroscopicity of nanoparticles as measured by the tandem differential mobility analyzer (TDMA)[312] is often invoked to provide insight into the particle composition. In the

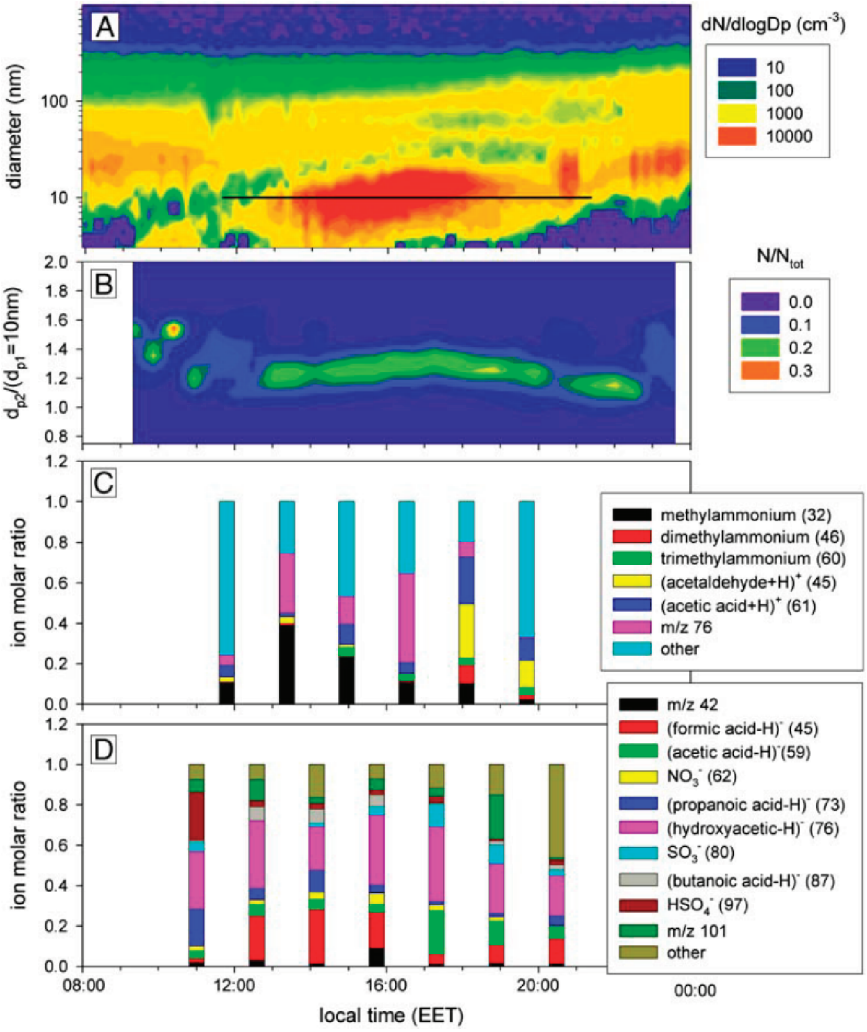

Figure 6. New particle formation in Hyytiälä, Finland, on Apr 9, 2007. (a) Particle size distributions; the black line marks the particle size analyzed by TDCIMS. (b) Hygroscopic growth factors obtained at 90% RH for 10 nm ambient particles. (c) Positive- and (d) negative-ion molecular compositions for the diameter indicated in a. Ion molar ratio is the average ion abundance divided by the total average ion abundance. (Reprinted with permission from ref 60. Copyright 2010 National Academy of Sciences.)

hygroscopicity—TDMA, ambient nanoparticles are dried, size selected by a nano-DMA, and then exposed to a 70—90% relative humidity. The change in the particle size caused by water uptake is detected by a second nano-DMA coupled with a CPC. Nanoparticles composed of sulfuric acid or ammonium sulfate increase in size significantly upon humidification, but those containing organic species grow only slightly or their size remains unchanged since most organics are hydrophobic or slightly hydrophilic. For instance, the hygroscopic growth factors of 10 nm nanoparticles measured during regional nucleation events in urban Atlanta in July and August 2002 were about 1.4, suggesting that particles are mostly composed of hygroscopic ammonium sulfate.[313] Another hygroscopicity-based technique utilizes four CPCs (two butanol and two water CPCs with different cutoff sizes) as a CPC battery.[314] Recent measurements of the water affinity of 2—9 nm nanoparticles with this CPC battery indicate that freshly nucleated particles are less hygroscopic than pure sulfuric acid or ammonium sulfate, implying that less hygroscopic compounds, presumably organics, are present even at the very early stage of particle growth.[315] Furthermore, the latter study indicates that the water affinity of particles decreases with increasing size, suggesting that the relative role of less hygroscopic organics in atmospheric particle growth becomes progressively more important for larger particles.[315] Another field study in Antarctica reveals that freshly nucleated particles have the smallest hygroscopic growth factors, which increase with particle aging, and organics are a significant component of newly formed particles.[230]

TDMA is often used with a thermal denuder in place of a humidifier to infer the chemical composition from volatility measurements of nanoparticles. For instance, 4—10 nm nanoparticles during nucleation events in Atlanta in July and August 2002 remained nonvolatile when heated to 100 °C, suggesting that sulfuric acid is transformed into less volatile ammonium sulfate and ammonium bisulfate salts.[313] By increasing the temperature of the thermal denuder to above 150 °C to evaporate more volatile components, such as sulfuric acid, ammonium bisulfate, and ammonium sulfate, volatility—TDMA can be used to identify the presence of nonvolatile organic components in nanoparticles.[60,313] In a field study in Melpitz, Germany, nonvolatile cores in 3—25 nm particles, presumably containing polymer-type organics, after heating the samples to 300 °C were suggested to

dx.doi.org/10.1021/cr2001756 |*Chem. Rev.* 2012, 112, 1957–2011

account for 20−40% of the measured nanoparticle growth.[225] Another volatility measurement of 5−60 nm particles heated to 280 °C showed the presence of nonvolatile cores in all particles in the rural atmosphere in Hyytiälä, Finland.[316] The relative ratio between the growth rate of ambient particles and their nonvolatile cores indicates that the nonvolatile mass is formed gradually in growing particles,[316] consistent with the results from hygroscopicity measurements.[315]

A combined volatility−hygroscopicity−TDMA has been utilized for simultaneous measurements of both volatility and hygroscopicity of 17−22.5 nm freshly nucleated nanoparticles in the east coast of Australia.[317] For the majority of particles, the composition is attributed to the internal mixture of sulfate and organic components, which originate from condensation of gas-phase sulfuric acid and low-volatility organics from marine/coastal precursors. Simultaneous measurements of volatile and hygroscopic properties of newly formed 20 nm particles in a eucalypt forest in south Australia also show that the particles are composed of sulfates and organics.[259] The amount of sulfate strongly depends on the availability of gas-phase sulfuric acid and typically represents a small fraction (6% or less). Also, the sulfate component is identified not as sulfuric acid but as a more neutralized form, i.e., either ammonium sulfate or bisulfate. The organic components have the same volatility and hygroscopicity as photo-oxidation products of monoterpenes, such as α-pinene.

Whereas water-based hygroscopicity−TDMA allows one to quantify water-soluble components, organic−TDMA utilizes subsaturated ethanol vapor to detect the presence of organics in nucleation mode particles.[318] In Hyytiälä, Finland, organic−TDMA measurements were used to corroborate chemical analysis of particle compositions by an Aerodyne aerosol mass spectrometer (AMS), low-pressure impactors, and a high-volume sampler. The growth factors of newly produced 10 and 50 nm particles upon uptake of ethanol vapor in organic−TDMA correlate strongly with the gas-phase concentration of monoterpene oxidation products, indicating that the organic constituents in particles smaller than 50 nm in diameter are at least partly similar to those in larger particles.[258,319] It is concluded that organic products from oxidation of biogenic emissions play a key role in determining the spatial and temporal features of the nucleation events.

3.1.3. Measurements of Charged and Neutral Atmospheric Clusters. Resolving the initial stages of new particle formation requires instruments capable of detecting atmospheric clusters as small as 1−2 nm. Although measurements of particles larger than about 3 nm have been conducted for about two decades, detection of smaller particles has become possible only recently. The largest obstacle to detection of small clusters by CPCs is the necessity to use the highly supersaturated vapor of a working fluid that results in the onset of homogeneous nucleation even in the absence of particles. A recent advance made by Winkler et al.[320,321] has overcome the barrier of homogeneous nucleation using an expansion-type CPC. Under appropriate conditions, the transition from heterogeneous to homogeneous nucleation is identified so that particles with diameters as small as 1.4 nm can be activated before the onset of homogeneous nucleation. A different approach is taken by Sipila et al.,[322,323] who achieved sub-2 nm detection using a pulse height analysis CPC to distinguish between particles formed by homogeneous nucleation of *n*-butanol vapor and those formed by heterogeneous nucleation on clusters. Alternatively, to achieve a high saturation ratio while avoiding homogeneous nucleation, working fluids that have a low vapor pressure and a high surface tension at room temperature are used. For instance, Iida et al.[324] utilize diethylene glycol (DEG) and oleic acid in the CPC to suppress homogeneous nucleation while activating sub-2 nm particles. Because the vapor pressures of DEG and oleic acid are much lower that that of *n*-butanol, particles grow to smaller sizes that are difficult to detect optically, and hence, a second conventional CPC is used as a "booster" to grow particles to an optically detectable size. Furthermore, the DEG CPC has been implemented into a new scanning mobility particle spectrometer for measuring number size distributions down to ~1 nm mobility diameter,[325] and the applicability of the new DEG SMPS for atmospheric measurements has been demonstrated during the Nucleation and Cloud Condensation Nuclei (NCCN) field campaign in Atlanta, GA, during summer 2009. Vanhanen et al.[326] report the development, calibration, and application of a continuous flow particle size magnifier (PSM) for detection of atmospheric clusters as small as ~1 nm. The PSM is based on previous designs introduced by Okuyama et al.[327] and Sgro and Fernández de la Mora[328] for laboratory measurements of small clusters in the sub-3 nm size range. The PSM operates using turbulent mixing of a cool air stream containing clusters with a heated clean-filtered air stream saturated with vapor of the working fluid to achieve a high saturation ratio. Similarly to the DEG CPC, clusters activated and grown by the PSM are too small to be detected directly. Thus, an external CPC is used to count activated clusters after their growth to an optically detectable size.

Atmospheric particles can also be produced through a nucleation process involving ions.[329] Because of the presence of a charge, molecular clusters that form around ions are more stable compared to the corresponding neutral clusters and ions can trigger nucleation under conditions when neutral nucleation does not occur. The concentration of atmospheric ions is controlled by the competition between production from galactic cosmic rays and radioactive decay and loss by ion−ion recombination and collisions with existing particles. The higher ion formation rates and the lower aerosol surface areas in the upper atmosphere suggest a preferential importance of ion-induced nucleation in the upper regions. A few instances of ion-induced nucleation have been inferred from field measurements in the upper atmosphere.[330]

Charged clusters can be detected by measuring the electrical current that arises when clusters arrive and discharge at specially designed electrodes. Using this approach, Tammet[331] and Mirme et al.[332] developed air ion mobility spectrometers to detect ambient charged clusters and particles down to about 0.4 nm, which is the size of molecular ions. In these instruments, ions are classified according to electrical mobility and detected simultaneously with an array of electrometers with a sensitivity corresponding to a minimum ion concentration of about 50 cm^{-3}. Two instruments of this type are currently available, the balanced scanning mobility analyzer (BSMA)[331] and the air ion spectrometer (AIS),[332] allowing detection of ions with mobility distributions corresponding to the size ranges of 0.4−7.5 nm and 0.4−55 nm, respectively. Also, on the basis of the AIS technique, a neutral cluster and air ion spectrometer (NAIS) has been developed for measurements of neutral clusters, down to 1.2−1.5 nm size.[333]

One of the most significant findings revealed by these new instruments is that charged and neutral sub-2 nm clusters appear

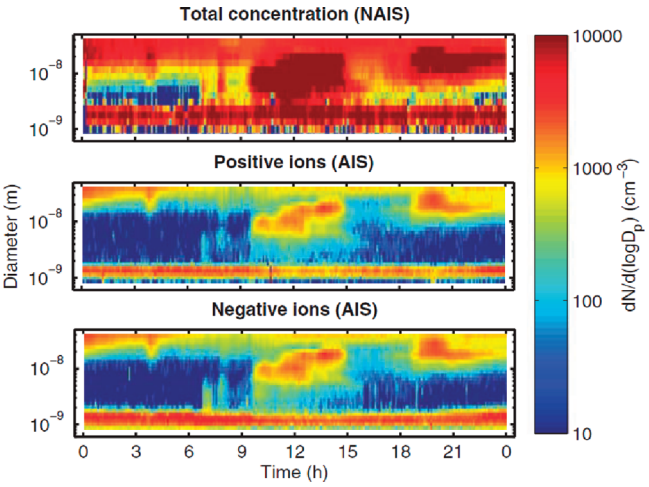

Figure 7. Evolution of particle number size distribution measured with the NAIS on a particle formation event day (Apr 23, 2006) in Hyytiälä, Finland. (Reprinted with permission from ref 333. Copyright 2007 American Association for the Advancement of Science.)

to be always present in ambient air, both during days with aerosol nucleation and also on days when new particle formation is not observed.[334] On the basis of simultaneous NAIS and AIS/BSMA measurements, neutral clusters are found to be present in substantially higher concentrations than ion clusters with a typical concentration ratio in the range of 10−100 (Figure 7).[333] Several studies[322,325,333,335] have demonstrated that atmospheric nucleation in the continental boundary layer is initiated at sizes of 1.5−2.0 nm and correlated strongly with the presence of small neutral clusters, in agreement with the earlier suggestion of Kulmala et al.[336] that thermodynamically stable clusters act as a source of new atmospheric particles. It is interesting to note that during cluster measurements in Atlanta by the DEG CPC tuned for efficient detection of sodium chloride particles but not of air ions of the same mobility, particles as small as 1 nm were detected only during nucleation events but not at other times.[325] The correlation between the concentration of gas-phase sulfuric acid and the formation rate of both charged and neutral clusters in a boreal forest indicates a short time delay on the order of 10 min between the two parameters.[12] Similarly to the previous studies, atmospheric nucleation is found to start from sizes close to 2 nm and the events are clearly associated with higher sulfuric acid concentrations and a lower condensation sink (a smaller surface of pre-existing aerosols) than on the nonevent days. Furthermore, airborne measurements provide clear evidence for the existence of neutral clusters not only in the boundary layer but also in the entire atmospheric column up to the tropopause.[337] Manninen et al.[338] provide a detailed report of continuous measurements of atmospheric clusters and nanoparticles in the size range ∼1−42 nm that were conducted within the EUCAARI project in a wide variety of environments, including coastal and continental locations as well as different altitudes, from the boundary layer to the free troposphere.

A number of studies of new particle formation in the lower atmosphere,[333,339,340] including measurements of the ion mobility[341] and overcharging ratios[342] for freshly nucleated particles, conclude that although ions are involved in most of the identified particle formation events, the ion-mediated fraction is small compared to the neutral pathways. For instance, Manninen et al.,[343] extending the analysis approach of Kulmala et al.[333] to a comprehensive set of ambient nucleation data in a boreal forest, estimated that ion-mediated nucleation contributes about 10% to new particle formation. In contrast, Yu and Turco,[61] applying a different analysis methodology to the same data as Manninen et al.,[343] suggested that most of the neutral particles detected at sizes around 2 nm are initially formed on smaller ionic cores, which are neutralized before the particles have a chance to grow to the 2 nm size. Overall, the subject of relative contributions of ion and neutral nucleation pathways remains controversial,[61,344−346] and a significant role of ion-induced nucleation in the middle and upper atmosphere cannot be ruled out presently.

Although the instruments described above can detect the presence and measure the size of small clusters, their resolution is insufficient to draw conclusions about the cluster chemical composition. Junninen et al.[347] recently developed an atmospheric pressure interface-time-of-flight (APi-TOF) mass spectrometer to study the chemical makeup of naturally occurring ambient ions in the mass-to-charge range up to 2000 Th. The APi-TOF features sufficiently high accuracy, mass resolution, and sensitivity for determination of compositions of small ions present in total concentrations of 400−2000 cm^{-3}. Atmospheric ions are identified based on their exact masses, utilizing a combination of Kendrick analysis and correlograms with additional information, such as proton affinities and isotopic patterns of the potential candidates. The instrument has been successfully evaluated in the laboratory using nebulized sulfuric acid−ammonia clusters[347] and deployed in measurements of charged clusters present in ambient air.[347−349] At an urban site in Helsinki[347] and a boreal forest site in Hyytiälä,[348] negative ions are dominated by strong organic and inorganic acids (e.g., malonic, nitric, and sulfuric acid), whereas positive ions consist of strong bases (e.g., alkyl pyridines and quinolines). Bisulfate and its clusters, including the $H_2SO_4 \cdot HSO_4^-$ dimer and the $(H_2SO_4)_2 \cdot HSO_4^-$ trimer, are the most abundant negative ions. During the strongest nucleation events, the H_2SO_4 tetramer and a tetramer cluster with ammonia are also detected. The performance of APi-TOF has been compared against that of AIS and BSMA mobility spectrometers and good agreement was observed, especially for sizes above 200 Da.[349] The mass and mobility spectrometers complement each other, with the APi-TOF providing chemical information limited to relatively small ions (<2.5 nm diameter), whereas the mobility spectrometers are better suited for quantitative number concentration measurements up to 40 nm. Furthermore, the BSMA and AIS methods are used to infer a transmission function for the APi-TOF, making it possible to obtain quantitative estimates of the concentrations of chemically identified ions.[349]

Recently, Zhao et al.[350] used a sensitive atmospheric pressure CIMS with two alternative charged/neutral cluster separation methods to measure low concentrations of neutral clusters formed during nucleation events, extending the instrumentation for measuring sulfuric acid in the atmosphere[236] and sulfate clusters in the laboratory[351−353] (see section 3.2.7). The instrument, Cluster−CIMS, has been calibrated using an electrospray high-resolution DMA technique and deployed in the field. At moderately polluted urban and relatively remote forested sites in Colorado, neutral sulfuric acid clusters containing up to four sulfuric acid molecules were detected with concentrations reaching 10^4 cm^{-3} during relatively strong nucleation events.[350] For a given concentration of gas-phase sulfuric acid, the forested site

shows significantly more efficient production of sulfate clusters than the urban site. During subsequent measurements in Atlanta, GA, the trend in concentrations of sulfate clusters detected by the Cluster−CIMS was compared against measurements of clusters by a DEG SMPS.[354] Both cluster instruments agree with each other and also with conventional aerosol mobility spectrometers operating in the 3−10 nm size range. Since the total concentration of small clusters measured by the Cluster−CIMS during nucleation events exceeds those of sulfuric acid trimers and tetramers by an order of magnitude, it is not obvious why the Cluster−CIMS data including only sulfate clusters agree so well with the DEG SMPS measurements. It is suggested that only clusters experiencing condensational growth in the atmosphere undergo condensational growth in the DEG CPC, because the activation efficiencies of clusters in the DEG CPC depend on their composition.[354] On the contrary, the electrometers used in instruments such as the NAIS detect all clusters and molecular ions, even those that do not result in new particle formation, and hence may overestimate the concentration of nucleating clusters.

3.2. Laboratory Studies

3.2.1. Binary Nucleation of H_2SO_4−H_2O. Sulfuric acid−water vapor nucleation was first proposed in the theoretical study of Doyle,[216] who pointed out that the phase change in this system may occur in the presence of about 1 part per trillion (ppt) level H_2SO_4 even at low relative humidity (RH). Although later studies showed a somewhat higher nucleation threshold, about 0.1−1 part per billion (ppb),[355−357] the notion that sulfuric acid represents the most prominent atmospheric nucleation agent remains valid. Early experiments of the binary sulfuric acid−water nucleation were carried out using expansion chambers,[358,359] a thermal diffusion chamber,[360] and turbulent mixing chambers.[180,361] A qualitative agreement of the experimental results from the diffusion and adiabatic expansion chambers with those from mixing chamber is notable because the former results were obtained in supersaturated water vapor whereas the relative humidity in the latter work was kept below 40%. A common feature of the early experiments is that gaseous sulfuric acid is introduced from evaporation of liquid solutions, and its concentration in the nucleation zone is calculated using thermodynamic data and various assumptions rather than that being measured experimentally. Also, nucleated particles in the mixing chamber experiments are required to grow by condensation of sulfuric acid to a size of larger than 20−30 nm before they can be detected, possibly leading to considerable underestimation of the nucleation rate because of undercounting of smaller particles. However, the problem of undercounting is minimal for the expansion and diffusion chamber experiments, since nucleated particles grow quickly to detectable droplets by condensation of water in highly supersaturated water vapor. The nucleation threshold ($J \approx 1$ cm^{-3} s^{-1}) obtained in experiments conducted in the 10−30 °C temperature range and using subsaturated water vapor corresponds to 10^{10}−10^{11} molecules cm^{-3} H_2SO_4, in agreement with predictions by the binary homogeneous nucleation theory.[180,357]

The study of Ball et al.[181] represents the first laboratory investigation of binary nucleation with an experimentally determined concentration of gaseous sulfuric acid. Sulfuric acid vapor was introduced into the nucleation flow chamber in a flow of carrier gas that passed above a liquid H_2SO_4 sample. The concentration of sulfuric acid vapor was measured by a CIMS downstream the nucleation zone and corrected to account for losses between the nucleation zone and the mass spectrometer.

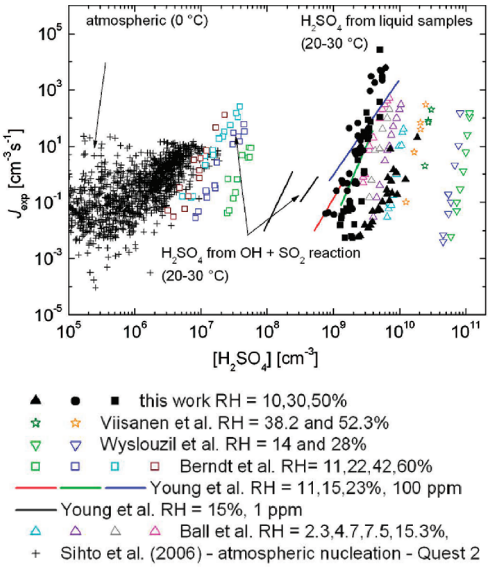

Figure 8. Comparison of homogeneous nucleation rates as a function of sulfuric acid concentration from different research groups against atmospheric nucleation data obtained during the Quest 2 campaign in Hyytiälä, Finland. References in the legend: this work,[182] Viisanen et al.,[180] Wyslouzil et al.,[361] Berndt et al.,[365] Young et al.,[184] Ball et al.,[181] and Sihto et al.[364] (Reprinted with permission from ref 182. Copyright 2010.)

An ultrafine particle condensation nucleus counter with a detection limit extended to about 3 nm was utilized to measure the concentration of freshly nucleated particles. The measured nucleation threshold at 295 K corresponds to 6×10^{10} molecules cm^{-3} H_2SO_4 in the nucleation zone at a 15% relative humidity. The critical nucleus composition derived from the slope of the nucleation rate dependencies corresponds to ∼8 molecules of H_2SO_4 and 5 molecules of H_2O. Several later laboratory studies, using sulfuric acid vapor from a liquid reservoir, measured a comparable threshold H_2SO_4 concentration for binary nucleation, corresponding to 10^9−10^{10} molecules cm^{-3} to achieve an observable nucleation rate.[57,58,182] As shown in Figure 8, the nucleation rate obtained in these measurements exhibits a similar steep dependence on the gaseous sulfuric acid concentration, in agreement with predictions by classical binary nucleation theory[357,362] but in contrast with a much weaker dependence measured for new particle formation in the atmosphere.[363,364]

Considerably different and variable results are obtained in the laboratory studies by Berndt et al.[185,186,365] using gaseous sulfuric acid generated in several ways, including evaporation of liquid samples and reaction of SO_2 with chemically and photochemically produced hydroxyl radical (see section 2.2.5). Substantial differences exist between the results obtained with the sources of H_2SO_4 from in-situ production in the chemical reactions and a liquid reservoir.[186] With H_2SO_4 from the liquid source, the nucleation rates generally agree with those from previous experimental studies. However, for H_2SO_4 produced chemically or photochemically from oxidation of SO_2, the nucleation threshold occurs at concentrations as low as 10^7 molecules cm^{-3}, closer to the H_2SO_4 concentration typically measured in the atmosphere during nucleation events. Similar measurements are reported in the work of Benson et al.[366] and Young et al.,[184] but the threshold H_2SO_4 vapor concentrations are at least 1 order of magnitude

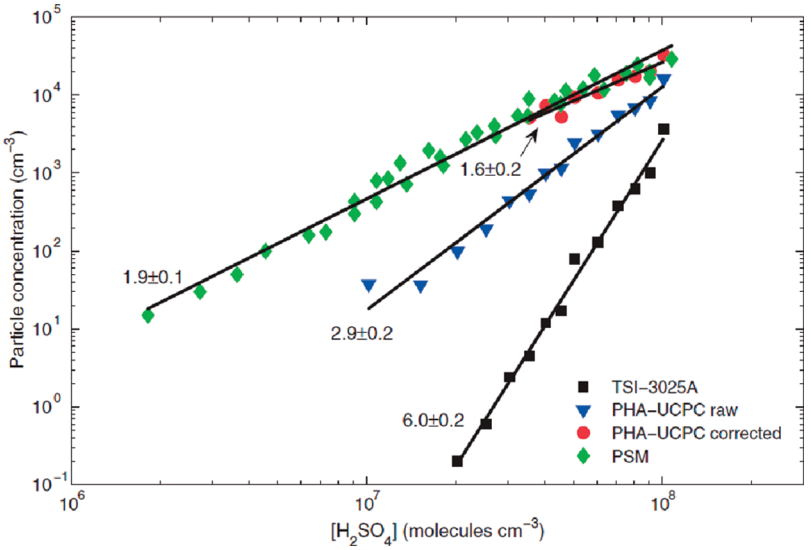

Figure 9. Comparison of TSI-3025A, PHA-UCPC, and PSM data. In the case of PHA-UCPC, both raw data—in which the diameter dependency of the counting efficiency is neglected—and the final, corrected data are shown. With a particle size approaching 3 nm, the different series merge. Slopes of the fittings are given in the figure. The experiment was performed in the IfT-LFT with a 115 s residence time using in-situ-produced H_2SO_4. The match of the PSM data and the corrected PHA-UCPC data suggests that PSM has a close-to-unity detection efficiency for the particle size range of 1.5−3 nm. (Reprinted with permission from ref 59. Copyright 2010 American Association for the Advancement of Science.)

higher than those measured by Berndt et al.[185,186,365] The chemical compositions of the critical nucleus derived from experiments with in-situ H_2SO_4 production are comparable between the two groups (3−5[186] and 3−8[184] H_2SO_4 molecules) and only slightly lower than those obtained in the previous studies using sulfuric acid from liquid samples.

The differences among the various previous studies may be attributable to the differences in the experimental details of the measurements. In the experiments conducted by Berndt et al.,[185,186,365] the concentration of H_2SO_4 was not directly measured but instead calculated from the concentrations of SO_2 and OH in the nucleation reactor. The concentration of OH was also estimated from the titration reactions in the presence of several organic compounds or carbon monoxide. When using such chemical reaction sources as ozonolysis of alkenes and ozone photolysis, hydroxyl radical is produced throughout the whole length of the nucleation chamber, providing continuous generation of sulfuric acid for nucleation and growth. On the contrary, the experiments by Benson et al.[366] and Young et al.[184] produced sulfuric acid photochemically in the mixing region only and measured its concentration by CIMS. Sulfuric acid vapor then passed to the nucleation/growth region of the flow chamber, where its concentration quickly decreased because of wall loss.

Even in the presence of continuous H_2SO_4 production, the derived low steady-state concentrations of sulfuric acid in the experiments of Berndt et al.[365] cannot explain the measured particle growth rates solely by H_2SO_4 condensation, indicating possible contaminants or alternative growth mechanisms. Since the contribution from organic oxidation products, e.g., carboxylic acids,[57] was ruled out by conducting experiments with carbon monoxide as a tracer instead of organic compounds,[365] unorthodox SO_2 oxidation products were invoked to account for the fast nucleation and growth rates.[367,368] Alternatively, the presence of an additional source of gaseous H_2SO_4 from photoexcitation of SO_2 by ultraviolet light[369] or an underestimated concentration of H_2SO_4 in the nucleation zone[370,371] has been proposed to explain the discrepancies in the study by Berndt et al.

In recent laboratory studies by Kulmala and co-workers, rapid binary nucleation was detected at atmospherically relevant concentrations of sulfuric acid and with a slope of the nucleation rate ranging from 1 to 2, indicating a critical nucleus that consists of one or two sulfuric acid molecules.[59,372,373] This work also revealed that the results from the binary nucleation experiments are independent of the source of gaseous sulfuric acid. The difference between these results and previous laboratory measurements has been explained by the use of more sensitive particle detectors, including a PSM and a PHA-UCPC, which extend over the previous detection limit of 3 nm and allow counting particles as small as 1.5 nm (Figure 9).[59] An insufficient growth and lower counting efficiency are suggested to cause most of the discrepancies with the earlier laboratory studies. The disagreement between experiments performed using H_2SO_4 produced chemically in situ and from a liquid sample is explained from the different H_2SO_4 concentration profiles along the nucleation chamber. In the experiments using in-situ H_2SO_4 production, particles have sufficient time to grow to detectable sizes because of a nearly constant H_2SO_4 concentration. In contrast, for the case of a liquid sample as a point source, the H_2SO_4 concentration decreases rapidly with time and growth of particles is limited. Hence, Sipila et al.[59] provide an explanation for the apparent disagreement in the nucleation rates measured using the H_2SO_4 sources from in-situ production and a liquid sample and conclude that sulfuric acid alone can explain atmospheric nucleation rates in most locations without participation of ammonia or organic substances.

It should be pointed out that in the previous studies using higher concentrations of sulfuric acid the measured nucleation rate may be insensitive to the cutoff size of the particle detector, since the growth rates of freshly nucleated particles are significantly faster at higher H_2SO_4 concentrations. Furthermore, under high H_2SO_4 concentrations, trace levels of base contaminants (e.g., ammonia

and amines) may be efficiently removed by heterogeneous nucleation on the chamber surfaces and their concentrations in the nucleation region can be negligible, which is in contrast to the case for the experiments with continuous H_2SO_4 generation. In fact, two mechanisms may be in effect in previous studies that utilize H_2SO_4 from a liquid source. Nanoparticles produced at high initial H_2SO_4 concentration during the nucleation pulse can be formed through a binary mechanism, whereas sub-3 nm nanoparticles produced at the end of the nucleation zone at much lower H_2SO_4 concentration may nucleate through a ternary mechanism involving trace contaminants. To address this question, further advancement in analytical instrumentation for chemical analysis of nanoparticles, neutral molecular clusters, and nucleating precursors is required (see section 3.2.7).

The finding by Sipila et al.[59] raises an important question on whether one or two sulfuric acid molecules are sufficient to form a critical nucleus at the temperatures and concentrations of sulfuric acid corresponding to the lower troposphere from a thermodynamics viewpoint.[1] Laboratory experiments and analysis of field measurements[374,375] suggest that this may be plausible but only if other stabilizing species are involved in nucleation and are present in the critical nucleus. For instance, organic compounds from anthropogenic and biogenic sources may assist the nucleation process either directly, e.g., by amines,[372,376] or following atmospheric photo-oxidation, such as by organic acids from aromatics[57] and monoterpenes.[58] As to be discussed in the following sections, the presence of 10^8-10^{10} molecules cm^{-3} levels of amines or organic acids considerably enhances nucleation in the water−sulfuric acid system via formation of strongly hydrogen-bonded clusters between the organic molecules and sulfuric acid.[58,377,378]

3.2.2. Ternary Nucleation of $H_2SO_4-H_2O$ Involving Ammonia and Amines. Ammonia is a ubiquitous atmospheric gas with a typical mixing ratio between 0.1 and 10 ppb over the continental lower atmosphere,[82] and its interaction with sulfuric acid significantly lowers the partial pressure of H_2SO_4 through formation of ammonium sulfate and bisulfate salts.[10] Theoretical studies demonstrate that the presence of ammonia at ppt level mixing ratios enhances the nucleation rate in the sulfuric acid−water system by stabilizing the critical nucleus.[379,380] One of the first laboratory accounts of the role of ammonia in the $H_2SO_4-H_2O$ nucleation was reported by Kim et al.[381] in a study of new particle formation in the $NH_3/SO_2/H_2O$/air mixtures exposed to α-irradiation. Although no direct measurements of H_2SO_4 and NH_3 concentrations were performed and part per million (ppm) mixing ratios of the reactants were merely estimated, this early study produced two important observations. First, the measured particle number concentrations remain constant when NH_3 mixing ratios are varied between 0.7 and 4 ppm, in agreement with the ternary nucleation theory that for a NH_3 level higher than 100 pptv the enhancement effect diminishes.[382] Second, the enhancement in new particle formation upon addition of NH_3 depends on the H_2O concentration, decreasing from 9 to 50 at a low H_2O mixing ratio (50 ppm) to from 2 to 4 at H_2O mixing ratios exceeding 1000 ppm. This is in noticeable disagreement with the theoretical calculations, which predict that the nucleation rate in the ternary system is humidity independent.[383]

Ball et al.[181] confirmed the earlier findings in experiments conducted under well-controlled conditions using significantly lower, 80−170 parts per trillion, concentrations of ammonia. Addition of NH_3 increases the nucleation rate by a factor of 10−1000 with a larger value corresponding to a higher concentration of ammonia and a lower relative humidity. Although the concentration of ammonia was estimated indirectly from the dilution ratios of NH_3 added to the nucleation flow chamber, the concentration of sulfuric acid ($10^{10}-10^{11}$ molecules cm^{-3}) was measured directly by CIMS, allowing application of the nucleation theorem to the concentration dependence of the nucleation rate. The presence of NH_3 decreases the number of H_2SO_4 molecules in the critical nucleus, from 8 to 5 and from 12 to 8 at 15% and 5% relative humidities, respectively. In a more recent study, Benson et al.[384] employed two CIMS to simultaneously measure H_2SO_4 and NH_3 with the initial concentrations in the range of 10^8-10^9 molecules cm^{-3} and 10−50 ppb ($\sim 2 \times 10^{11}-1 \times 10^{12}$ molecules cm^{-3}), respectively. From the dependence of the nucleation rate on the ammonia concentration, the number of NH_3 molecules in the critical nucleus is estimated to be less than 2. In the relative humidity range of 4−42%, the numbers of H_2SO_4 (9−10) and H_2O molecules (6−15) in the critical nucleus are reduced in the presence of NH_3 to 6−8 and 4−10, respectively (Figure 10). The enhancement factor exponentially increases with decreasing relative humidity and decreasing concentration of sulfuric acid, reaching a maximum value of 1000. In a subsequent study using a redesigned nucleation reactor, Benson et al.[385] observed a comparable nucleation threshold as in their previous study at significantly lower concentrations of sulfuric acid and ammonia, i.e., 10^6-10^7 molecules cm^{-3} and 0.08−20 ppb ($\sim 2 \times 10^9-5 \times 10^{11}$ molecules cm^{-3}), respectively, and the authors concluded fewer molecules of H_2SO_4 (3−5), H_2O (1−4), and NH_3 (1) in the critical nucleus.

Recently, Berndt et al.[372] have shown that addition of from 1.2×10^{11} to 1.2×10^{12} molecules cm^{-3} of NH_3, as measured by a commercial gas analyzer with a detection limit of 2.5×10^9 molecules cm^{-3}, promotes both the nucleation rate and the particle growth rate. The faster growth may be explained by a reduced evaporation of sulfuric acid from nanoparticles caused by stabilizing ammonia, because neutralization of sulfuric acid nanoparticles by ammonia alone does not lead to an observable growth.[58] Similarly as in the previous studies, the enhancement by NH_3 on the nucleation rate is more pronounced for dry conditions, by 1−2 orders of magnitude at 13% relative humidity but a factor of 2−5 at 47% relative humidity (1.2×10^{12} molecules cm^{-3} NH_3). However, these measurements show little change of the slope, i.e., $\Delta \log(J)/\Delta \log([H_2SO_4])$ in the presence of NH_3, in contrast to previous studies[181,384] indicating a significant decrease in the slope. It is suggested[372] that the insufficient counting efficiency of the commercial counters may affect the slopes derived in the studies by Ball et al.[181] and Benson et al.[384]

Although in the laboratory experiments nucleation in the presence of ammonia is enhanced by orders of magnitude relative to that in the binary system, the slope of the experimental nucleation rate with respect to sulfuric acid remains significantly higher than the value of 2 inferred from atmospheric measurements.[253,363] Furthermore, for comparable nucleation rates measured in the atmosphere and in laboratory, the concentration of sulfuric acid used in most laboratory experiments is higher than that in the atmosphere. Hence, either nucleation rates at much lower atmospheric H_2SO_4 concentrations are affected differently by the presence of ammonia or chemical species other than ammonia may be involved in the atmospheric nucleation process.

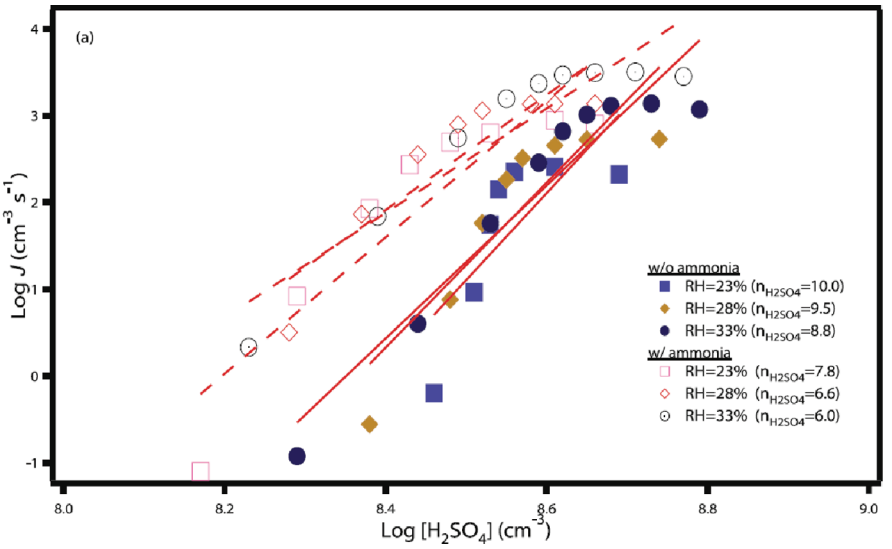

Figure 10. Measured nucleation rates for $H_2SO_4-H_2O-NH_3$ ternary homogeneous nucleation at 288 K as a function of the initial H_2SO_4 concentration. Initial $[NH_3]$ = 20 ppbv (4.6×10^{10} cm^{-3}) for the experiments in the presence of ammonia; measured nucleation rates for the $H_2SO_4-H_2O$ system are also included for comparison. Background $[NH_3]$ < 0.1 ppbv in the nucleation reactor. Solid lines are fits to the experimental data. (Reprinted with permission from ref 384. Copyright 2009 American Geophysical Union.)

Significant levels of dimethylamine measured in nanoparticles during atmospheric nucleation events[60,290,309] suggest that alkyl amines may contribute to aerosol nucleation and growth. Amines, organic derivatives of ammonia, are emitted by a range of natural and anthropogenic sources.[386] Typically present in the atmosphere at a much lower level than ammonia, amines are stronger bases and are expected to form more stable complexes and salts with sulfuric acid and/or organic acids.[378,387,388] Berndt et al.[372] reported a stronger enhancing effect on aerosol nucleation and growth in the presence of *tert*-butylamine than in the presence of ammonia. Their measurements at a 13% relative humidity with an estimated addition of about 10^{10} molecules cm^{-3} *tert*-butylamine show an enhancement in the particle concentration by about 2 orders of magnitude whereas extrapolation of the NH_3 data down to about 10^{10} molecules cm^{-3} suggests only a small or negligible effect. The enhancement of amine on the nucleation rate decreases with an increasing amine concentration but levels off for higher amine concentrations. This behavior is opposite to the observation for ammonia in the same study, which exhibits a linear enhancement with the ammonia concentration. Because of the strong enhancing effect of amines, measurements without amine addition can be influenced by a trace amine background below 10^9 molecules cm^{-3}, which corresponds to the detection limit of the gas-phase measurements in those experiments. Erupe et al.[376] also detected a significant enhancement of the nucleation rate in the presence of 180−1350 ppt (from 4.5×10^9 to 3.4×10^{10} molecules cm^{-3}) trimethylamine, measured by the CIMS. The number of H_2SO_4 molecules in the critical nucleus is estimated to be 4−6 without the amine and 4−5 in the presence of amine, depending on the relative humidity. Only one molecule of amine appears to be present in the critical nucleus, similarly to NH_3 addition. Both studies[372,376] conclude that amines are likely candidates in explaining the discrepancies between binary nucleation theory, laboratory studies, and atmospheric measurements. Considering the atmospheric amine concentrations in the range of 10^8-10^9 molecules cm^{-3} and higher close to the local sources,[386] it is expected that amines may play an important role in atmospheric nucleation of sulfuric acid and water vapors.

3.2.3. Nucleation of $H_2SO_4-H_2O$ Assisted by Organic Acids. Atmospheric measurements reveal that aerosols often contain a considerable amount of organic matter.[389] A large fraction of low-volatility organics in aerosols originates from photo-oxidation of volatile organic compounds, emitted in significant quantities into the atmosphere from anthropogenic and biogenic sources. To assess the role of organic acids in new particle formation, Zhang and coauthors investigated nucleation of several aromatic acids[57] and *cis*-pinonic acid[58] with H_2SO_4 and water vapors in a flow chamber. A marked increase in the particle concentration occurs when benzoic, *p*-toluic, *m*-toluic, or *cis*-pinonic acid vapor is added to the $H_2SO_4-H_2O$ binary system. As shown in Figure 11a, with H_2SO_4 concentrations of about 3×10^9 molecules cm^{-3} and at a relative humidity of 20%, the presence of 4.9×10^9 to 7.2×10^9 molecules cm^{-3} *cis*-pinonic acid (CPA) increases the particle concentration by a factor from 3 to 7, respectively. The measured peak diameter of the particle distribution shifts slightly to a larger size with addition of organic acids, likely implying that the presence of organic acids enhances both nucleation and growth of newly nucleated particles. However, as discussed later in this section, diffferentiating the contributions of organics to nucleation and growth from the changes in size distributions in the absence of chemical analysis may be misleading. Figure 11b shows that the nucleation rate determined from measured particle concentrations and nucleation time increases by about an order of magnitude relative to the binary system. At lower relative humidities, addition of organic acids consistently leads to a larger enhancement of the nucleation rate. The nucleation rate also increases with increasing H_2SO_4 concentration for a constant concentration of the organic acid (Figure 11c).

The partial pressures of organic acids in those experiments are several orders of magnitude smaller than their corresponding saturation vapor pressures, and hence, the saturation ratio, *S*, is much smaller than unity. A high nucleation rate is also measured in the absence of added water vapor, indicating that the organic

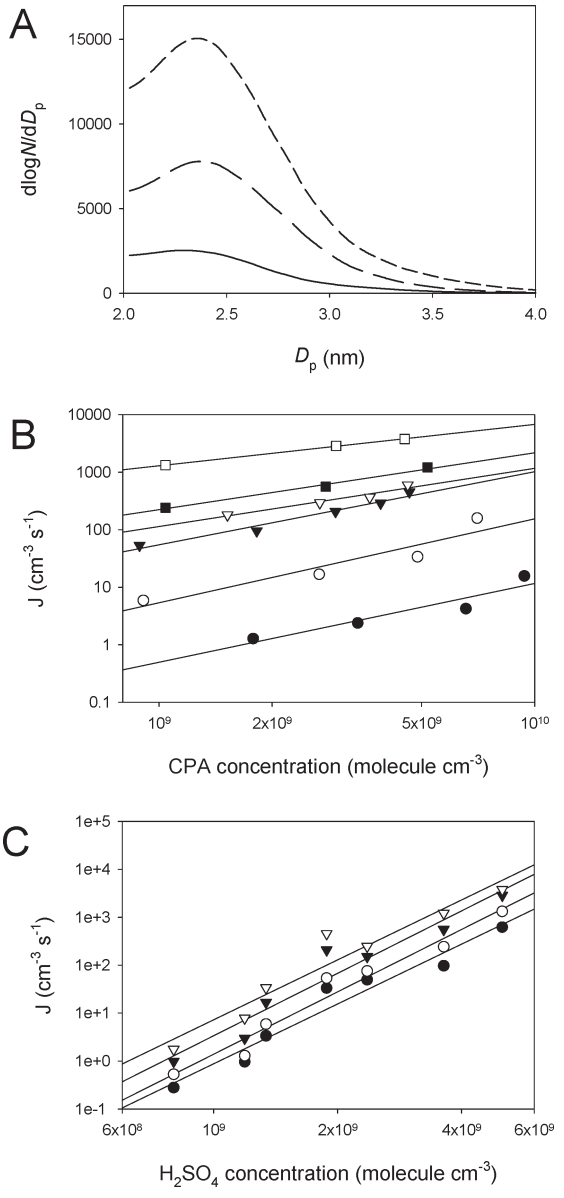

Figure 11. New particle formation in the presence of *cis*-pinonic acid (CPA), sulfuric acid, and water. (A) Size distribution of newly nucleated particles. Concentration of H_2SO_4 is 3×10^9 molecules cm^{-3}, and relative humidity is 20%. Concentration of CPA is 7.2×10^9 molecules cm^{-3} for the top curve (short dashed line), 4.9×10^9 molecules cm^{-3} for the middle curve (long-dashed line), and zero for the bottom curve (solid line). (B) Nucleation rate (J) as a function of CPA concentrations at 13% relative humidity. For the lines from top to bottom, the H_2SO_4 concentration varied from 5×10^9 (open squares), 3.6×10^9 (solid squares), 2.4×10^9 (open triangles), 1.9×10^9 (solid triangles), and 1.3×10^9 (open circles) to 0.8×10^9 molecules cm^{-3} (solid circles). (C) Nucleation rate as a function of the H_2SO_4 concentration at 13% relative humidity. For the lines from top to bottom, the CPA concentration varied from 6.1×10^9 (open triangles), 4.0×10^9 (solid triangles), and 1.4×10^9 molecules cm^{-3} (open circles) to zero (solid circles). All experiments were performed at 284 ± 2 K and a total pressure of 760 Torr. (Reprinted with permission from ref 58. Copyright 2009 National Academy of Sciences.)

acid−sulfuric acid interaction to form heteromolecular complexes is responsible for the enhanced new particle formation by reducing the nucleation barrier. In the absence of sulfuric acid, an individual organic acid or a mixture of two different types of organic acids do not lead to new particles, even at saturation ratios as high as 20−30. For instance, the minimum S required to produce detectable new particles is about 45 for benzoic acid and even higher for other acids.[57] The study by Zhang and coauthors is in contrast to an earlier environmental chamber study,[390] suggesting that organic aerosol nucleation occurs through formation of stable heterodimers between different organic acids, such as pinic and norpinic, which are the major products of α-pinene ozonolysis. A strong intermolecular binding force between different organic acids is proposed to play a key role in formation of the critical nucleus and its subsequent growth by Hoffmann et al.[390] However, unlike sulfuric acid−organic acid complexes, organic acid dimers have no vacant hydrogen acceptor/donor groups to promote subsequent cluster growth and cannot be stabilized by forming strongly bonded hydrates.[377,391] Indeed, water has a negligible influence on organic particle formation from organic acids because of their low water solubility.[57] Furthermore, the bonding energy of complexes represents only one of the factors that determine the rate of particle nucleation. Other physicochemical parameters, such as the surface tension and equilibrium vapor pressures of the multicomponent system, also influence new particle formation. For example, experimental measurements indicate a negligible effect of glutaric acid (pentandioic acid) on binary H_2SO_4−H_2O nucleation,[57] although the bonding energy of this organic acid with sulfuric acid is comparable to those of the aromatic acid−sulfuric acid complexes.[57,377,391]

The concentration dependencies of experimental nucleation rates obtained for the *p*-toluic acid−sulfuric acid−water vapor system[57] are examined using an approach based on the recent development of nucleation theorems[138] and multivariate statistical methods to provide a direct estimate of the molecular content of the critical nucleus.[139] It is determined that the critical ternary nucleus contains 1−2 molecules of *p*-toluic acid and approximately 8 molecules of sulfuric acid. A similar analysis of the experimental nucleation rates obtained for the *cis*-pinonic acid−sulfuric acid−water system yields one *cis*-pinonic and 3−5 sulfuric acid molecules in the critical nucleus,[58] where the hydrophobic organic acid part enhances the stability of the hydrophilic sulfuric acid counterpart (Figure 12). Direct analysis of the chemical composition of nucleated nanoparticles using the TD-ID-CIMS confirms the critical nucleus composition derived on the basis of the nucleation theorem.[58] As shown in Figure 13, sulfuric acid (H_2SO_4 and H_2SO_4−H_2SO_4 dimer) is significantly more abundant than CPA (CPA and CPA−H_2SO_4 heterodimer) in collected nanoparticles (the size ranging from 3 to 13 nm and a peak diameter of about 7 nm, with a mass ratio of about 1000 to 1 between H_2SO_4 and CPA). In general, condensation on nanoparticles is greatly suppressed because of enormously elevated equilibrium vapor pressures from the curvature (Kelvin) effect. Sulfuric acid condensation on newly nucleated particles can be efficiently promoted by simultaneous condensation of water molecules that prevents evaporation of H_2SO_4 and leads to practically irreversible growth process. In contrast, condensation of CPA on nanosized particles is limited because of its low solubility and lack of stabilization by hydration. Thus, the initial growth from the critical nucleus to the detectable 2−3 nm particles occurs exclusively by condensations of H_2SO_4 and H_2O. While enhancing formation of the critical nucleus by forming a stable complex with sulfuric acid, organic acids

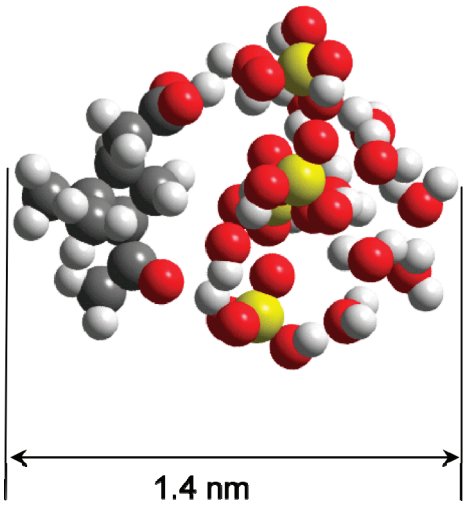

Figure 12. Molecular dynamic simulation of a critical nucleus consisting of 1 *cis*-pinonic acid, 4 sulfuric acids, and 10 water molecules. Carbon, sulfur, oxygen, and hydrogen atoms are represented by black, yellow, red, and gray spheres, respectively. The organic acid portion (left) is connected to the cluster via the carboxylic functional group. (Reprinted with permission from ref 58. Copyright 2009 National Academy of Sciences.)

contribute negligibly to growth of newly nucleated nanoparticles. The observed increase in the particle size in the presence of organic acids[57,58] is likely explained by the fact that faster nucleation produces nanoparticles earlier in the chamber and extends the growth time. Growth, however, occurs solely by condensation of sulfuric acid, similarly as in the binary nucleation case.

Since the magnitude of the enhancement from organic acids on the binary nucleation is comparable to that reported in the presence of ammonia,[181,384] nucleation assisted by organic acids likely explains high aerosol concentrations measured in polluted environments[392] because large concentrations of organic acids are produced by emissions and photochemical oxidation of anthropogenic and biogenic hydrocarbons. Aromatic acids, such as benzoic, *p*-toluic, and *m*-toluic, are products from photochemical degradation of aromatic hydrocarbons emitted from automobiles in the urban atmosphere and have been identified in the particle phase.[393,394] Pinonic acid is formed from reactions of α-pinene with ozone and the hydroxyl radical and represents an important constituent of ultrafine particles over forests.[257,289]

3.2.4. Nucleation of Iodine Oxides. Field studies reveal that bursts of new particles at different coastal sites correlate with sunlight, low-tide periods, and elevated concentrations of gas-phase iodine species.[226,265,269] Several laboratory studies, stimulated by field measurements, investigated the chemistry relevant to coastal new formation events, including near UV photolysis of CH_2I_2,[267,395] and formation of iodine oxides from the reaction of iodine atoms with O_3.[396] Hoffmann et al.[267] conducted a series of experiments in a 100 L reaction chamber to measure the chemical composition of aerosol particles formed after photodissociation of CH_2I_2 in the presence of O_3 using online atmospheric pressure CIMS (APCI/MS). On the basis of the mass spectrometric results and the molecular properties of iodine oxides, self-nucleation of iodine oxides was suggested as an efficient source of natural condensable materials for new particle formation in

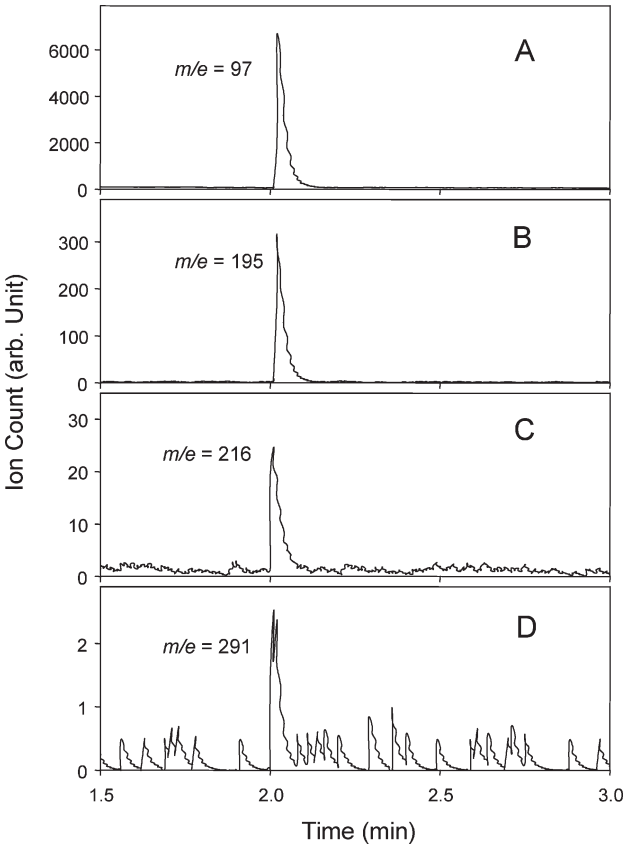

Figure 13. TD-ID-CIMS composition analysis of nanosized particles formed from ternary nucleation in the H_2SO_4−CPA−H_2O system. Ion signals for (a) HSO_4^-, (b) $HSO_4^-\cdot H_2SO_4$, (c) CPA$\cdot O_2^-$, and (d) $HSO_4^-\cdot$CPA represent H_2SO_4, $H_2SO_4\cdot H_2SO_4$ dimer, CPA, and CPA$\cdot H_2SO_4$ heterodimer, respectively. The ratio between CPA and H_2SO_4 is about 1:1000 in the collected particle mass. (Reprinted with permission from ref 58. Copyright 2009 National Academy of Sciences.)

coastal environments

$$CH_2I_2 + h\nu_{(nearUV)} \rightarrow I + CH_2I \quad (3.1)$$

$$I + O_3 \rightarrow IO + O_2 \quad (3.2)$$

$$IO + IO \rightarrow OIO + I \quad (3.3)$$

$$OIO + OIO \rightarrow I_2O_4 (or IO^+IO_3^-) \quad (3.4)$$

$$I_2O_4 + nOIO \rightarrow [-I-O-IO_2-O-]_{(1+n/2)} \quad (3.5)$$

Jimenez et al.[395] investigated new particle formation from the same chemical system in a 28 m^3 Caltech chamber. Rapid homogeneous nucleation is observed in the CH_2I_2 mixing ratio extending over 3 orders of magnitude, down to a level of 15 ppt, which is comparable to measured total gas-phase iodine species concentrations in coastal areas. Particles formed under dry conditions are fractal agglomerates. At higher relative humidity (65%) the nucleation and growth behavior remain similar as under dry conditions but particles are more compact and dense. Chemical analysis of larger particles in the chamber using an Aerodyne Aerosol Mass Spectrometer reveals that they are composed mainly of iodine oxides and water and/or iodine

dx.doi.org/10.1021/cr2001756 |*Chem. Rev.* 2012, 112, 1957–2011

oxyacids. Shrinking of particles upon humidification confirms that they are aggregated rather than compact. From comparison between the particle compositions, hygroscopic behavior, and nucleation and growth rates in laboratory and field measurements, photooxidation of CH_2I_2 and other organo−iodine compounds has been suggested as the mechanism responsible for coastal nucleation. Burkholder et al.[397] measured new particle formation from UV photolysis of CF_3I and CH_2I_2 in the presence of excess ozone in a 70 L Teflon reactor and analyzed the experimental results using a coupled chemical−aerosol model, assuming a single-component homogeneous nucleation of OIO. Application of the parameters derived from this model in an atmospheric box model suggests that the averaged IO and OIO concentrations reported in the field measurements using long path absorption[398,399] are insufficient to account for significant aerosol production in the coastal ocean marine boundary layer. Burkholder et al.[397] further proposed that inhomogeneous local sources of iodine oxides, i.e., "hot" spots with elevated iodine species emissions, may account for the observed aerosol production bursts.

Identification of molecular iodine[400] at higher levels than those of diiodomethane and other organo−iodide species in the marine boundary layer and a faster photolysis rate of I_2 in the atmosphere indicate that molecular iodine may be the dominant source of iodine atoms, leading to new particle formation in seaweed-rich coastal regions (eq 3.6)[396,401,402]

$$I_2 + h\nu_{(\text{visible})} \rightarrow I + I \qquad (3.6)$$

The work by McFiggans et al.[401] demonstrates that ultrafine iodine-containing particles can be produced by intertidal macroalgae exposed to ambient levels of ozone in 10 L reactors. The composition and morphology of nanoparticles are similar to those formed in the chamber by photo-oxidation of diiodomethane or in the oxidation of molecular iodine by ozone. Atomic iodine involved in the observed particle bursts is more likely (by a factor of 1000) to result from photolysis of molecular iodine rather than diiodomethane. Another laboratory experiment by Saunders and Plane[396,402] shows that iodine oxide nanoparticles are generated photochemically from I_2 in the presence of O_3. The nanoparticles exhibit fractal morphologies consistent with agglomerative coagulation and have an O/I ratio of 2.45 ± 0.08, indicating that they are composed of I_2O_5. According to quantum chemical calculations, gas-phase I_2O_5 is thermodynamically feasible and involves a series of exothermic oxidation reactions of the I_2O_2, I_2O_3, and I_2O_4 by O_3.[396] Sellegri et al.[403] employed a simulation chamber during a BIOFLUX (quantifying coastal BIOgenic aerosol and gas FLUX) campaign to further elucidate the role of I_2 in new particle formation from seaweeds and to quantify the amount of I_2 emitted and new particles formed by a given seaweed loading. A 2 m^3 chamber is filled with selected species of seaweeds from the Mace Head area and flushed with particle-free atmospheric air. Particle concentrations in the 3.0−3.4 nm size range produced in the chamber are positively correlated with gaseous I_2 concentrations emitted by the seaweeds, and both I_2 and particle concentrations are directly positively correlated with the seaweed mass. The source rates and growth rates determined from the chamber experiments were used in conjunction with seaweed coverage in and around this region to produce local emission inventories using a mesoscale dispersion model.

3.2.5. Ion-Induced Nucleation. Two types of laboratory experimental approaches are utilized to study ion-induced nucleation. The first approach involves measurements of new particle formation in the presence of ionizing radiation to determine the macroscopic influence of ions on the nucleation rate. In the second approach, molecular reactions between ions and neutral molecules are investigated to understand the underlying mechanisms of nucleation and growth of charged clusters.

Vohra et al.[404] investigated the possible role of radon and its daughters in the conversion of gaseous sulfur dioxide into particulate sulfate in the atmosphere using a reaction vessel with several hundred ppb levels of SO_2, O_2, and C_2H_4 and showed that the presence of atmospheric levels of radon enhances particle generation in the vessel. Raes et al.[405] compared the capability of UV light, γ-radiation, and their combination to produce particles in a mixture of SO_2, NO_2, and synthetic air. In the presence of UV, γ-radiation enhances particle production even at low dose rates. Since γ-radiation alone at low dose rates does not transform SO_2 into H_2SO_4, this observation of enhanced particle formation is interpreted as ion-induced nucleation. Kim et al.[406] used alpha-ray radiolysis of $SO_2/H_2O/N_2$ gas mixtures to investigate the competition between ion-induced and binary homogeneous nucleation processes. The measured ratios of the charged to uncharged particle fractions are indicative of the importance of ion-induced nucleation. On the basis of a comparison between the measured electrical mobility distributions for positively charged and negatively charged particles, ion-induced nucleation was found to be activated more strongly by negative ions than by positive ions. In a later study by the same group, addition of NH_3 enhances particle formation but decreases the charged fraction.[381] Svensmark et al.[407] investigated aerosol nucleation in a 7 m^3 reaction chamber in air containing 25 ppb ozone and 230 ppb sulfur dioxide upon UV photolysis and ionization (1000−6000 ions cm^{-3}). Production of new aerosol particles is linearly proportional to the concentration of negative ions with nucleation rates of the order of 0.1−1 cm^{-3} s^{-1}.

Duplissy et al.[408] reported the results of a pilot experiment performed at the CERN Proton Synchrotron in preparation for the CLOUD (Cosmics Leaving OUtdoor Droplets) experiment with the aim to study the possible influence of cosmic rays on clouds. A total of 44 nucleation events were studied, with particle nucleation rates of 0.1 and 100 cm^{-3} s^{-1} (for particles larger than 3 nm) and growth rates of 2−37 nm h^{-1} at H_2SO_4 concentrations typically around 10^6 molecules cm^{-3} or less. From analysis of the charged fraction, several of the aerosol nucleation events appear to have a contribution from ion-induced nucleation and ion−ion recombination to form neutral clusters, providing evidence for ion-induced nucleation or ion−ion recombination as sources of particles. It is also noted that although the measurements support involvement of sulfuric acid in the nucleation, its low level is insufficient to explain the observed rapid growth rates, suggesting the presence of additional trace vapors in the aerosol chamber, although their identity is largely unknown. Recently, Enghoff et al.[409] investigated sulfuric acid nucleation in a 50 L stainless steel chamber at atmospheric pressure under ionization from a 580 MeV electron beam and a gamma source. A clear contribution from ion-induced nucleation to new particle formation under atmospherically relevant sulfuric acid and ion concentrations has been detected. Also, simalr results from two different ionization sources indicate that the nature of the ionizing radiation is unimportant, implying that

inexpensive ionization sources can be used for investigations of ion-induced nucleation instead of expensive accelerator beams.

In addition to observations of enhancement in new particle formation in the presence of ions, a large number of experimental studies have been conducted to investigate ion clustering in the sulfuric acid−water system. The major goal of such studies is to measure the thermochemical parameters of the stepwise cluster formation reactions in order to develop kinetic models that accurately predict nucleation rates. Although a large number of reactions need to be evaluated to accurately describe the kinetics of cluster growth, the obtained thermochemical parameters for the initial few clustering steps allow estimation of the nucleation rates. Unlike neutral molecular clusters,[351] which require special approaches such as transverse CIMS for analysis, charged clusters are directly observable by mass spectrometry without an ionization source. Furthermore, a high-efficiency atmospheric pressure interface can be used to sample naturally occurring ambient ions from atmospheric pressure into the high vacuum of the mass spectrometer.[347]

Castleman and coauthors[410] used a mass spectrometer to investigate the thermodynamics of clustering of water, CO_2, and SO_2 with a large number of different core ions. In a recent study by this group, formic acid is shown to promote growth of positively charged water clusters by forming multiple hydrogen bonds.[411] Lovejoy[412] determined the rate coefficients and products for reactions of protonated sulfuric acid and water clusters $H^+(H_2SO_4)_m(H_2O)_n$ with water, ammonia, and a large number of organic compounds. The cluster ions are generated in an external ion source, and the reactions are studied in a quadrupole ion trap. Later, Froyd and Lovejoy[413,414] investigated the thermodynamics of small positively and negatively charged sulfuric acid−water clusters. It is shown that although a stable population of the $H^+(H_2O)_w$ cluster ions can be present in the atmosphere, incorporation of the first H_2SO_4 molecule to form $H^+(H_2SO_4)(H_2O)_w$ is thermodynamically unfavorable at 270 K.[413] As a result, no significant growth or subsequent nucleation of the $H^+(H_2SO_4)_s(H_2O)_w$ system is anticipated in the middle or lower troposphere. Small negative cluster ions, on the contrary, have a lower affinity for H_2O but a higher affinity for H_2SO_4.[414] Effective solvation of the HSO_4^- core ion by H_2SO_4 ligands results in a stable $HSO_4^-(H_2SO_4)_s$ backbone, and subsequent incorporation of H_2O molecules further stabilizes these clusters and allows for stepwise growth by addition of more H_2SO_4. The pressure and temperature dependences of thermal decomposition of $HSO_4^-(HNO_3)_y$ and $HSO_4^-(H_2SO_4)(HNO_3)$ were studied in an ion trap,[415] and the results were used to verify a master equation for thermal decomposition.[416] The thermodynamics for growth and evaporation of small cluster ions containing H_2SO_4 and H_2O obtained in previous studies have been incorporated into a kinetic aerosol model to investigate the rate of ion-induced nucleation under different atmospheric conditions.[417] The model predicts that the binary negative-ion H_2SO_4/H_2O mechanism can be an efficient source of new particles in the middle and upper troposphere but not in the boundary layer. Similar experiments were conducted by Wilhelm et al.[418] and Sorokin et al.,[419] showing that sulfuric acid has a stronger affinity for hydrated negative ions than positive ions, and hence, positive-ion clusters are less likely to grow under typical tropospheric conditions.

3.2.6. Chemical Composition, Reactivity, and Thermodynamics of Nucleating Clusters. Formation of complexes involving sulfuric acid, water, ammonia, and other species represents an important first step toward larger clusters and eventually nanoparticles. Understanding the mechanism of nucleation requires the knowledge of both the concentrations and the chemical composition of nucleating clusters. Although clusters can be size classified based on their electrical mobility,[325,333] the size resolution in such measurements is insufficient to provide information about the cluster molecular composition. A high degree of mass resolution and molecular specificity can only be achieved with the use of mass spectrometry (MS). Several different instrumental approaches based on mass spectrometry have been developed and successfully employed over the past decade to study molecular composition, thermodynamics, and reactivity of prenucleation clusters.

The first group of MS methods detects clusters that carry a positive or negative charge, such as clusters formed via the ion-induced nucleation mechanism. In a study of Goken and Castleman,[411] positively charged clusters containing 2−30 water molecules were generated by discharge and exposed to formic acid in a flow reactor at a 0.3 Torr total pressure to elucidate the role of organic acids in cluster nucleation and growth. The charged clusters were sampled from the flow reactor through a nose cone and analyzed directly by a quadrupole mass spectrometer. In the presence of formic acid, the distribution of clusters shifts to larger sizes, indicating that the acid promotes cluster growth by forming multiple hydrogen bonds within the hydrogen-bonding network of the cluster structure.

Bzdek et al.[420] investigated the kinetics and thermodynamics of exchange of amines for ammonia in small (1−2 nm diameter) ammonium bisulfate and ammonium nitrate clusters using Fourier transform ion cyclotron resonance mass spectrometry (FT-ICR-MS). Positively charged ammonium salt clusters produced by electrospray ionization are mass selected in a quadrupole and then transferred to the ICR cell, where they react with di- and trimethylamines. High mass resolution and accuracy FT-ICR-MS measurements allow for identification of the ion cluster composition before and after the reaction. Uptake coefficients of amines are close to unity, and the Gibbs free energy changes for substitution reactions are determined to be exothermic, −7 kJ/mol or more negative. Fast exchange of dimethylamine for ammonia is also observed in ammonium methanesulfonate clusters.[421] The reaction kinetics of ammonium bisulfate clusters with dimethylamine has been investigated as a function of the cluster size for clusters containing n = 1−10 bisulfate ions[422]

$$[(NH_4)_n(HSO_4)_{n-1}]^+ + (CH_3)_2NH \rightarrow [(NH_4)_{n-1}(CH_3)_2NH_2(HSO_4)_{n-1}]^+ + NH_3 \quad (3.7)$$

Although the displacement of the first several ammonium ions by dimethylamine occurs with near unit efficiency, the displacement of the final ammonium ion is size dependent because in larger clusters an ammonium ion can be trapped in an inaccessible core region, rendering difficult exchange. Dimethylamine is also observed to add onto existing dimethylaminium bisulfate clusters above a critical size, and didimethylaminium sulfate formation is more favorable as the cluster size increases. The results of the two studies suggest that complete exchange of ammonia in small clusters by amine may occur within several seconds to minutes even for the ambient amine concentration in the low ppt level.[420,422] Hence, being a stronger base than ammonia, amines not only are more efficient in stabilizing sulfuric acid−water clusters but can also rapidly replace ammonium

in nascent pre- and postcritical clusters. Very recently, the reactivity of dimethylamine and ammonia with negatively charged $[(HSO_4)(H_2SO_4)_x]^-$ and $[(NH_4)_x(HSO_4)_{x+1}(H_2SO_4)_3]^-$ sulfuric acid−ammonia clusters was also investigated.[423]

Dimethylamine substitution for ammonia in $[(NH_4)_x(HSO_4)_{x+1}(H_2SO_4)_3]^-$ clusters is nearly collision limited. Subsequent addition of dimethylamine to neutralize H_2SO_4 is within 1 order of magnitude of the substitution rate, but dimethylamine addition to $[(HSO_4)(H_2SO_4)_x]^-$ clusters is not observed. Addition of ammonia to unneutralized clusters occurs at a 2−3 orders of magnitude slower rate than incorporation of dimethylamine by either mechanism. It has been concluded that whereas amine chemistry may occur even in small ambient positive ions, for negative ions it will be important only when the ions grow to larger sizes (>m/z 400).[423]

It should be noted that small clusters in these studies are charged, and it is unclear whether the results are directly applicable to neutral clusters, which are often considered to be prevalent in the atmosphere.[333] According to quantum chemical calculations, bonding of nitrogen bases to sulfuric acid in clusters can be significantly reduced in the presence of a negative charge[378,424,425] or enhanced in the presence of a positive charge.[426] Indeed, experimental measurements have confirmed that the distributions of ionic species produced by electrospray of an ammonium sulfate solution in both positive and negative polarities differ significantly.[423] In positively charged clusters all sulfuric acid is present as bisulfate, whereas in negatively charged clusters the degree of sulfuric acid neutralization depends on the cluster size. In large clusters, with a decreasing role of charge, both positively and negatively charged cluster compositions converge toward ammonium bisulfate.

To understand the details of neutral cluster nucleation, measurements of the chemical composition of neutral clusters have been conducted using both indirect and direct approaches. Hanson and Eisele[217] determined the diffusion coefficient of H_2SO_4 vapor in humidified nitrogen to indirectly quantify the hydration state of gaseous sulfuric acid. Accounting for the hydration of sulfuric acid molecules in the gas phase is important for accurate calculation of binary nucleation rates because hydrates stabilize the vapor, hindering nucleation. The measurements indicate that about one-half of the H_2SO_4 molecules become hydrated at 8% relative humidity and form a dihydrate at higher relative humidity.[217] The derived Gibbs free energies of the sulfuric acid monohydrate (−3.6 kcal mol^{-1}) and dihydrate (−2.3 kcal mol^{-1}) at 298 K are in reasonable agreement with the hydration energies calculated by classical hydrate theory,[427,428] which assumes that the thermodynamics of bulk solutions is directly transferable to small clusters. The thermodynamics of hydration derived from the measurements of individual molecular clusters is crucial in reconciling the discrepancies between the results obtained by quantum chemical calculations, which predict less hydration, and the results of Monte Carlo simulations, which predict more extensive hydration than the classical hydrate theory.[429]

Hanson and Eisele[351] also introduced a direct approach to measure the concentration, composition, and thermodynamics of neutral clusters using transverse CIMS mass spectrometry. In this method, the clusters are ionized through ion−molecule reaction with the nitrate ion, NO_3^-. Varying the ion−molecule reaction time in a transverse ionization source maintained at atmospheric pressure allows for separation of the contribution of interfering ion-neutral clustering reactions (eq 3.8) from ionization of neutral clusters (eq 3.9)

$$HSO_4^- + H_2SO_4 \rightarrow HSO_4^-(H_2SO_4) \quad (3.8)$$

$$(H_2SO_4)_2 + NO_3^- \rightarrow HSO_4^-(H_2SO_4) + HNO_3 \quad (3.9)$$

This approach has been employed in laboratory studies to measure the composition of neutral molecular clusters of sulfuric acid in the presence of water[351,353] and ammonia.[352] In experiments conducted under temperatures and water concentrations that are typical of the middle-to-upper troposphere and the high latitudes, the steady-state ratios of neutral molecular clusters of sulfuric acid containing from two to eight H_2SO_4 molecules were measured.[351] The large clusters are comparable to the critical nucleus size derived on the basis of nucleation theorem from laboratory nucleation experiments.[181] The positive correlation between cluster growth and concentrations of water and sulfuric acid along with the size of a critical nucleus corresponding to the sulfuric acid tetramer (at 240 K) are in qualitative agreement with bimolecular nucleation theories. In the presence of ammonia, molecular clusters $(H_2SO_4)_n(NH_3)_m$, where n = 2−6 and m = 0 to n − 1, can be detected at temperatures up to 285 K,[352] much warmer than those necessary to form detectable levels of clusters in the H_2SO_4−H_2O system without ammonia (240 K[351]). For typical NH_3 and H_2SO_4 concentrations of about 2×10^9 molecules cm^{-3}, the cluster concentrations are estimated to be on the order of 10^6 molecules cm^{-3}. It is suggested that the critical, particle-forming cluster likely contains two H_2SO_4 molecules at 275 K, corresponding to the species $(H_2SO_4)_2 \cdot NH_3$. Furthermore, the thermodynamic data for formation of sulfuric acid dimers and trimers in the presence of water vapor, derived in a study by Hanson and Lovejoy,[353] indicate that the dimer is the least stable (i.e., critical) cluster with respect to evaporation of H_2SO_4 at 240 K, 20% relative humidity, and $[H_2SO_4] > 5 \times 10^8$ molecules cm^{-3}, whereas for the trimer and larger clusters the growth rates are faster than the evaporation rates. The Gibbs free energies of cluster formation at 242 K and 26% relative humidity, obtained from the measured cluster distributions, are −8.7, −11.2, and less than −12 kcal mol^{-1} for dimers, trimers, and the larger clusters, respectively. The data have been used to place limits on the atmospheric nucleation rate for the neutral H_2SO_4/H_2O mechanism. The neutral binary nucleation is concluded to be slower than the ion-induced nucleation for most conditions found in the middle and upper troposphere and is three to four orders slower than the classical theory predictions for all conditions.[353] The large discrepancy between the CNT and experimental data is likely due to the small size of the critical nucleus at lower temperatures when the liquid drop approximation is expected to be inaccurate. At room temperature, the larger critical nucleus contains eight or more H_2SO_4 molecules and the most recent classical theories[95,357] agree within an order of magnitude with early laboratory measurements of binary nucleation.[57,180,181,361]

Although all of the MS-based methods described above are capable of detecting molecular clusters up to 1000 amu (1.2 nm mobility diameter) either in the laboratory settings or ambient air, the resulting mass spectra are complex and require consideration of additional constraints, such as selective ionization, relative ion stability, accurate mass measurement, or tandem MS to provide an accurate molecular assignment. Detection sensitivity is another factor that may limit identification and quantification

of atmospheric molecular clusters. Although the total concentration of all clusters may be relatively high, the concentration of individual clusters at any particular mass is often as low as only a few percent of the total cluster concentration, in the range of 10^3-10^4 cm^{-3}, which is close to the detection limit of current mass spectrometric techniques.[350] Many nucleating clusters may be relatively weakly bound, further complicating efforts to determine their chemical makeup because of partial or complete evaporation of water, ammonia, and organic molecules from the clusters upon sampling through a dry curtain flow into the high-vacuum region of the mass spectrometer. The evaporation effect prohibits direct measurements of the hydration state of clusters and may cause an underestimation of the cluster nitrogen base content. Furthermore, as discussed in section 3.1, it is plausible that not all ions detected by these methods necessarily correspond to nucleating clusters. Although the MS methods are still in their infancy and often require additional simultaneous measurements to gain conclusive information on the chemical speciation, they show great potential as tools to follow the entire nucleation process, from subcritical clusters to nanoparticles.

3.2.7. Other Species. The substantial differences between binary nucleation rates measured in various experiments using in-situ production and liquid sources of H_2SO_4[186] invoked a number of theoretical studies aiming to account for the experimental discrepancies. For instance, the lack of nucleation enhancement from sulfuric acid additionally introduced from the liquid reservoir coupled to in-situ chemically generated H_2SO_4 and suppression of nucleation in the presence of NO_x have led to the suggestion that substances other than H_2SO_4 may trigger new particle formation and growth in the HO + SO_2 experimental system and possibly in the atmosphere.[367] Computational and modeling studies[368,430,431] further corroborated the hydrates of HSO_5, H_2SO_5, and $H_2S_2O_8$ from SO_2 oxidation as potential species responsible for nucleation. Alternatively, a stable complex $HO_2-H_2SO_4$[432] has been proposed to explain faster than expected nanoparticle growth rates.[365] However, formation of these species in the SO_2 + OH reaction has not been directly confirmed in laboratory experiments or ambient measurements.

A key role of oxidation products of organic compounds has been suggested in determining the spatial and temporal features of the atmospheric nucleation events.[258] A mechanism for the reaction of sulfuric acid with stabilized Criegee intermediates from ozonolysis of monoterpenes has been postulated on the basis of quantum chemical calculations to account for new particle formation events in the atmosphere assisted by organics.[433] Also, the variation in nucleation measurements between a series of photooxidation experiments in the 27 m^3 PSI (Paul Scherrer Institute) environmental chamber in the presence of 1,3,5-trimethylbenzene (TMB), NO_x, and SO_2 is significantly reduced if unidentified low-volatility organic compounds are assumed to participate together with sulfuric acid in the nucleation process.[188]

3.3. Theoretical and Computational Studies

Complexes and clusters bridge the gap between the molecular and the macroscopic scales, i.e., between individual molecules of nucleating vapors and aerosol particles. As discussed in the previous section, the scarce data on the chemical composition and thermochemical properties of atmospheric nucleating clusters limits the knowledge of their dynamics, hindering efforts to accurately predict atmospheric nucleation rates. Currently, atmospheric new particle formation is still poorly understood at the fundamental molecular level. Theoretical methodologies, including quantum chemical, molecular dynamics, and Monte Carlo methods, provide an opportunity for studying the properties of atmospheric nucleating clusters which contain tens to hundreds of molecules at the molecular level.

Molecular clusters are bonded together by noncovalent van der Waals interactions of varying strength, including dispersive, electrostatic, polarization, and hydrogen-bonding interactions. Also, in larger clusters, a chemical reaction of proton transfer may occur between interacting molecules, leading to additional cluster stabilization. The advantage of quantum chemical methods is that the interaction in molecular clusters is explicitly accounted for, including the effects of breaking and forming chemical bonds on the hydrogen-bond network of the cluster. The geometrical structures of a cluster as a whole and also of individual molecules and ions within the cluster can be obtained from theoretical calculations. The free energies of cluster formation can be computed from the electronic energies and the thermal contributions to enthalpies and entropies, which are typically evaluated using simple rigid rotor and harmonic oscillator models. Furthermore, the data from quantum chemical calculations are often used to construct interaction potentials for MD and MC methods. One disadvantage of quantum chemical methods is that the computational time required for energy and gradient evaluation is significant, restricting the size of molecular systems and the number of cluster configurations that can be probed. On the contrary, MD and MC methods utilizing classical interaction potentials are significantly less computationally expensive, allowing treatment of clusters consisting of thousands of molecules. Whereas MD simulations capture the dynamics of cluster formation, MC is an effective tool for sampling the cluster configuration space and obtaining average formation free energies and critical nucleus sizes. Also, explicit consideration of both cluster dynamics and chemistry can be accomplished using hybrid MD-quantum chemical methods, albeit at a significant computational cost.

3.3.1. Quantum Chemical Calculations. Due to the large affinity for water, gaseous sulfuric acid in the atmosphere exists in various hydrated forms; hence, the stabilizing effect of hydration needs to be taken into account when calculating the nucleation rate. In the absence of reliable experimental data, a large number of quantum chemical studies have been conducted to determine the structures and stabilities of various sulfuric acid hydrates, $(H_2SO_4)_m(H_2O)_n$, where $m = 1-3$ and $n = 0-9$.[434−443] Although all the studies conclude that deprotonation of sulfuric acid and formation of ions occur only in larger hydrated clusters, there is little agreement regarding the minimum number of water molecules (3−8) required to stabilize the resulting ion pair. The relative concentrations of free and hydrated sulfuric acid molecules calculated from the free energies of cluster formation obtained in different studies also show a significant variability.[444] It should be noted that even small variations in the estimated interaction energies between molecules in nucleating clusters have enormous consequences on the calculated overall nucleation rate. For example, a free energy change of −0.5 kcal mol^{-1} for addition of H_2O monomer increases the nucleation rate of water by 10 orders of magnitude.[96] Although atmospheric clusters contain a fewer number of monomer molecules (ten or less) than pure water clusters (50 monomer molecules) and the uncertainties in the stepwise free energy change may have different signs and partially cancel out, this sensitivity of J on ΔG has dramatic consequences on the level of calculation accuracy

dx.doi.org/10.1021/cr2001756 |Chem. Rev. 2012, 112, 1957–2011

required to predict the thermodynamics and kinetics of nucleation. Furthermore, the availability and reliability of experimental data on sulfuric acid clusters are rather limited, and it is rather difficult to determine the absolute accuracy of different theoretical methods. Although the thermodynamics of sulfuric acid dimers and trimers has been experimentally quantified using the transverse CIMS,[352,353] the hydration state of these clusters is unknown because water is prone to evaporation from the clusters under vacuum conditions. Also, the free energies of formation of sulfuric acid mono- and dihydrates have been only estimated indirectly.[217]

The discrepancies between the results of various quantum chemical studies arise from a number of factors, including use of different levels of theory and electron correlation, basis set completeness, treatment of the basis set superposition error, and use of the harmonic oscillator approximation.[72,444] Most of the studies of sulfuric acid−water clusters are based on electronic structure DFT methods. Although DFT is computationally effective, its performance in describing weakly bound systems is subject to debate; particularly, there is little agreement on whether DFT is superior to simple correlated methods, such as MP2, in describing hydrogen bonding. For some reference data sets, parametrized density functionals[445] often reproduce experimental binding energies very well but their transferability to different types of systems is questionable. Additionally, DFT results cannot be systematically improved, whereas correlated ab initio methods, despite producing larger errors when used with small basis sets, generally are more reliable because the results can be systematically improved using higher order correlation and larger basis sets. A significant limitation of the correlated ab initio methods is their prohibitively high computational costs. A common approach to obtain accurate thermochemical data for clusters is to use a two-step scheme, in which the geometry and vibrational frequencies are calculated at a lower order correlation level, such as MP2 with a moderate basis set or even at the DFT level, and then a single-point energy for the frozen geometry is calculated at a higher level, such as MP4 or CCSD(T).[377,442] A promising approach to reduce the computational costs of the correlated methods is resorting to the resolution-of-identity (RI) approximation to reduce the number of four-center, two-electron integrals. Using RI-MP2 and RI-CC2 methods for clusters composed of sulfuric acid, ammonia, and amines, Kurtén et al.[378] achieved an accuracy comparable to that of the full methods but at a much lower computational cost. Another source of discrepancies, the presence of many local minima on the cluster potential energy surface, can be partially overcome by obtaining initial guess structures via conformational searches using Car−Parrinello MD or semiempirical MC sampling.[446]

Since the binary homogeneous nucleation alone cannot explain the nucleation rates measured in the continental atmosphere boundary layer, the involvement of ammonia,[181,372,384] amines,[372,376] and organic acids[57,58] has been suggested on the basis of laboratory studies, which demonstrate that the presence of these species has a clear enhancement effect over the sulfuric acid−water vapor system. In the absence of experimental data, current knowledge of the structures and thermodynamics of neutral clusters involving the various species is based solely on theoretical calculations. The properties of H_2SO_4−H_2O−NH_3 clusters have been reported in a large number of publications.[377,391,424,437,442,447−449] The binding energy between sulfuric acid and ammonia is stronger ($\Delta G \approx -7$ kcal mol^{-1}) than that between sulfuric acid and water ($\Delta G \approx -3$ kcal mol^{-1}). In the absence of water, the H_2SO_4−NH_3 system is hydrogen bonded, with H_2SO_4 acting as the hydrogen-bond donor and NH_3 as the acceptor (Figure 14). In the presence of several water molecules, proton transfer occurs from H_2SO_4 to NH_3. The presence of ammonia also strengthens the binding of sulfuric acid molecules to the clusters, increasing the stability of clusters containing two or more sulfuric acid molecules.[448] The stabilizing effect of ammonia is likely to increase for clusters of larger size. It is concluded[449] that depending on the temperature, ammonia concentrations of 10 ppb to 10 ppm are required to obtain cluster compositions corresponding to ammonium bisulfate; the ratios corresponding to ammonium sulfate are unlikely in the first steps of atmospheric nucleation. Overall, theoretical and experimental studies agree that although ammonia enhances the rate of the sulfuric acid−water nucleation, the effect is rather modest to explain the observed new particle formation rates in the atmosphere.

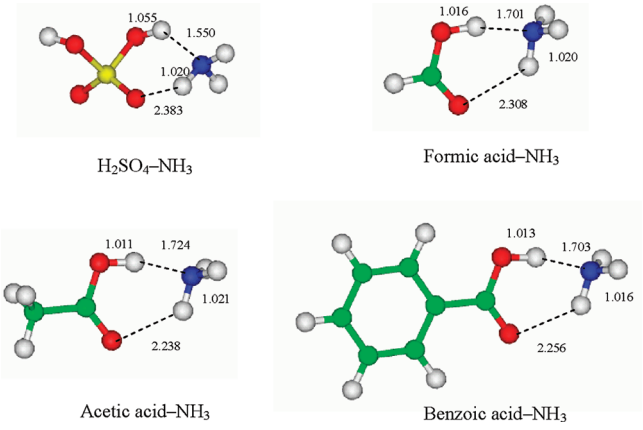

Figure 14. Optimized geometries of the complexes of sulfuric acid, organic acids, and ammonia obtained at the B3LYP/6-31G(d,p) level. (Reprinted with permission from ref 377. Copyright 2009 American Chemical Society.)

Recently, in a search for other compounds that can stabilize sulfuric acid by reducing its saturation vapor pressure, attention has been directed to organic bases, amines. Like ammonia, amines are able to form salts with strong inorganic acids under atmospheric conditions. Also because of higher proton affinity of amines,[450] proton transfer can occur more easily for amine−acid clusters than for ammonia−acid clusters, leading to stronger binding. Moreover, on the basis of thermodynamic evaluations amines may be able to form stable salts with organic acids.[387] Kurtén et al.,[378] using high-level ab initio methods RI-MP2 and RI-CC2, demonstrated that complexes of sulfuric acid with amines are stronger bound (ΔG from −10 to −17 kcal mol^{-1}) than those of sulfuric acid with ammonia ($\Delta G \approx -7$ kcal mol^{-1}) as shown in Figure 15. However, most amine complexes with negative bisulfate ion are only somewhat more strongly bound than the corresponding $NH_3 \cdot HSO_4^-$. In the case of larger cluster structures containing two H_2SO_4 molecules or one H_2SO_4 molecule and one HSO_4^- ion, amines, unlike ammonia, assist growth by stepwise attachment of H_2SO_4 molecules to both neutral and ionic clusters. The difference in complexation free energies for amine- and ammonia-containing clusters is suggested to be large enough to overcome the mass-balance effect caused by the 2−3 orders of magnitude lower concentration of amines than that of ammonia in the atmosphere.[378] This implies that amines are more important than ammonia in

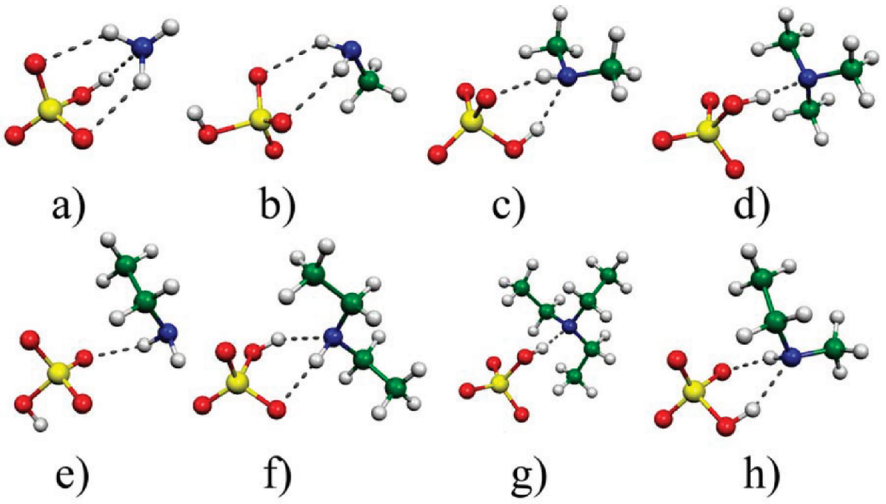

Figure 15. Structures of dimer clusters containing sulfuric acid and ammonia or various amines: (a) $H_2SO_4 \cdot NH_3$, (b) $H_2SO_4 \cdot CH_3NH_2$, (c) $H_2SO_4 \cdot (CH_3)_2NH$, (d) $H_2SO_4 \cdot (CH_3)_3N$, (e) $H_2SO_4 \cdot CH_3CH_2NH_2$, (f) $H_2SO_4 \cdot (CH_3CH_2)_2NH$, (g) $H_2SO_4 \cdot (CH_3CH_2)_3N$, (h) $H_2SO_4 \cdot (CH_3CH_2)NH(CH_3)$. Hydrogen bonds are indicated by dashed lines. Color coding: yellow = sulfur, red = oxygen, blue = nitrogen, green = carbon, and white = hydrogen. (Reprinted with permission from ref 378. Copyright 2008.)

enhancing neutral and especially ion-induced sulfuric acid−water nucleation in the atmosphere. In a subsequent study,[388] the thermodynamics of hydration for clusters composed of one ammonia or one dimethylamine molecule together with 1−2 sulfuric acid and 0−5 water molecules has been studied.

Dimethylamine is found to enhance attachment of sulfuric acid to the clusters much more efficiently than ammonia when the number of water molecules in the cluster is either zero or greater than two. Hydrate distributions obtained on the basis of the calculated free energies show that the two-acid clusters containing dimethylamine remain unhydrated in the troposphere, suggesting that dimethylamine assists atmospheric sulfuric acid nucleation much more effectively than ammonia. Nadykto et al.[451] using DFT calculations confirmed that the sulfuric acid−amine−water complexes are more thermodynamically stable than the sulfuric acid−ammonia−water complexes but suggested that addition of the second sulfuric acid to the amine−sulfuric acid complex is not sufficiently exothermic to account for the difference in typical atmospheric concentrations of ammonia and amines. The later conclusion, however, was debated by Kurtén,[452] prompting further research to address the existing uncertainties in thermochemical data of clusters and atmospheric concentrations of amines.

Following the experimental measurements of the enhancement of aromatic organic acids on the binary nucleation of sulfuric acid and water by Zhang et al.,[57] heteromolecular and homomolecular neutral and charged complexes of various organic acids have been the subject of several quantum chemical investigations (Figure 16).[377,391,453,454] A large number of organic acids, including formic, acetic, benzoic, *cis*-pinonic, maleic, malic, pyruvic, phenylacetic, and tartaric acids, are found to stabilize neutral H_2SO_4−H_2O clusters similarly to or even stronger than ammonia.[377,391,454] On the contrary, oxalic acid forms relatively weak neutral clusters with sulfuric acid, water, and ammonia.[453] However, the interaction of oxalic acid within positively charged $(C_2H_2O_4)(H_3O^+)$, $(C_2H_2O_4)(NH_4^+)$, and $(C_2H_2O_4)(H_3O^+)(H_2SO_4)$ clusters is strong and further enhanced by hydration. The interaction of larger organic acids with H_3O^+ is also very strong, with the corresponding free energies far exceeding those of the $(H_3O^+)(H_2SO_4)$ and $(H_3O^+)(H_2SO_4)_2$ formation.[454] Thus, the abundant organic acids may possess a substantial capability of stabilizing both neutral and positively charged prenucleation clusters, enhancing atmospheric new particle formation rates. Aerosol model simulations indicate that formation of organic acid−sulfuric acid complexes, by reducing the nucleation barrier, may be responsible for the observed enhancement of the binary H_2SO_4−H_2O nucleation in the presence of subppb levels of organic acids.[392]

Hydrogen bonding represents the first step in cluster formation and affects the stability and growth rate of clusters through the interaction with sulfuric acid and other trace species. In the sulfuric acid−organic acid complexes (Figure 16), unlike in the complexes of sulfuric acid with ammonia or amines (Figures 14 and 15), proton transfer is not energetically feasible. The driving force for formation of the complexes between organic acids and sulfuric acid is solely hydrogen-bonding interaction, and its strength determines the thermodynamic stability of these complexes. Zhao et al.[377] explored the structures, energetics, and topology of different hydrogen-bonded complexes composed of sulfuric acid, organic acid, ammonia, and water using several ab initio and DFT quantum chemical methods. Geometrical analysis shows that the organic acid−sulfuric acid complexes possess a pair of hydrogen bonds, one strong and one of medium strength, but for organic acid−ammonia complexes the corresponding hydrogen bond pair is much weaker. The binding energies of the organic acid−sulfuric acid complexes are several kcal mol^{-1} higher than those for the organic acid−ammonia complexes. Formation of strong hydrogen bonds in the organic acid−sulfuric acid complexes can be explained by a well-established resonance-assisted hydrogen-bonding theory. Furthermore, topological analysis employing quantum theory of atoms in molecules (QTAIM) shows that the charge density and the Laplacian at bond critical points (BCPs) of the hydrogen bonds of the organic acid−sulfuric acid complexes are positive, falling in the range or exceeding the range of one strong and one medium-strength hydrogen-bond criteria.[377] A notable topological feature of the organic acid−sulfuric acid complexes is a nearly planar, 6- or 8-membered cyclic ring structure with a pair of hydrogen

dx.doi.org/10.1021/cr2001756 |*Chem. Rev.* 2012, 112, 1957–2011

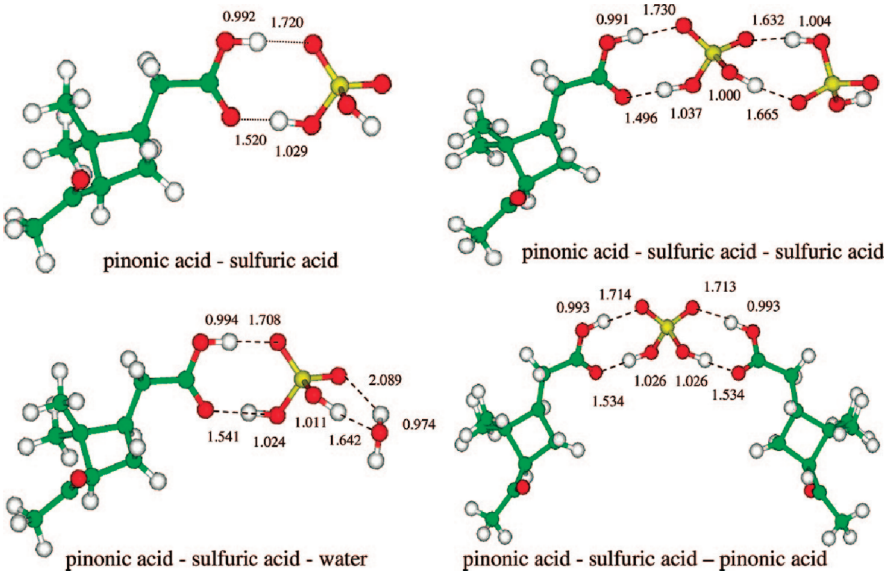

Figure 16. Optimized geometries of the complexes of sulfuric acid, *cis*-pinonic acid, and water obtained at the B3LYP/6-31G(d,p) level. (Reprinted with permission from ref 377. Copyright 2009 American Chemical Society.)

bonds, and the BCPs are close to the hydrogen nuclei, consistent with the topological structures of H_2SO_4−H_2O and H_2SO_4−NH_3 determined by Kurtén et al.[442] In addition, in the cases of strong hydrogen-bonding interactions, the total electronic energy density is found to be negative, showing a partially covalent character, but for medium and weak hydrogen bonds, only electrostatic interactions are present.[377]

Quantum chemistry calculations have also been used to investigate the underlying mechanism relevant to ion-induced nucleation for which sufficient experimental data exist on the thermochemistry of HSO_4^--based[414] and $H_2S_2O_7^-$-based[455] ion clusters. Nadykto et al.[89,456] showed that the sign preference in ion-induced nucleation, which manifests itself in water preferring to nucleate more efficiently on negatively charged ions, arises from the molecular structure of small charged clusters and can be explained and predicted by quantum chemical calculations. Furthermore, the stabilizing effect of ammonia on formation of negatively charged cluster hydrates is ruled out.[425] Although the concentration of positively charged H_2SO_4 clusters is small, most of them are expected to contain ammonia under typical atmospheric conditions.[426] Kurtén et al.[443] and Ortega et al.[424] also conclude that the role of ammonia in negative-ion-induced sulfuric acid−water nucleation is likely to be significantly smaller than in neutral sulfuric acid−water nucleation.

3.3.2. Molecular Dynamics and Monte Carlo Simulations. Since classical MD and MC methods do not allow for bond formation or breaking, their application in describing the structure, dynamics, and energetics of atmospheric nucleating clusters is far from straightforward. When clusters grow by stepwise addition of sulfuric acid, water, or base (e.g., NH_3 or amine) molecules, at a certain stage H_2SO_4 dissociates and water or the base becomes protonated. One approach is to represent the dissociating system as a mixture of water, base, sulfate/bisulfate ion, and proton entities. In this approach, a proton can be described as a unit charge using an interaction potential that reproduces O−H bond energies of hydronium ion and sulfuric acid and the N−H bond energy of the base, which are all on the order of 100 kcal mol^{-1}. However, because of the strong bonding, such a system is locked into a local minimum because protons rarely change their positions during a simulation, in contradiction with the experimental observation of a rapid proton transfer in water, with an activation energy of only a few kcal mol^{-1}. Development of an accurate dissociative model for the H_2SO_4/H_2O/base system using this approach requires construction of detailed interaction potentials, including explicit polarizabilities and three-body potentials, to describe the change in the entire electronic structure of the molecules, with breaking of one of the O−H or N−H bonds and formation of another upon proton transfer. An alternative and somewhat unconventional model approach is proposed by Kathmann and Hale[457] by assigning a partial charge to a proton. In this study, effective atom−atom potentials have been developed using ab initio data obtained at a HF/DZV+P level and fitted to yield approximate agreement with the experimental bulk solution surface tension and partial vapor pressures at 298 K. The effective atom−atom potentials are applied in a Bennett Metropolis Monte Carlo calculation to determine free energy differences for small neighboring sized sulfuric acid−water clusters of fixed composition.

Another approach is to treat the dissociated and undissociated states as distinct entities and to evaluate the occurrence of dissociation by comparing the energies of the systems composed of dissociated and undissociated states. Since a proton exists most of the time as a part of sulfuric acid, hydronium ion, or protonated base rather than as a free ion and the second dissociation of sulfuric acid is negligible compared to the first, one can introduce water, hydronium ion, sulfuric acid, bisulfate ion, and protonated base as the constituent species. Each species is modeled as a set of interaction sites rigidly or flexibly held together at a representative geometry. Although nonadditive interactions, arising from molecular polarizabilities and three-body interactions, play an important role in both the energetics and the structures of clusters, a pairwise additive potential is universally employed in most studies because of significantly low computational effort involved in calculations. For instance, Kusaka et al.[112] developed a classical mechanical model representation of the H_2SO_4/H_2O binary system in a Monte Carlo

mixed ensemble simulation to sample different configurations of clusters and evaluate the cluster free energies. The model potential is constructed on the basis of previously reported ab initio calculations of Kurdi and Kochanski[434] in combination with experimental data. The clusters obtained in the simulations are highly nonspherical and for a given number of acid molecules show several structurally different but energetically similar conformations. The dissociation behavior of H_2SO_4 in a cluster differs markedly from that in bulk solution, depending strongly on the assumed value of the free energy of the proton transfer from H_2SO_4 to water. No dissociation occurs in small clusters. The probability of having a $(HSO_4^-)(H_3O^+)$ ion pair increases in larger clusters, but the ion pairs remain in contact and about 240 water molecules are required to observe the behavior which resembles that in bulk solution.

Similarly, Ding et al.[458] used the available ab initio data for sulfuric acid hydrates[438] to construct a reliable potential model of sulfuric acid−water interactions in small clusters suitable for both molecular dynamics and Monte Carlo simulations. Interaction potentials for sulfuric acid (H_2SO_4), bisulfate ion (HSO_4^-), hydronium ion (H_3O^+), and water (H_2O) are included. The model reproduces well previous ab initio data and agrees with the hydration data obtained experimentally by Hanson and Eisele.[217] However, large differences in the energies of the clusters exist in comparison with those obtained using Monte Carlo models by Kusaka et al.[112] and Kathmann and Hale.[457] Also, it is found that bisulfate and hydronium ions are well separated rather than present as contact pairs as in a previous study.[112] Simulations of larger clusters indicate that the hydronium ion is always present at the surface of the cluster while the bisulfate ion exists inside the cluster, resulting in a large dipole moment.[458] A cluster with a large dipole moment is expected to nucleate and grow at a faster rate by attracting polar molecules from the gas phase. Also, a larger total binding energy of the ion-containing clusters reduces cluster evaporation. From the difference in the stabilities of the clusters composed of molecular and dissociated sulfuric acid it is concluded that the presence of three water molecules is sufficient to deprotonate H_2SO_4 in the clusters containing one sulfuric acid. Furthermore, addition of a second sulfuric acid does not inhibit deprotonation.

Matsubara et al.[459] utilized a rigid version of the potential model by Ding et al.[458] and calculated only intermolecular forces with the intramolecular geometries frozen to reduce the computational cost. This modified model is applied in molecular dynamics simulations to investigate the binary nucleation in the water−sulfuric acid vapor mixture to explore the structure of the hydrated clusters. The system consists of 10 000 vapor molecules and 10 000 carrier gas molecules (argon) in a cube with a 586 nm side. A periodic boundary condition is applied in three dimensions. When the sulfuric acid concentration or water saturation is low, nucleation does not occur within the simulation time (20 ns), although small hydrates are formed. In other cases, nucleation is clearly observed and coagulation of hydrated sulfuric acid (or bisulfate ion) clusters represents the major growth mechanism. The rate of coagulation is larger for clusters enriched with sulfuric acid molecules and lower for highly hydrated clusters. This behavior is explained by the molecular-scale structure of the hydrates, which consists of the sulfuric acid cores surrounded by the diffuse water shells. As extensive hydration stabilizes the sulfuric acid clusters, their rapid growth by coagulation is only possible before the sulfuric acid cores are completely enclosed in a water shell.

Toivola et al.[460] used molecular dynamics to compare the interaction between sulfuric acid and water molecules in stable clusters and at a planar liquid−vapor interface. The system includes 100−2000 molecules, and the molar fraction of H_2SO_4 was varied from 0.01 to 0.6. Following Ding et al.,[458] two different potential models are considered, including undissociated sulfuric acid and H_2SO_4 dissociated in the presence of water to form bisulfate (HSO_4^-) and hydronium (H_3O^+) ions. For H_2SO_4 mole fractions smaller than 0.1, in the unprotonated case sulfuric acid in the clusters is located preferentially at the surface whereas at a planar interface no enhanced surface activity is observed. In the protonated case, the bisulfate ions are present at the center of the cluster and the hydronium ions are present on the surface when the sulfuric acid concentration is small. The presence of ions destabilizes the clusters at higher compositions and the planar interfaces at all compositions. It is suggested that the observed destabilization may be associated with the deficiency of the potential model and that new interaction potentials based on larger clusters and higher acid concentrations may be required. As shown by Choe et al.,[461] using the first-principle molecular dynamics simulations based on density functional theory in conjunction with norm-conserving pseudopotentials, the structural features of aqueous sulfuric acid solutions have a strong dependency on the H_2SO_4 concentration in the 0.84−10.2 M range. Particularly, the Grötthuss-type proton transfer mechanism (proton hopping) becomes ineffective at higher concentrations because the ions from the dissociation of sulfuric acid disrupt the hydrogen-bond network of water.

In the most advanced approaches, first-principle molecular dynamics, atomic nuclei are treated according to classical mechanics while the electronic degrees of freedom are treated explicitly by density functional theory or semiempirical quantum chemistry. No model potential needs to be specified; instead, the energy is calculated on the fly at each step of the simulation. Although this approach is capable of explicit treatment of nuclear quantum effects, such as proton transfer, its application is currently limited to investigating dynamics that occurs on a time scale of the order of tens-to-hundreds of picoseconds and is not yet practical in evaluating free energy. Using first-principles Car−Parrinello molecular dynamics simulations, Anderson et al.[462] showed that the presence of two sulfuric acid molecules in $(H_2SO_4)_m \cdot \text{base} \cdot (H_2O)_6$ clusters ($m = 1-2$) is always sufficient to form a double ion already during the initial geometry optimization. Growth of such a double-ion cluster likely proceeds without encountering a nucleation free energy barrier. For clusters containing only one H_2SO_4 molecule, the acid remains protonated throughout the entire simulation (~30 ps) for the base-free and NH_3-containing clusters but dissociates after about 1.5 and 9.5 ps for the methylamine- and pyridine-containing clusters. The initial transfer of the proton is induced by formation of H_4SO_5, followed by a bound Eigen ion, $(HSO_4^-) \cdot (H_3O^+)$, that is stable for only 0.2−0.5 ps before the proton is transferred again either to the base or to a second water molecule. For all clusters with two sulfuric acid molecules and a base present, the base remains protonated (HB^+) throughout the entire simulation. For these clusters, only one out of six cases exhibits a contact ion pair. In most cases, acid and base are separated by one or two water molecules, contrary to many previously reported static calculations, showing direct H bonding between the acid and the base. In the base-free cluster with two sulfuric acids, one acid molecule is preferentially dissociated and a contact ion pair (with

a direct H bond) is present for about 90% of the time when the acid is deprotonated.

Kakizaki et al.[119] utilized a recently developed semiempirical PM6 method to study the structures and dynamics of small hydrated sulfuric acid clusters $H_2SO_4(H_2O)_n$ (n = 1−9). Low-energy structures of clusters optimized at the PM6 level agree reasonably well in terms of geometrical parameters and energies with those from previous ab initio and density functional theory studies with the exception that PM6 somewhat overemphasizes bifurcated hydrogen-bonded structures, with two protons of a water molecule forming a hydrogen bond to the same acceptor atom. Direct dynamics simulations performed on hydrated sulfuric acid clusters (n = 1−6) by the path-integral molecular dynamics approach (PIMD), i.e., using PM6 potential energies and their gradients, show that the H_2SO_4 dissociation probability increases with increasing cluster size and that contact-ion-pair structures are dominant in the proton-dissociated clusters. A comparison with the classical MD results suggests that nuclear quantization significantly enhances thermal fluctuations, presumably due to larger zero-point vibrational amplitudes of hydrogen atoms, leading to liquid-like structures for the hydrated clusters even at 250 K, while the corresponding classical MD clusters are solid-like. Sulfuric acid does not dissociate in small tri- and tetrahydrate clusters despite the comparable stability of ionic and neutral structures, and proton transfer from sulfuric acid to water only occurs in clusters containing five or more water molecules.

3.4. Parameterizations of Atmospheric Nucleation

Field measurements and laboratory experiments show that atmospheric nucleation events are closely associated with the sulfuric acid concentration. To represent this dependence in atmospheric models, several theories and parametrizations have been developed, including classical binary and ternary homogeneous nucleation, ion-mediated nucleation, activation-type nucleation, and kinetic nucleation. With the exception of the kinetic CNT formulation, e.g., by Yu[463] and Sorokin et al.,[95] the theoretical methods described in sections 2.1 and 3.4, which involve explicit consideration of cluster distributions or cluster dynamics, e.g., DNT, DFT, MD, and MC, are yet to receive broad application in atmospheric nucleation studies because of lacking the required interaction potentials or being computationally expensive.

Widely used parametrization of the binary homogeneous nucleation by Vehkamaki et al.[357] is based on classical theory, and nucleation is a function of the surface tension, density of the solution, and equilibrium vapor pressures of sulfuric acid and water above the solution. This parametrization is a revision to the one previously developed by Kulmala et al.[464] and corrected for the activity coefficients and errors made in the kinetic assumptions in the previous parametrization, based on the classical theory developed by Wilemski.[465] Yu adopted a slightly different approach to develop a self-consistent kinetic homogeneous nucleation model for the H_2SO_4−H_2O system, assuming water vapor concentration to be high enough that binary homogeneous nucleation can be treated as a quasi-unary nucleation process for H_2SO_4 in equilibrium with water vapor.[362,463,466,467] Ammonia, because of its relatively high concentration in the troposphere and ability to decrease the vapor pressure of sulfuric acid above a solution, can enhance the binary nucleation rate, and the classical ternary homogeneous nucleation model has been introduced to account for the effect of NH_3 on H_2SO_4−H_2O homogeneous nucleation.[379] Korhonen et al.[380] considered hydrate formation during ternary nucleation, and later Napari et al.[383] incorporated a refined hydrate model in an improved theory of ternary nucleation. This theory, however, significantly overpredicts the experimentally observed nucleation rates, e.g., up to 30 orders of magnitude in the presence of ppt level of NH_3. By considering the energetics of small H_2SO_4−NH_3−H_2O clusters, Vehkamaki et al.[468] demonstrated that sulfuric acid and ammonia may produce hydrate-like clusters of ammonium bisulfate in the vapor phase, and later Anttila et al.[469] showed that when clustering is taken into account the ternary nucleation rates are closer to the binary nucleation rates, typically over by 1 or 2 orders of magnitude. Yu[470] developed another approach based on a kinetic semiequilibrium model containing a fitted stabilizing factor to achieve agreement with experiments. The kinetic model assumes that H_2SO_4 dominates cluster growth and nucleation, whereas H_2O and NH_3 are secondary species influencing the cluster composition and the evaporation coefficient of H_2SO_4 from the clusters. To account for the effect of atmospheric ions, Yu[471] developed a second-generation ion-mediated nucleation model, which incorporates new thermodynamic data[418] and physical algorithms[472,473] and explicitly treats evaporation of clusters. This model is built upon an earlier version of the IMN model,[329] which has been improved using experimental measurements to constrain H_2SO_4 monomer hydration and incorporating recently determined energetics of small neutral H_2SO_4−H_2O clusters.[362] The IMN theory differs substantially from classical ion-nucleation theory,[474] which is based on a simple modification of the free energy associated with formation of a critical nucleus to include the effect of charge. The classical approach does not properly account for the kinetic limitation to embryo development and does not consider the important contribution of neutral clusters resulting from ion−ion recombination. On the contrary, IMN theory explicitly considers the kinetic effect of charge on cluster growth rates and formation of neutral clusters from neutralization of charged clusters. The present IMN model, however, is limited to the binary system and does not account for species other than H_2SO_4 and H_2O.

Although the CNT-based binary and ternary homogeneous nucleation parametrizations are widely used in atmospheric modeling studies, they tend to considerably underestimate particle formation rates, especially within the PBL.[475] Furthermore, the functional dependence of atmospherically measured particle formation rates on the sulfuric acid vapor concentrations is much weaker than that predicted by the binary nucleation theory.[363] Most ambient measurements suggest that the nucleation rate is correlated with the sulfuric acid vapor concentration to the power of 1−2.[50,54] This discrepancy between atmospheric measurements and binary nucleation theory likely implies participation of other species in nucleation, in addition to sulfuric acid, such as ammonia, amines, and organic acids.[1] Such species can stabilize the nucleating clusters, reducing H_2SO_4 evaporation and enhancing the nucleation rates. Hence, atmospheric nucleation may be limited by vapor−cluster collisions, rather than by a competition between condensation and evaporation assumed in the classical theory. If all nucleating clusters are stable, consideration of a free energy barrier in the nucleation rate calculations is likely unnecessary. For instance, in the presence of high concentrations of ammonia, clusters may be efficiently stabilized as ammonium bisulfate. In the kinetic model,[374,476] the critical nucleus is assumed to form through bimolecular collisions of sulfuric acid and sulfuric acid-containing clusters, cluster evaporation is neglected,

and the nucleation rate is proportional to the square of the sulfuric acid concentration, i.e., $P = 2$ in eq 3.10

$$J = k[H_2SO_4]^P \quad (3.10)$$

Neglecting evaporation of small clusters is not well justified, and a recent study suggests that explicit treatment of cluster evaporation is required for quantitative understanding of the dynamics of atmospheric clusters.[477]

Alternatively, atmospheric new particle formation may be represented by a two-step process,[336] consisting of nucleation of thermodynamically stable neutral or ion clusters followed by activation of clusters to observable particles.[478] According to this activation model,[333,478] nucleation occurs through activation of small clusters containing one sulfuric acid molecule and the nucleation rate is linearly proportional to the sulfuric acid concentration, i.e., $P = 1$.

The involvement of organic vapors has been suggested to explain the variation in the nucleation rate coefficient in eq 3.10 between four measurement sites during 2007−2009 EUCAARI campaigns, and an alternative eq 3.11 is proposed.[264] According to this equation, the intersite variation is substantially smaller when the heteromolecular homogeneous nucleation between H_2SO_4 and organic vapors (NucOrg) is assumed to take place in addition to homogeneous nucleation of H_2SO_4 using a constant k_{NucOrg} for all sites

$$J = k_{NucOrg}[H_2SO_4]^m[NucOrg]^n \quad (3.11)$$

In a sectional atmospheric chemistry and aerosol dynamics box model developed by Pirjola et al.[479] to simulate ultrafine particle formation and growth from the seaweed chamber in the coastal environment, thermodynamically stable clusters are formed by dimer nucleation of OIO vapor and the precursor is assumed to be molecular I_2 emitted by seaweed. The modeled results show a good agreement with the chamber measurements performed during the BIOFLUX campaign, confirming that I_2 emissions and nucleation of iodine oxides can largely explain the coastal nucleation events. In the aerosol dynamical box model developed by Vuollekoski et al.,[480] the nucleating vapor is assumed to be iodine dioxide (OIO) and three nucleation mechanisms are included, i.e., kinetic nucleation of OIO ($K \times [OIO]^2$), activation of clusters by OIO ($A \times [OIO]$), and sulfuric acid-induced activation of clusters containing OIO ($B \times [OIO] \times [H_2SO_4]$). Although all nucleation mechanisms provide reasonable results for coastal environments, kinetic nucleation fails to reproduce growth of newly formed particles up to 10 nm with the only available condensable vapors being OIO and sulfuric acid. The sensitivity studies indicate that growth of newly formed particles can be assisted by any low-volatility vapors present in concentrations exceeding 10^9 molecules cm^{-3}. Thus, marine new particle formation involving iodine oxides is not likely to produce particles of the size of CCN, except potentially over very large phytoplankton blooms or via condensation of additional low-volatility vapors.

Recent modeling studies[481−483] have shown that estimations of aerosol concentrations in the PBL can be considerably improved when using activation or kinetic nucleation parametrizations. Since few measurements[264] are available that provide information on the spatial distribution of the rate coefficient k in eq 3.10, most previous studies assumed a single median value for the entire atmosphere. Typically, kinetic and activation-type nucleation parametrizations produce similar agreement with observed monthly mean condensation nuclei (CN) concentrations[481,483] but do not allow one to resolve the nature of the acutal nucleation mechanism (via a barrier or barrierless). Comparisons with aerosol observations from many sites around the world[483] show that parametrization of nucleation is a promising way to improve the performance of global models, although the results exhibit highly temporal variability with occasionally unrealistically high number concentrations. Another model analysis of land-, ship-, and aircraft-based measurements by Yu et al.[484] indicated that among six widely used H_2SO_4 nucleation schemes only the ion-mediated nucleation can reasonably account for both absolute values and spatial distributions of particle number concentrations in the entire troposphere. Binary homogeneous nucleation significantly underpredicts particle number concentrations in the lower troposphere and is also insignificant in the upper troposphere, contrary to previous conclusions. Empirical activation and kinetic nucleation parametrizations significantly overpredict the particle number concentrations over tropical and subtropical oceans. Overall, the relative role of neutral and ion-mediated mechanisms in the atmospheric nucleation remains controversial.[61,333,344−346]

4. GROWTH OF NANOPARTICLES IN THE ATMOSPHERE

As discussed previously, aerosol nucleation occurs in two distinct stages, i.e., formation of a critical nucleus (~1 nm in size) and spontaneous growth of the critical nucleus to a larger size, both occurring from gas-phase molecules, such as H_2SO_4, water, ammonia, and other species. Atmospheric new particle formation can be observed only if freshly nucleated particles grow to a detectable size, which is currently about 1.5−3 nm.[1,59,322,323,328,372] The fate of freshly nucleated particles is determined by the competition between scavenging by preexisting particles and growth to larger particles. The relative rates at which those particles are lost by coagulation and grow to a larger size determine whether new particle formation events can be observed and how fast nanoparticles grow into CCN.

Coagulation loss of particles occurs when the particles suspended in air come into contact with each other because of the Brownian motion. The coagulation sink, F_{coag}, determines how rapidly nucleated aerosol particles are removed through coagulation[82]

$$F_{coag} = N_{dnuc} \sum_j K_{dnuc,dj} N_j \quad (4.1)$$

where N_{dnuc} is the number concentration of the nuclei, N_j is the number concentration of particles in a size class j, and $K_{dnuc,dj}$ is the Brownian coagulation coefficient between particles of diameter d_{nuc} and d_j.[82,485] Since the coagulation sink, F_{coag}, is linearly proportional to the number concentration of preexisting particles, N_j, new particle formation events are less frequently observed when the background aerosol number concentration is high. Furthermore, since the Brownian coagulation coefficient $K_{dnuc,dj}$ is larger when the difference between the size of nuclei d_{nuc} and preexisting particles d_j is larger,[82] coagulation loss is faster when the size distribution of preexisting particles shifts to bigger sizes.

Several mechanisms have been suggested to contribute to growth of organic aerosols, including condensation of low-volatility species, gas-to-particle partitioning of semivolatile species, and heterogeneous reactions.[486,487] Condensation of a gas-phase species onto a particle surface is dependent on its

ambient partial pressure (i.e., its atmospheric abundance) and the equilibrium or saturation vapor pressure of the species above a particle (i.e., its volatility), which is not only a function of temperature but also of the particle chemical composition and size. While soluble impurities in a particle decrease the equilibrium vapor pressure (known as the solution effect), the saturation vapor pressure over nanoparticles can be highly elevated because of the Kelvin effect. In addition to its atmospheric abundance and volatility, gas−particle partitioning of a species is also determined by its physicochemical properties (such as solubility) and the aerosol properties (such as available particle masses or volumes). Growth of nanoparticles from heterogeneous reactions is dependent on the volatility of the products formed in the particle phase. Although, gaseous aerosol precursors can be volatile, nonvolatile products formed from heterogeneous reactions provide an important pathway for growth of nanoparticles.[13] It has been hypothesized that heterogeneous reactions of certain organic compounds facilitate growth of nanoparticles by overcoming the Kelvin barrier.[486] In this section, the mechanisms of nanoparticle growth by condensation and heterogeneous reactions is discussed.

4.1. Role of the Kelvin (Curvature) Effect in Growth of Nanoparticles

The Kelvin effect represents a major limitation in the spontaneous growth of nanoparticles, particularly for freshly nucleated particles with a size of 1−2 nm. Condensation of a gas-phase species onto a particle surface occurs when the ambient partial pressure of the compound far away from the particle exceeds its saturation vapor pressure over the particle.[82] Mathematically, the condensational flux of a gas-phase molecule toward the particle is proportional to this partial pressure difference (i.e., the ambient pressure minus the saturation pressure). The saturation vapor pressure over the particle, p_A, is increased over a curved surface, as illustrated by the Kelvin equation

$$p_A = p_A^\circ \exp\left(\frac{2\sigma M}{RT\rho_l r}\right) \quad (4.2)$$

where p_A° is the vapor pressure of A over a flat surface, σ is the surface tension, M is the molecular weight of A, R is the gas constant, T is the temperature, ρ_l is the liquid-phase density of A, and r is the radius of the particle. The Kelvin equation provides a thermodynamic description of the saturation vapor pressure over the particle: the equilibrium pressure increases with decreasing particle size. Hence, condensation of chemical species onto nanoparticles in the atmosphere is considerably suppressed, particularly for newly nucleated particles. Although the surface tension of a particle may decrease somewhat as soluble organics condense, its value is dominated by sulfuric acid, water, and ammonium sulfate for small particles at the early stage of growth, being at least 70 dyn cm^{-1}.[488] In addition, the molecular weight M and density ρ_l together define the molar volume of the species (i.e., $v = M/\rho_l$, the volume occupied by one mole of the species in the condensed phase), which varies with the chemical composition (with a general increasing trend with increasing molar mass). Although the bulk-phase vapor pressures of most organic compounds decrease with increasing molecular mass (or number of carbon atoms), because of the increasing molar volume, the Kelvin barrier is highly elevated such that the occurrence of condensation on nanometer-sized particles is largely implausible even for organics with low volatility,[486] unless these organic

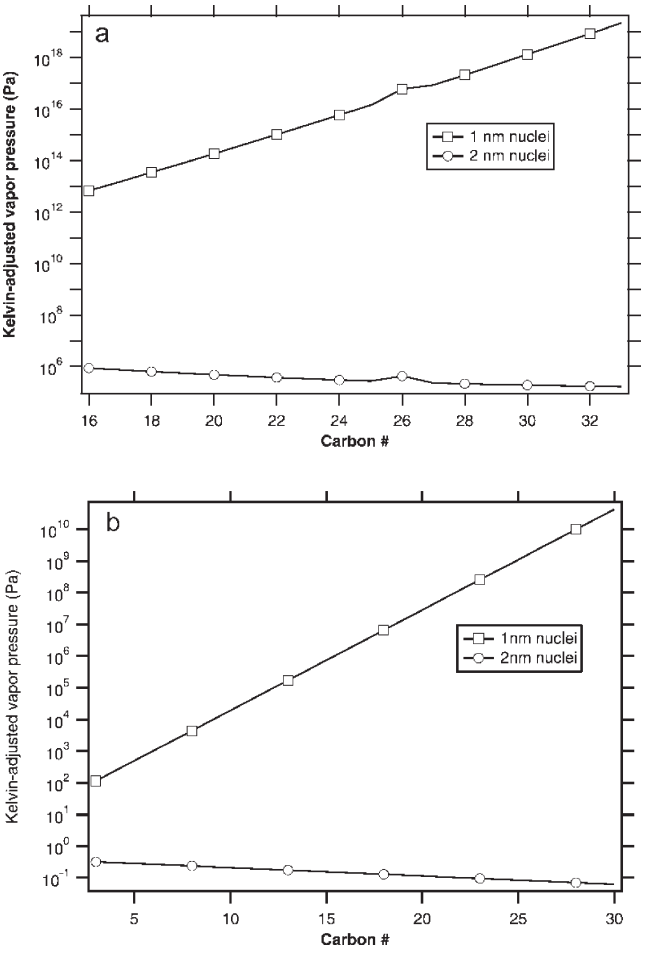

Figure 17. Kelvin-adjusted vapor pressures of (a) alkanes and (b) diacids as a function of the number of carbon atoms for 1 and 2 nm clusters. (Reprinted with permission from ref 486. Copyright 2002 by the American Geophysical Union.)

molecules are highly soluble in aqueous solutions.[489] The role of the Kelvin effect is demonstrated in Figure 17, showing the Kelvin-adjusted vapor pressures of alkanes and diacids as a function of number of carbon atoms in their molecules above 1 and 2 nm clusters.[486] Hence, the preferable candidates for condensational growth of nanoparticles include low-volatility compounds of a low molar volume, most likely with the presence of polar functional groups (e.g., hydroxyl, carboxyl) that can be stabilized by interaction with water or acid.

Kulmala et al.[489] introduced a theoretical framework to explain and quantify formation of organic nanoparticles in the atmosphere. The thermodynamic interactions between organic and inorganic compounds in growing clusters and particles are formulated by a theory analogous to the Köhler theory, which describes formation of cloud droplets due to spontaneous condensation of water vapor. The nano-Köhler theory differs from the conventional one in that it describes the activation of inorganic stable nanoclusters into aerosol particles in a supersaturated organic vapor that initiates spontaneous and rapid growth of clusters. An organic compound is assumed to be fully soluble in aqueous solution, i.e., it does not form a separate solid phase but is totally dissolved into the solution. This cluster activation theory shows that an equilibrium condition may occur at 3−4 orders of magnitude lower saturation ratios of the organic

vapor above an aqueous bisulfate cluster than that required for the pure organic clusters, i.e., the clusters behave as nuclei for organic aerosol nucleation. For instance, cluster activation theory explains the linear dependence between the formation rate of 3 nm particles and the gaseous sulfuric acid concentration.[478]

Since the Kelvin effect leads to reduced equilibrium aqueous concentrations of organic compounds in the particle phase, growth of nanoparticles by gas−particle portioning for semivolatile organic compounds is highly implausible under atmospheric conditions. Furthermore, limited solubility in nanoparticles due to the Kelvin effect can contribute to a suppressed growth by heterogeneous chemical reactions on nanoparticles, to be discussed in section 4.3.

4.2. Condensation

Condensational growth is a commonly accepted mechanism for nanoparticle growth in the atmosphere. For a gas-phase molecule, the condensation sink to nuclei/aerosol surfaces determines how rapidly gas-phase molecules condense onto pre-existing aerosols and depends strongly on the shape of the aerosol size distribution.[490] The condensation rate of a gas-phase molecule, F_{con}, into a particle of a radius, r, is often defined using the continuum/transition regime theory[464]

$$F_{con} = N_r \times 4\pi r \beta_M D(C - C_r) \quad (4.3)$$

where N_r is the number concentration of the particle with a radius r, β_M is the transitional correction factor for the condensational mass flux,[491] D is the diffusion coefficient of the gas-phase molecules, C is the ambient concentration of the gas-phase molecule, and C_r is the concentration of the gas-phase molecules corresponding to the saturation vapor pressure for the gas-phase molecule over the particle with a radius of r. Hence, at a given gas-phase molecule concentration, the condensation rates for smaller nuclei/particles tend to be smaller, directly because of the size term in the condensation rate equation and indirectly because of the much elevated saturation vapor pressure that arises from the Kelvin effect.

4.2.1. Condensation of Sulfuric Acid. The saturation vapor pressure of gaseous H_2SO_4 over its aqueous solutions at typical ambient temperatures and humidities corresponds to a 10^2-10^8 molecules cm^{-3} concentration range with a lower value in more dilute solution and at lower temperatures.[82] Atmospheric gas-phase sulfuric acid is mainly formed from photochemical oxidation of SO_2 and dimethyl sulfide in the presence of molecular oxygen and water, and hence, normally its concentration peaks around noon.[82,251,286] Ambient concentrations of gas-phase H_2SO_4 are typically in the range of 10^5-10^7 molecules cm^{-3} during the daytime, frequently exceeding the saturation vapor concentration over an aqueous solution. Due to random collisions, sulfuric acid molecules come into contact with existing particles, leading to condensational growth of particles. H_2SO_4 molecules that condense on particles are efficiently stabilized by simultaneous condensation of H_2O molecules that hinders evaporation of H_2SO_4, leading to practically irreversible condensation.[58] The stabilization of H_2SO_4 assisted by H_2O occurs via formation of hydrogen bonds between H_2SO_4 and H_2O molecules, followed by proton transfer to form H_3O^+ and HSO_4^- ions.[377,439,443] The concentration of water vapor in ambient air is sufficiently high ($10^{16}-10^{17}$ molecules cm^{-3}), and the water content of nanoparticles is in rapid equilibrium with the ambient relative humidity. Also, in the presence of basic gases, such as NH_3 and alkylamines, H_2SO_4 in the nanoparticles is converted to ammonium sulfate[492,493] and alkylaminium sulfate[13] salts, which have a lower volatility than H_2SO_4, resulting in further stabilization.[60,313]

The first detection of atmospheric gas-phase sulfuric acid was accomplished indirectly on the basis of measurements of stratospheric negative ions by Arnold and Fabian.[494] Later, Eisele and Tanner[236] introduced a highly sensitive direct technique for detection of gaseous H_2SO_4 using an atmospheric pressure selected ion CIMS. In this method sulfuric acid is converted to ions through reaction with the nitrate reagent ion (eq 4.4), and the ions are then detected by the mass spectrometer

$$H_2SO_4 + NO_3^-(HNO_3)_n \rightarrow HSO_4^-(HNO_3)_n + HNO_3 \quad (4.4)$$

Recently, this method has been modified by introducing an atmospheric pressure ion drift tube to constrain the ion flight path and reduce ion wall losses.[286] These two approaches are very robust and can detect sulfuric acid at concentrations as low as $(2-5) \times 10^4$ molecules cm^{-3}. Using these mass spectrometric techniques, a number of ambient measurements of the gas-phase H_2SO_4 have been performed.[236,251,253,364] A recent computational study suggests that in the presence of amines the measured sulfuric acid concentration may be underestimated because the H_2SO_4−amine clusters are charged less efficiently than H_2SO_4.[495] However, the validity of this conclusion based on theoretical results is yet to be confirmed, since theoretical calculations often contain large uncertainties in energetic predictions.[451,452]

In ambient studies, a power law relationship between ambient sulfuric acid concentrations and atmospheric particle formation rates is often observed.[253,364,374] However, this relationship does not necessarily imply that condensation of sulfuric acid plays a dominant role in nanoparticle growth. Simultaneous measurements of nanoparticle growth rates and gas-phase H_2SO_4 concentrations show that H_2SO_4 typically accounts for only 5−50% of the measured growth.[222,225,250,496,497] In addition to condensation of sulfuric acid, intramodal coagulation of nucleation mode particles and extramodal coagulation of nucleation mode particles with preexisting particles also contribute to the observed growth rate,[222] as described in section 5. Comparisons of calculated nanoparticle growth rates to ambient measurements indicate that the three mechanisms described above do not account for all the growth processes during new particle formation events in Atlanta[222] and Beijing.[250] Hence, other species in addition to sulfuric acid also contribute to nanoparticle growth.

4.2.2. Condensation of Low-Volatility Organics. Direct condensation of organic vapors of low volatility, such as organic acids, has been suggested as a potential additional mechanism for growth of atmospheric nanoparticles.[2] Although calculation using the Kelvin equation suggests that the saturation vapor pressure of organics over nanoparticles is much elevated,[486] the condensation process of organic acids that contributes to nanoparticle growth may involve formation of hydrogen bonding between organic acids and H_2SO_4 and/or H_2O molecules, analogous to that of sulfuric acid. Quantum chemical calculations show that stable complexes between organic acid (e.g., pinonic acid, formic acid, acetic acid, and benzoic acid) and sulfuric acid molecules can be formed through double hydrogen bonding.[377] The interaction between selected organic monodicarboxylic acids (benzoic, maleic, malic, pyruvic, phenylacetic, and tartaric acids) and dicarboxylic acid (oxalic acid) with nucleation

precursors and charged trace species leads to a decrease in free energy and can enhance the successive condensation of H_2SO_4 and H_2O in neutral and positively charged nanoparticles.[391,453,454]

There are rather limited laboratory experiments that investigate the direct condensation of organic acids onto nanoparticles. Chemical composition analysis of nanoparticles formed from the $H_2SO_4-CPA-H_2O$ ternary nucleation using a TD-ID-CIMS clearly shows that sulfuric acid (in the forms of H_2SO_4 and $H_2SO_4-H_2SO_4$ dimer) is far more abundant in the mass spectra than pinonic acid (pinonic acid and pinonic acid$-H_2SO_4$ heterodimer), with a mass ratio of ~1000 to 1 between H_2SO_4 and pinonic acid even if the gaseous concentrations of the two species are comparable.[58] The suppressed condensation of pinonic acid on nanosized particles is explained by its low solubility and lack of stabilization by other molecules such as H_2O, although hydrogen bonding can be formed. On the other hand, TDCIMS measurements of the composition of ambient 10−33 nm diameter particles formed from nucleation in Tecamac, Mexico show the presence of carboxylic and hydroxy carboxylic organic acids.[309] The average ion molar ratios for organic acids and other species suggest that organic compounds play a dominant role in the observed high nanoparticle growth rate.[309] In another study, combined laboratory investigation and field measurements using TDCIMS and ultrafine hygroscopicity TDMA confirm that alkylaminium−carboxylate salts contribute significantly to nanoparticle growth.[60] The discrepancy in the role of organic acids in nanoparticle growth can be potentially explained by heterogeneous reactions, i.e., the synergistic effects involving organic acids and alkylamines in the gas-phase and sulfuric acid in the particulates, rather than direct condensation of organic acids.

4.3. Heterogeneous Reactions

Heterogeneous atmospheric chemistry encompasses interaction between gaseous species and aerosols, cloud droplets, hydrometeors (falling rain, sleet, snow, etc.), and surface waters as well as chemical transformations and photochemical processes occurring within those condensed systems.[23,498,499] In this review, we focus on the heterogeneous reactions between organic vapors and H_2SO_4 nanoparticles that contribute to nanoparticle growth. Heterogeneous reactions are initiated with the accommodation of gas-phase organic vapor into the particles, which is limited by the Kelvin effect. Subsequent particle-phase reactions can proceed via various reaction mechanisms. For instance, heterogeneous reactions can be acid catalyzed, and hence, their rates are dependent on particle acidity. Also, pre-existing organics in nanoparticles can exert synergetic effects on the uptake of other species.[500] Formation of hygroscopic products can lead to further growth of nanoparticles through the uptake of H_2O. When chemical reactions are reversible, partial shrinking of grown particles may occur when the concentration of organic vapor decreases.[501]

Over the past decade, numerous studies have investigated heterogeneous reactions responsible for growth of larger particles using H_2SO_4 particles suspended in air and deposited on solid substrates and also using bulk aqueous H_2SO_4 solutions.[487] However, uptake of gaseous vapors on nanoparticles is significantly different from that on bulk solution surfaces.[501] The gas−particle interaction is determined by gas-phase diffusion, mass accommodation, and liquid-phase diffusion and reaction. For nanoparticles, the rate-liming step in the heterogeneous reactions often corresponds to mass accommodation, i.e., incorporation of organic species into nanoparticles. For sufficiently volatile organic species partitioning is highly suppressed because of the curvature effect, leading to negligible particle-phase concentrations of the organics and hindrance in the heterogeneous reactions on nanoparticles. Furthermore, care must be excised when applying the results of laboratory experiments to atmospheric nanoparticle growth, since the occurrence of particle-phase reactions is related to the concentrations of the organic vapors and the particle residence time. In laboratory experiments, the gaseous concentrations of organic vapors are typically higher than those in the atmosphere, but a shorter gas−particle interaction time is employed.

Due to the technical challenges, studies that directly investigate heterogeneous reactions of various organics on nucleation mode nanoparticles are rather sparse. Using a TDMA technique, the mobility size change of H_2SO_4 nanoparticles has been measured due to exposure to a series of organic species, summarized in Table 1.[13,501] In addition, TDCIMS and TD-ID-CIMS have been employed in both field and laboratory studies to obtain the chemical composition of nanoparticles.[13,60,309,501]

4.3.1. Ammonia. Ammonia is the primary basic gas and the most important neutralization agent for atmospheric particulates.[82] The heterogeneous uptake coefficient of NH_3 on bulk H_2SO_4 surfaces increases as a function of acid concentration and reaches unity at >55 wt % H_2SO_4.[492,493] The reaction products include NH_4^+ and HSO_4^- or SO_4^- in the aqueous phase (Scheme 1).

Two previous studies have measured the growth factor of H_2SO_4 nanoparticles upon neutralization by NH_3, both of which use the TDMA technique.[58,502] The uptake of NH_3 by H_2SO_4 particles is generally accompanied by release of H_2O, effectively resulting in ammonia replacing water in the particle phase.[502] At relative humidity < 5%, a growth factor of 0.988−1.05 is observed for 10−60 nm H_2SO_4 particles, with a larger value for smaller particles.[502] An increase or decrease in particle diameter upon neutralization is governed by the initial weight percent of H_2SO_4. An approximate cut value of the mass concentration of H_2SO_4 is 78 wt %, suggesting that at relative humidity below 5% H_2SO_4 particles with a diameter smaller than about 45 nm can grow to a larger size when neutralized by NH_3.[502] At higher relative humidity (25% and 75%), such as in another experimental study by Zhang et al.,[58] no apparent growth or shrinkage is observed when 6−30 nm H_2SO_4 particles are exposed to NH_3 (about 3×10^{14} molecules cm^{-3}). Thus, the role of ammonia to growth of atmospheric nanoparticles is limited to stabilizing the particle-phase sulfuric acid and depends on the availability of gaseous sulfuric acid.

4.3.2. Amines. Low molecular weight alkylamines are highly volatile.[386,503] The ambient concentrations of individual gas-phase alkylamines, on the basis of rather limited measurements, range from 0.3 to 4.2 ng m^{-3} in the marine atmosphere[504] to 231−562 μg m^{-3} in a location near a commercial dairy.[505] Generally, the concentrations of amines are expected to be at least an order of magnitude lower than that of ammonia in the atmosphere, except perhaps in the immediate vicinity of amine emission sources.[506] Being strong organic bases, amines react with nitric and sulfuric acids to form particle-phase aminium nitrate and aminium sulfate.[506,507] The heterogeneous reaction of gaseous alkylamines is a stepwise process involving partitioning of amines into the liquid phase, which is governed by Henry's Law, and subsequent liquid-phase reaction, leading to formation

Table 1. Growth Factors (D_p/D_0) Measured by Nano-TDMA upon Exposure of Sulfuric Acid Nanoparticles to Different Organic Vapors[a]

		growth factor D_p/D_0					
organics	relative humidity, %	4 nm	6 nm	8 nm	10 nm	15 nm	20 nm
glyoxal[b]	7	1.02 ± 0.02			1.22 ± 0.03	1.46 ± 0.03	1.53 ± 0.02
	20	1.02 ± 0.01			1.28 ± 0.03	1.64 ± 0.04	1.93 ± 0.04
methylglyoxal[c]	6	1.01 ± 0.02	0.99 ± 0.01		1.01 ± 0.01		1.01 ± 0.01
	20	1.01 ± 0.02	1.02 ± 0.01		1.02 ± 0.01		1.01 ± 0.01
	50		1.01 ± 0.01		1.01 ± 0.01		0.99 ± 0.01
2,4-hexadienal[b]	7	1.02 ± 0.02	1.02 ± 0.02	1.05 ± 0.02	1.08 ± 0.02	1.10 ± 0.03	1.13 ± 0.02
	12	1.02 ± 0.02	1.02 ± 0.02	1.03 ± 0.02	1.04 ± 0.02	1.08 ± 0.02	1.09 ± 0.03
	20	1.01 ± 0.01	1.01 ± 0.01	1.01 ± 0.01	1.01 ± 0.01	1.01 ± 0.01	1.01 ± 0.01
trimethylamine[b]	6	1.10 ± 0.01	1.12 ± 0.01		1.18 ± 0.01		1.18 ± 0.01
	45	1.12 ± 0.02	1.18 ± 0.01		1.19 ± 0.01		1.23 ± 0.01
ethanol[c]	6	1.01 ± 0.01			1.00 ± 0.01		1.00 ± 0.01
1-butanol[c]	3	1.02 ± 0.02			1.01 ± 0.01		1.01 ± 0.01
	7	1.02 ± 0.02			1.00 ± 0.01		1.00 ± 0.01
	15	1.01 ± 0.02			1.01 ± 0.01		1.00 ± 0.01
1-heptanol[c]	6	1.00 ± 0.01			1.00 ± 0.01		1.00 ± 0.01
1-decanol[c]	6	1.00 ± 0.01			1.00 ± 0.01		1.01 ± 0.01

[a] Adapted with permission from ref 501. Copyright 2011 American Chemical Society. [b] Reference 13. [c] Reference 501.

Scheme 1

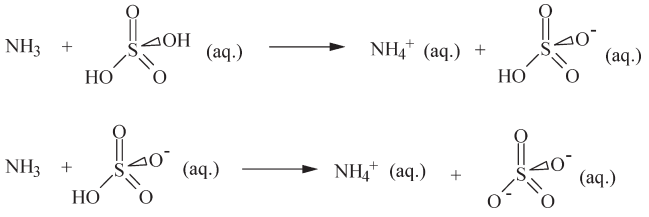

Scheme 2

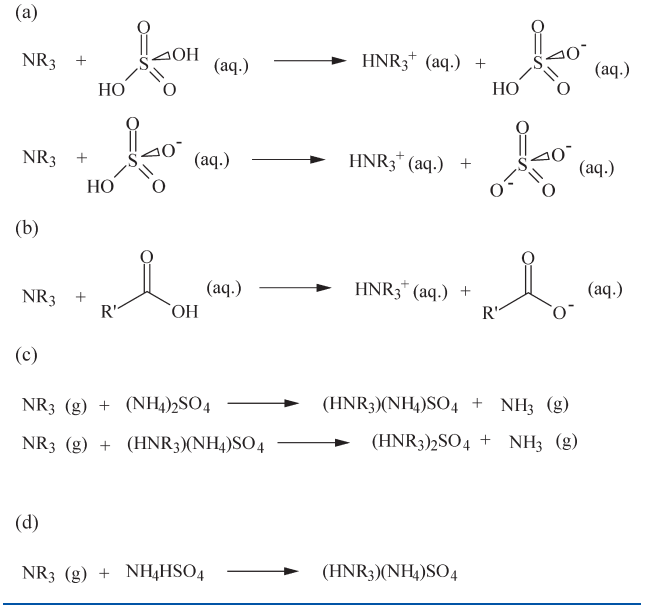

of aminium ions (Scheme 2a). The uptake coefficient γ measured for several different alkylamines on sulfuric acid solutions is about 10^{-2} and depends only weakly on H_2SO_4 concentration or temperature.[307]

Nano-TDMA experiments indicate that H_2SO_4 nanoparticles exposed to trimethylamine increase in size with a growth factor in the range of 1.10 for 4 nm particles to 1.23 for 10−20 nm particles (Figure 18c and Table 1).[13] The reduction in the growth factor for smaller particles is caused by the Kelvin effect. Since neutralization of the particle-phase sulfuric acid by amines is first order with respect to formation of aminium sulfate, the reaction rate is linearly dependent on the amine concentration, likely explaining the reduced but still a noticeable particle growth even at the size of 4 nm. Chemical analysis of nanoparticles exposed to amines by TD-ID-CIMS shows the presence of MS signals characteristic of aminium sulfate (Figure 19c and 19d).[13]

Using previously derived uptake coefficients,[307] it is estimated that the exposure time in those experiments is sufficiently long for gaseous trimethylamine to completely neutralize particulate sulfuric acid.[13] Growth of nanoparticles upon exposure to trimethylamine is more pronounced at higher relative humidity, because of the higher hygroscopicity of trimethylaminimiun sulfate,[508] which promotes additional uptake of water molecules by nanoparticles. The reaction between alkylamines and H_2SO_4 is expected to be completely irreversible, because the free energy change for the reaction corresponds to a rather large equilibrium constant.[378]

Amines can also contribute to new particle growth through formation of organic aminium salts between amines and organic acids. A recent thermodynamic modeling study on the relative contribution of ammonia and amines in forming organic salts and the corresponding decrease in volatility of these species suggests that amines may be an important contributor to organic salt formation (Scheme 2b).[387] Very recently, chemical composition analysis of atmospheric nanoparticles confirmed the coexistence of aminium cations and carboxylate anions in particles as small as 8−10 nm.[60]

dx.doi.org/10.1021/cr2001756 |Chem. Rev. 2012, 112, 1957–2011

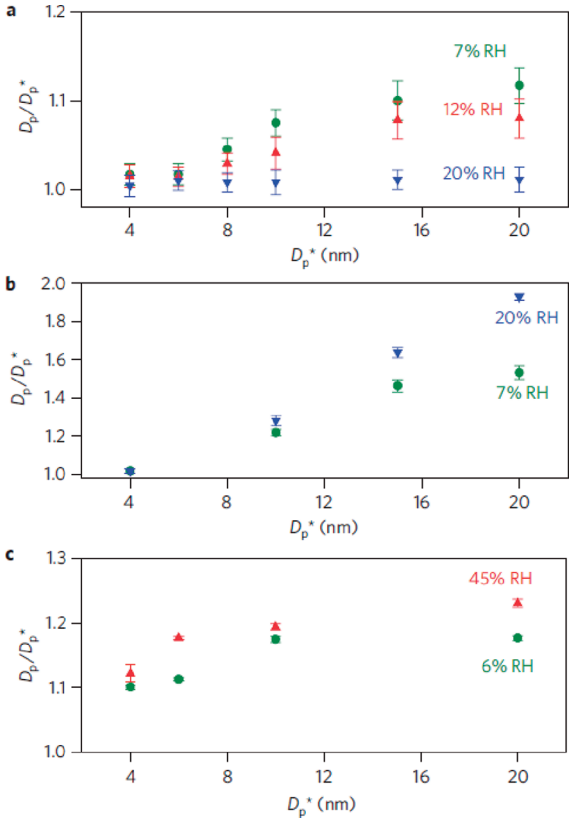

Figure 18. Particle growth factor (D_p/D_p^*) upon exposure to organic vapors: (a) 2,4-hexadienal, (b) glyoxal, (c) trimethylamine. All experiments were performed at 298 ± 2 K and a total pressure of 760 Torr. (Reprinted with permission from ref 13. Copyright 2010 Macmillan Publishers Limited.)

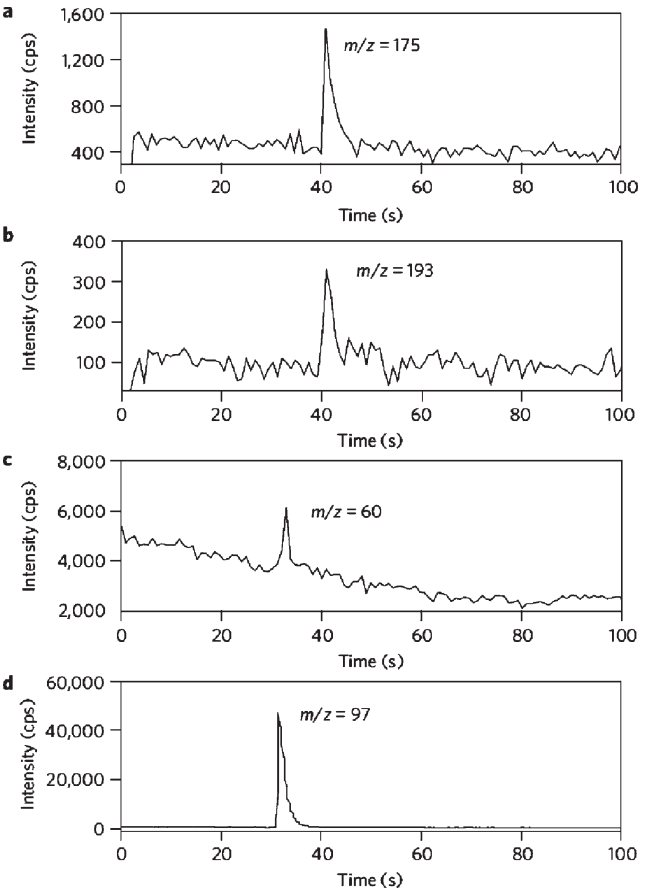

Figure 19. TD-ID-CIMS analysis of particle composition after exposure to 2,4-hexadienal and trimethylamine vapors: (a) mass at $m/z = 175$ for particles exposed to 2,4-hexadienal, assigned as a protonated aldol with loss of H_2O, $[C_{12}H_{16}O_2 + H - H_2O]^+$; (b) mass at $m/z = 193$ for particles exposed to 2,4-hexadienal, assigned as a protonated aldol, $[C_{12}H_{16}O_2 + H]^+$; (c) mass at $m/z = 60$ for particles exposed to trimethylamine, assigned as a protonated trimethylamine, $[(CH_3)_3N + H]^+$; (d) mass at $m/z = 97$ corresponding to HSO_4^-. The reagent ions were H_3O^+ and CO_3^-/CO_4^- for a–c and d, respectively. The sample was heated to 300 °C to completely evaporate the collected mass, starting at about 40 (a and b) and 30 s (c and d). (Reprinted with permission from ref 13. Copyright 2010 Macmillan Publishers Limited.)

In addition to neutralization reactions, amines can displace ammonium cations in ammonium nitrate and ammonium sulfate salts (Scheme 2c). The measured uptake coefficient is found to vary in the range from 10^{-4} to near unity on clusters, nanoparticles, or bulk surfaces.[420,422,506,509,510] In the case of ammonium bisulfate, the competition between the amine substitution into ammonium bisulfate and the acid–base neutralization of amine and bisulfate is governed by the cluster/particle size. Neutralization is more favorable with an increasing cluster size,[420,422] and the process becomes a dominating process on bulk surfaces[510] (Scheme 2d). Although uncertainties still exist that warrant further research on the reactions of amines with ammonium salts, this displacement pathway involving amines is likely to lead to further growth of neutralized nanoparticles because of the larger size of aminium ions than ammonium ions.

4.3.3. Aldehydes. Compounds with a carbonyl group (aldehydes and ketones) are emitted into the atmosphere from both anthropogenic and biogenic sources and also formed directly in the atmosphere from the photochemical degradation of volatile organic compounds.[82] The ambient concentrations of carbonyls are highly variable, in the range of tens of ppt to a few ppb, with the most abundant species normally being formaldehyde.[511] In acidic aqueous media, carbonyl compounds are known to engage in various reactions, such as hydration, polymerization, hemiacetal/acetal formation, aldol condensation, or cationic rearrangement.[512,513] Using thermodynamic calculations, Barsanti and Pankow[387] concluded that whereas particle-phase reactions of ketones and small aldehydes are not relevant for organic aerosol formation, aldol condensation of hexanal and higher aldehydes and reactions of α-dicarbonyls (glyoxal and methylglyoxal) may contribute to particle growth. Reactive and physical uptake of various carbonyl compounds has been widely measured in droplet train reactor or flow tube reactor experiments (e.g., by Jayne et al.[514] and Zhao et al.[515]). Experimental studies using bulk sulfuric acid solutions show that octanal, 2,4-hexadienal, and other larger aldehydes, while having negligible hydration rates, undergo protonation and enolization followed by aldol condensation and formation of large unsaturated polymers at high acidity.[515]

Aldol condensation has been proposed to contribute to growth of secondary organic particles of larger sizes. Jang and co-workers performed a series of smog chamber and flow tube experiments to study particle growth via acid-catalyzed reactions of volatile organic compounds, such as octanal and 2,4-hexadienal, and conclude that reactions of various aldehydes can remarkably increase the secondary organic aerosol mass production.[516–520] However, little

aerosol growth is observed in a chamber study by Kroll et al.[521] when H_2SO_4 aerosol seed particles are exposed to much lower concentrations of different carbonyls, including formaldehyde, 2,4-hexadienal, octanal, 2,3-butanedione, 2,4-pentanedione, glutaraldehyde, and hydroxyacetone. Hemiacetal formation from uptake of hexanal on moderately concentrated sulfuric acid submicrometer aerosols (30%) is experimentally observed, although very high concentrations of hexanal (up to 0.009 atm) are used.[522] An electrodynamic balance study on the reaction between octanal vapor and single levitated H_2SO_4 droplets also suggests that the reactive uptake of aldehydes into acidic particles may not be an important pathway in secondary organic aerosol formation under typical atmospheric conditions.[523]

The interaction of higher aldehydes with H_2SO_4 nucleation mode nanoparticles has been directly studied by a nano-TDMA.[13] Using 2,4-hexadienal as a model compound, it is observed that particle growth increases with decreasing relative humidity (Figure 18a and Table 1). In the particle size range of 4−20 nm, the growth factors reach the highest value at 7% relative humidity and the lowest one at 20% relative humidity for a given size. Also, the growth factor is size dependent, being close to unity for 4−6 nm particles but increasing for particles larger than 6−8 nm and reaching a value of 1.1 for 20 nm particles. Heterogeneous interaction between 2,4-hexadienal and nanoparticles is a two-step process that involves dissolution (partitioning) of gas-phase molecules in the particles followed by protonation and chemical reactions of the dissolved molecules. Highly elevated saturation vapor pressure above smaller particles caused by the Kelvin effect limits the solubility of 2,4-hexadienal in the particle phase, reducing the rate of the particle-phase reaction. The net result on the particle growth rate depends on the kinetic order of the reaction. Since polymerization of 2,4-hexadienal corresponds to a second- or higher-order reaction with respect to the organics to form aldol products,[515] the rate of this reaction is strongly dependent on the concentration of the organic species in the particle phase. Hence, the heterogeneous uptake of 2,4-hexadienal is nearly completely inhibited in nanoparticles smaller than about 4 nm. On the contrary, neutralization of sulfuric acid by amines described in the previous section is a first-order reaction and the rate is less dependent on the amine concentration, resulting in a noticeable particle growth even at the size of 4 nm.

Formation of aldol products in sulfuric acid nanoparticles exposed to 2,4-hexadienal is clearly evident from the chemical analysis of nanoparticles by TD-ID-CIMS (Figure 19a and 19b).[13] A clear increase in the organic constituents corresponding to the aldol products is also observed in attenuated total reflection infrared spectra of deposited sulfuric acid particles exposed to 2,4-hexadienal.[501] A decrease in the aldol signal upon terminating exposure to 2,4-hexadienal suggests that this reaction is partially reversible. Aldol condensation is initiated by protonation and enolization of 2,4-hexadienal in the presence of sulfuric acid, and the following reaction between protonated 2,4-hexadienal and enol leads to the aldol products (Scheme 3).[515] Since newly formed atmospheric particles are likely highly acidic, aldol condensation represents a plausible route contributing to their growth.

4.3.4. α-Dicarbonyls. α-Dicarbonyls are significantly more reactive than simple carbonyls. Typical α-dicarbonyls found in the atmosphere include glyoxal and methylglyoxal generated from photochemical oxidation of biogenic and anthropogenic hydrocarbons.[524−526] The ambient concentrations of glyoxal and methylglyoxal are comparable, ranging from 10 ppt to 1 ppb or even higher in more polluted areas.[527−531] Both glyoxal and methylglyoxal have been shown to contribute to growth of secondary organic aerosol of larger sizes.[517,532,533]

Scheme 3

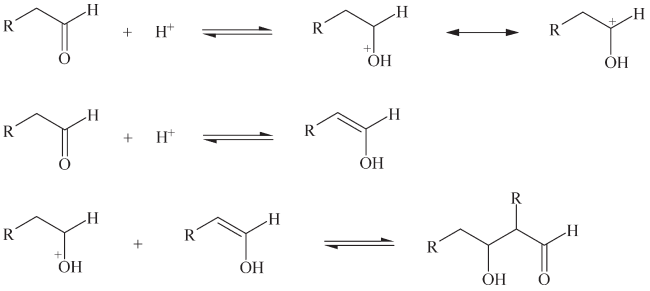

Experiments using the nano-TDMA suggest that while H_2SO_4 nanoparticles exposed to glyoxal experience noticeable growth with growth factors in the range of 1.00−1.93 (Figure 18b and Table 1),[13] similar particles do not show an appreciable change in size when exposed to methylglyoxal.[501] When exposed to glyoxal, H_2SO_4 nanoparticles show a larger growth at higher relative humidity, i.e., lower acidity and higher water activity, suggesting a hydration and self-oligomerization reaction mechanism in the presence of acid catalysis.[13] Although a number of previous studies report a correlation between the reactive uptake of glyoxal and particle acidity,[516,534,535] several other studies indicate that the acidity of the seed particles has an insignificant effect on glyoxal uptake.[521,536] Similarly as in the case of 2,4-hexadienal,[13] no growth is observed upon reaction of glyoxal with of 4−6 nm particles, but the growth factor increases for particles larger than 6−8 nm and reaches a value of 1.9 for 20 nm particles.

The chemical composition of H_2SO_4 nanoparticles exposed to glyoxal has been examined using TD-ID-CIMS.[13] Since the specific ion−molecule reaction rates used for chemical ionization of organic molecules with similar functional groups are similar,[537] oligomers exhibit little discrimination on their sizes during analysis, allowing quantification of oligomers in the particle phase. The TD-ID-CIMS results suggest that glyoxal oligomers are composed of 2−5 glyoxal monomer units, with the trimer being the most abundant (Figure 20).[13] The mass to charge ratios of the observed MS traces allow one to infer the molecular structures and suggest that oligomers are formed through an acid-catalyzed hemiacetal formation mechanism (Scheme 4a),[13] similarly to the routes that glyoxal oligomers are formed during water evaporation from cloud droplets[536] and glyoxal uptake on aqueous aerosols.[535] Other previous studies using bulk solution or larger particles also suggest that glyoxal oligomer formation occurs via aldol condensation (Scheme 4b)[538] and that organosulfate forms by the acid-catalyzed reaction of hydrated glyoxal with sulfuric acid (Scheme 4c).[534,539]

Experiments involving large seed particles suggest that formation of glyoxal oligomers according to the acid-catalyzed pathway is partially reversible.[521,540] Formation of glyoxal oligomers in a deposited H_2SO_4 droplet layer also displays a partially reversible behavior, as monitored by attenuated total reflection-Fourier transform infrared spectroscopy.[501]

Although H_2SO_4 nanoparticles of 4−20 nm diameter do not display any growth when they are exposed to methylglyoxal at 6−50% relative humidity,[501] evidence suggests that methylglyoxal is nevertheless an important precursor of larger secondary

dx.doi.org/10.1021/cr2001756 |Chem. Rev. 2012, 112, 1957–2011

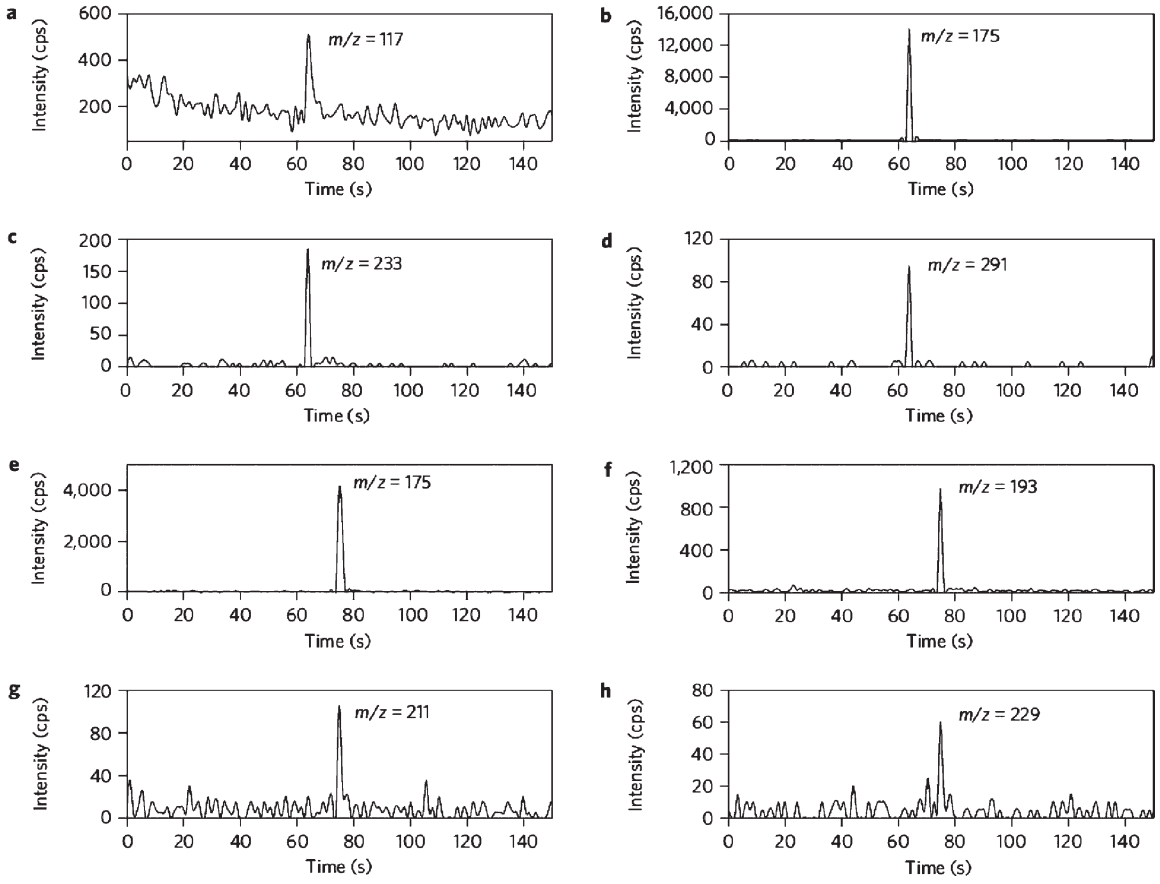

Figure 20. TD-ID-CIMS analysis of particle composition after exposure to glyoxal vapor. (a−d) Represent protonated glyoxal dimer through pentamer: (a) mass at $m/z = 117$, assigned as a protonated glyoxal dimer with a loss of H_2O, $[C_4H_6O_5 + H - H_2O]^+$; (b) mass at $m/z = 175$, assigned as a protonated glyoxal trimer with a loss of H_2O, $[C_6H_8O_7 + H - H_2O]^+$; (c) mass at $m/z = 233$, assigned as a protonated glyoxal tetramer with a loss of H_2O, $[C_8H_{10}O_9 + H - H_2O]^+$; (d) mass at $m/z = 117$, assigned as a protonated glyoxal pentamer with a loss of H_2O, $[C_{10}H_{12}O_{11} + H - H_2O]^+$. (e−h) Four possible glyoxal trimers in equilibrium; ions shown are protonated trimers with a loss of H_2O: (e) mass at $m/z = 175$, corresponding to a fragment from a branched trimer with two C−O−C bonds and three terminal C═O groups, $[C_6H_8O_7 + H - H_2O]^+$; (f) mass at $m/z = 193$, corresponding to a fragment from a linear or branched trimer with two C−O−C bonds and two terminal C═O groups, or a monocyclic trimer with three C−O−C bonds and one terminal C═O group, or a dual-cyclic trimer with four C−O−C bonds and no terminal C═O groups, $[C_6H_{10}O_8 + H - H_2O]^+$; (g) mass at $m/z = 211$, corresponding to a fragment from a linear or branched trimer with two C−O−C bonds and one terminal C═O group, or a monocyclic trimer with three C−O−C bonds and no terminal C═O groups, $[C_6H_{12}O_9 + H - H_2O]^+$; (h) mass at $m/z = 229$, corresponding to a fragment from a linear or branched trimer with two C−O−C bonds and no terminal C═O groups, $[C_6H_{14}O_{10} + H - H_2O]^+$. The sample was heated to 300 °C to completely evaporate the collected mass, starting at about 65 (a−d) and 75 s (e−h). For simplicity, the sulfate peak is not shown but is similar to that in Figure 19. (Reprinted with permission from ref 13. Copyright 2010 Macmillan Publishers Limited.)

organic aerosols.[532,541,542] Formation of methylglyoxal oligomers occurs via aldol condensation reactions (Scheme 5a) on the basis of the product analysis of aerosol composition by an aerosol mass spectrometer,[543] in contrast to a hydration and polymerization mechanism to form hemiacetal products (Scheme 5b) from a study where uptake of methylglyoxal is measured over bulk liquid H_2SO_4 surfaces.[541] A recent chemical composition study of methylglyoxal oligomers produced using electrospray-mass spectrometry suggests that aldol condensation of methylglyoxal is a favorable mechanism under simulated cloud conditions (pH = 4−5), while the hydration/acetal formation mechanism becomes predominant at pH < 3.5.[542]

Although the detailed mechanisms for glyoxal and methylglyoxal self-oligomerization are still lacking, the difference in the heterogeneous reactivity of these two α-dicarbonyls on nanoparticles can be explained by the difference in the rate and degree of hydration, resulting in different effective Henry's law constants. The effective Henry's law constant for glyoxal[521] is at least 3 orders of magnitude larger than that of methylglyoxal,[541] leading to a significantly lower aqueous concentration of methylglyoxal in nanoparticles for similar gas-phase concentrations of glyoxal and methylglyoxal in the nano-TDMA experiments.[13,501]

4.3.5. Alcohols. Methanol and ethanol are the primary simple alcohols that have been identified in air, with concentrations in the ∼1−20 and ∼0.2−1 ppb ranges, respectively, in rural areas.[511] Other alcohols identified in the atmosphere have generally much lower concentrations. The uptake of a series of alcohols by bulk H_2SO_4 solutions has been investigated using various techniques, including the flow tube reactor and the Knudsen cell.[544−548] In dilute sulfuric acid, alcohols interact mostly through a reversible physical absorption by solution, with a Henry's law constant increasing with increasing acidity. In concentrated sulfuric acid, uptake occurs due to the reversible formation of alkyl hydrogen sulfate (eq 4.5) and/or dialkyl sulfate (eq 4.6)

Scheme 4

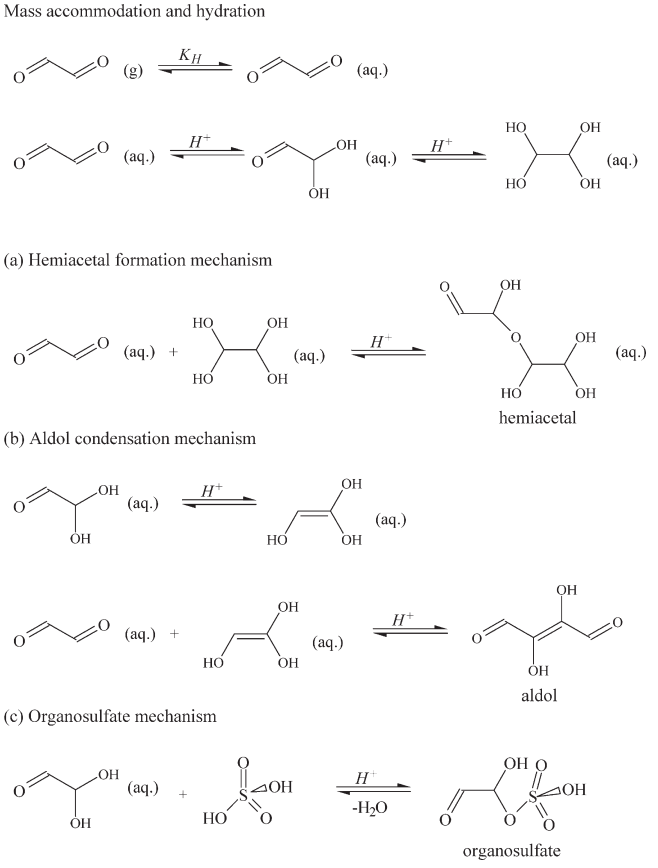

$$ROH + H_2SO_4 \rightleftarrows ROSO_3H + H_2O \quad (4.5)$$

$$ROH + ROSO_3H \rightleftarrows (RO)_2SO_2 + H_2O \quad (4.6)$$

At lower temperatures, the equilibrium shifts to the right-hand side of the reactions, promoting formation of sulfate esters. However, because of the strong temperature dependence of the rate constant for direct reaction of alcohols with sulfuric acid, formation of sulfate esters is kinetically infeasible at lower temperatures.[549] From the dependence of the reaction rate and equilibrium constant on temperature and acidity, it is concluded that heterogeneous reactions between alcohols and sulfuric acid are unlikely of importance in the lower atmosphere except in the case of freshly nucleated aerosols with high acid concentrations.[549]

Wang et al.[501] investigated the heterogeneous reaction of ethanol, 1-butanol, 1-heptanol, and 1-decanol with 4−20 nm H_2SO_4 nanoparticles by the TDMA method at relatively high acidity (50−75 wt %) and the alcohol gaseous concentrations of 10^{13}−10^{16} molecules cm^{-3}. No observable growth is detected within the accuracy of experimental measurements (Table 1), suggesting that esterification of alcohols by H_2SO_4 may contribute negligibly to growth of freshly nucleated particles in the atmosphere, where concentrations of alcohols and particle acidities are substantially lower. This conclusion is in agreement with the lifetime of alcohols estimated by Minerath et al.[549] from the reaction rate between alcohols and H_2SO_4 at high acidity using the atmospheric concentrations of alcohols and the time scale for nucleation growth. In another study, Vaattovaara et al.,[319]

Scheme 5

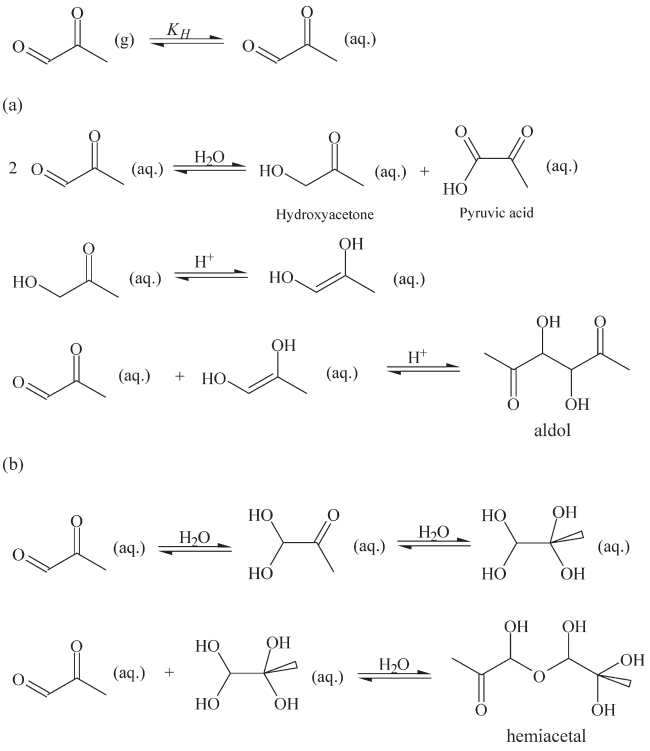

using an ultrafine organic TDMA, observed growth with 6−50 nm seed nanoparticles composed of NH_4HSO_4, H_2SO_4/NH_4HSO_4, citric acid, benzoic acid, and tartaric acid exposed to ethanol at a 72−86% saturation ratio. However, physical partitioning of ethanol vapor, instead of heterogeneous reaction, may be responsible for the observed particle growth because an extremely high ethanol concentration is used in those experiments. A dependence of the growth factor on the initial particle size is noted at ~3% relative humidity.[319] Thermodynamic calculations suggest that the Kelvin effect alone cannot account for the magnitude of the observed variation in the growth factor for particles smaller than 20 nm. The change in the chemical composition of smaller particles due to the higher Laplace pressure from the excess free energy at the highly curved nanoparticle surface is proposed to explain the measured trend.[319]

4.3.6. Other Species. A diversity of organic compounds is present in the atmosphere, many of which possess multiple functional groups that may lead to different types of heterogeneous reactions and possibly contribute to nanoparticle growth. For example, epoxide, cyclic ether with three ring atoms, reacts rapidly with water in acidic medium.[550] Recently, it has been shown that under pristine conditions isoprene is oxidized primarily to hydroxyhydroperoxides and that further oxidation of hydroxyhydroperoxides by the OH radical leads efficiently to formation of dihydroxyepoxides (i.e., epoxydiols).[551] Surratt et al.[552] suggest that secondary organic aerosol formation can be enhanced by the reactive uptake of dihydroxyepoxides, by the acid-catalyzed ring opening of the epoxide in the particle phase, followed by subsequent addition of H_2O, inorganic sulfate, or a 2-methyltetrol and a hydroxyl sulfate ester present in the aerosol phase. A series of laboratory studies have been carried out to measure the bulk hydrolysis reaction kinetics for a number of epoxides, including those formed from the OH radical-initiated reaction of isoprene, and to assess the potential of diol and

dx.doi.org/10.1021/cr2001756 |*Chem. Rev.* 2012, 112, 1957–2011

hydroxyl sulfate ester formation from reactions of epoxides on tropospheric aerosols[550,553,554] using a nuclear magnetic resonance technique. These results suggest that the isoprene-derived dihydroxyepoxides undergo efficient hydrolysis under atmospheric conditions, even in mildly acidic or pH-neutral particles. The hydrolysis reactions of epoxides may hence provide a viable alternative to the kinetically and thermodynamically inefficient reactions between alcohols and sulfuric acid[549] and explain the observation of sulfate esters (organosulfates) in secondary organic aerosols in ambient air and in laboratory chamber studies.

The coexistence of different types of organic compounds in the atmosphere may result in a synergistic effect that also contributes to growth of nanoparticles. For example, chemical analysis of ambient nucleation mode aerosols suggests the presence of formate, acetate, and propionate.[60] However, laboratory experiments indicate that even organic acids of lower volatility, such as *cis*-pinonic acid, do not significantly contribute to nanoparticle composition.[58] This apparent discrepancy between ambient measurements and laboratory experiments can be explained by a synergistic effect between organic acids and alkylamines in ambient air, forming stable salts, reducing the volatility of both components.

5. NUMERICAL TREATMENT OF AMBIENT NANOPARTICLE NUCLEATION AND GROWTH RATES

5.1. Measured Nucleation and Growth Rates

In ambient studies, the number distribution of nucleation mode particles evolves with time and can be well fit with a log-normal distribution that is characterized by the total particle number concentration, N, the geometric mean particle diameter, D_g, and the geometric standard deviation, σ_g. Since the existing analytical methods cannot detect the critical nucleus, only the formation rate of larger particles of the diameter D_p can be measured, rather than the true atmospheric nucleation rate. The particle formation rate, J_D, is defined as the flux of particles growing past the size D_p. When the effects of both coagulation and transport are small compared to the particle production, J_D can be written as[50]

$$J_D = \frac{\Delta N_{D_p, D_{p,\mathrm{Max}}}}{\Delta t} \tag{5.1}$$

where $N_{D_p,D_{p,\mathrm{Max}}}$ is the total particle number concentration in the size range $[D_p, D_{p,\mathrm{Max}}]$ and $D_{p,\mathrm{Max}}$ is the maximum size the critical nucleus can reach during a time of the particle formation event, Δt. This approximation offers a simple formula to estimate new particle formation rate in relatively clean, homogeneous air masses. However, this approach may significantly underestimate the true particle production rate when the nuclei number concentration or the pre-existing particle concentration is high[50] or when an air mass is inhomogeneous and rapid mixing of particles nucleated takes place at the measurement site. The apparent particle growth rate, GR, is then expressed as

$$GR = \frac{\Delta D_g}{\Delta t} \tag{5.2}$$

Note that this equation fails in the case of fast continuous nucleation producing new particles during particle growth.[50] The apparent growth rate of nucleated particles determined from field measurements is typically 1−20 nm h^{-1}.[50,51]

5.2. Condensation Sink of Low-Volatility Vapor

Assuming growth of particles is solely due to condensation of low-volatility vapors,[464] the growth rate can also be expressed as[555−557]

$$\frac{dD_p}{dt} = \frac{4 m_v \beta_M D C}{D_p \rho} \tag{5.3}$$

where m_v is the molecular mass of condensable vapor, β_M is the transitional correction factor for the condensational mass flux,[491] D is the diffusion coefficient of the gas-phase molecules, C is the vapor concentration, and ρ is the particle density. This equation can be integrated from $D_{p,0}$ to D_p to obtain

$$C = \frac{\rho}{\Delta t D m_v}\left(\frac{{D_p}^2 - {D_{p,0}}^2}{8} + \left(\frac{2}{3\alpha} - 0.312\right)\lambda_v (D_p - D_{p,0}) + 0.623{\lambda_v}^2 \ln\frac{2\lambda_v + D_p}{2\lambda_v + D_{p,0}}\right) \tag{5.4}$$

where α is the mass accommodation coefficient and λ_v is the mean free path of the gas molecules.

It should be noted that this approach uses a continuum regime expression together with a transition regime correction factor, e.g., Fuchs−Sutugin,[556] assuming that the condensing molecules have a negligible size compared to aerosols and that the particles have negligible mobility compared to vapor molecules. Such approximations are obviously not valid at the initial stage of particle growth. Using a correction factor that is obtained by equating the generalized coagulation rate, a new analytical expression that includes transition regime effects on growth, molecule size effects on the collision cross section, and particle mobility effects on the relative collisional speeds can be developed.[558,559] Detailed theory and analytical equations have been provided elsewhere.[559]

Furthermore, the flux of low-volatility vapors to the pre-existing particle population, CS, is defined as[556,560]

$$CS = 4\pi D CS' \tag{5.5}$$

where D is the diffusion coefficient of the gas-phase molecules. The condensation sink CS' is integrated over the aerosol size distribution

$$CS' = \int_0^\infty r\beta_M(r) n(r) dr = \sum_i \beta M_i r_i N_i \tag{5.6}$$

where β_M is the transitional correction factor for the condensational mass flux,[491] r_i is the radius of particles in a size class i, and N_i is the number concentration of particles in a size class i.

An alternative approach has been developed to describe the condensation sink of gas-phase molecules, where the Fuchs surface area, A_{Fuchs}, is used to account for the fact that pre-existing atmospheric particles have sizes that fall in the transition between free molecular and diffusional cluster transport regimes.[261,374] The relationship between CS' and A_{Fuchs} is given by the following

$$CS' = \frac{\bar{c} A_{\mathrm{Fuchs}}}{16\pi D} \tag{5.7}$$

where is $\bar{c}$ the mean thermal speed of the gas-phase molecule.[374]

5.3. Combined Growth Including Condensation and Intramodal/Extramodal Coagulation

As discussed above, most analyses of ambient new particle growth rates assume that measured modal growth rates are due to condensation alone. Recently, a numerical method has been

developed to elucidate the contribution of the intramodal coagulation of nucleation mode particles, extramodal coagulation of nucleation mode particles with preexisting particles, and condensation of H_2SO_4 to the nanoparticle growth.[222] In addition to nanoparticle growth by condensation of H_2SO_4, intramodal coagulation of nucleation mode particles leads to an increase in modal size, being more significant at a higher concentration of nucleation mode particles. Extramodal coagulation can also lead to an increase in the mean modal size of the nucleation mode particles, because smaller particles with higher diffusivities are depleted faster than larger particles.

If the nucleated particles are assumed to be dry ammonium sulfate with condensational growth limited by transport of gas-phase sulfuric acid molecules to the particle, the time rates of change of the modal parameters due to the above three mechanisms are approximate values because of applying a first-order transition regime correction in the free molecule regime. The time derivatives of the three modal parameters are obtained from the time derivatives of the zeroth, first, and second moments (M_k, $k = 0, 1, 2$) in particle volume ($v \equiv \pi {D_p}^3/6$) of the mode where

$$M_k(t) \equiv \int_{\text{mode}} v^k n(v,t) \mathrm{d} \ln v = N(t) \cdot {D_g}^{3k}(t) \cdot \exp\left[\frac{9}{2} k^2 \ln^2 \sigma_g(t)\right] \tag{5.8}$$

$$n(v,t) \equiv \frac{\mathrm{d}N}{\mathrm{d} \ln v} = \frac{1}{3} \frac{\mathrm{d}N}{\mathrm{d} \ln D_p} \tag{5.9}$$

For intramodal coagulation, the time derivatives of the moments are

$$\frac{\mathrm{d}M_k}{\mathrm{d}t} = \frac{1}{2} \int_{v_2} \int_{v_2} \left[(v_1 + v_2)^k - {v_1}^k - {v_1}^k\right] \times \beta(v_1, v_2) n(v_2, t) \mathrm{d} \ln v_1 \mathrm{d} \ln v_2 \tag{5.10}$$

where $\beta(v_1,v_2)$ is the Fuchs[485] transition regime collision frequency function for particles of volumes v_1 and v_2 and both integrals are over the nucleation mode.

For extramodal coagulation the time derivatives of the moments can be expressed as

$$\frac{\mathrm{d}M_k}{\mathrm{d}t} = \int_{v_2} \int_{v_2} v^k \beta(v_1, v_2) n(v_1, t) n(v_2, t) \mathrm{d} \ln v_2 \, \mathrm{d} \ln v_1 \tag{5.11}$$

where the outer integral (v_1) is over the nucleation mode and the inner integral (v_2) is over the extramodal region above the nucleation mode.

The rate of sulfuric acid condensation and neutralization process can be written as

$$\frac{\mathrm{d}M_k}{\mathrm{d}t} = N_s(t) \int_v \left[(v + v_n)^k - v^k\right] \beta(v, v_s) n(v, t) \mathrm{d} \ln v \tag{5.12}$$

where v_n and v_s are the respective volumes of $(NH_4)_2SO_4$ and H_2SO_4 molecules, N_s is the number concentration of H_2SO_4 molecules, where $\beta(v,v_s)$ is the Fuchs[485] transition regime collision frequency function for nucleation mode particles of volumes $v$and H_2SO_4 molecules of volumes v_s, and the integral is over the nucleation mode.

This approach has been used to calculate rates of sulfuric acid condensation, intramodal coagulation, and extramodal coagulation during nucleation events in Atlanta, GA, and Beijing, China, and a difference between the apparent growth rate and the sum of the three processes has been identified in some of nucleation events.[222,250] Since the concentrations of molecular clusters are likely 10−100 times lower than that predicted by the collision-controlled theory, condensation of molecular clusters contributes negligibly to measured growth rates.[222] Using the theoretical framework discussed above, Yue et al.[250] found that condensation of sulfuric acid and its subsequent neutralization by ammonia and coagulation contribute to less than 50% of the measured particle growth and concluded that organic compounds are an important contributor to growth of freshly nucleated particles.

5.4. Derivation of Nucleation Rates from Atmospheric Measurements

Nucleation theories suggest that freshly nucleated particles are initially on the order of 1 nm in diameter. However, existing measurement techniques can only detect particles of 1.5−3 nm in size.[1,56] In practice, the measured particle formation rate, J_D, is normally defined as the flux of particles exceeding the size D_p. Hence, it is possible to derive the actual nucleation rate (normally nucleation rate for 1 nm nuclei, J_1) from the measured nucleation rate J_D as a result of condensational growth in the atmosphere. To derive an analytical formula that describes the time evolution of the nuclei number concentration N during growth from their initial size D^* to some larger size D_p, the following assumptions are made: (1) the only important sink for the nuclei is their coagulation to larger pre-existing particles, (2) the nuclei grow by condensation at a constant rate, and (3) the pre-existing population of larger particles remains unchanged during nuclei growth.[560]

As discussed earlier (section 5.1), the apparent nucleation rate J_D, growth rate GR, and condensation sink CS' can be derived from the measurements of the time evolution of the particle size distribution in the size range $[D, D_{Max}]$. The actual nucleation rate J^* is then determined by the competition between condensation growth (GR) and scavenging (rate proportional to condensation sink CS')[478,560]

$$JD_p = J^* \left\{0.23 \left[\frac{1}{D_p} - \frac{1}{D^*}\right] \frac{CS}{GR}\right\} \tag{5.13}$$

where D^* is the size of the nuclei and normally estimated to be 1 nm. Setting the measured formation rate at 3 nm (J_3) gives

$$J_3 = J_1 \left\{-0.153 \frac{CS}{GR}\right\} \tag{5.14}$$

A similar approach has been developed to extrapolate the nucleation rate of 1 nm particles J_1 from time-shifted values of J_3 by incorporating the probability that a particle grows from 1 to 3 nm by vapor condensation before being scavenged by pre-existing aerosols.[253,261,374] The detailed theory and analytical equation can been found elsewhere.[253,261,374]

The estimated value of J_1 is then fit to the corresponding H_2SO_4 concentration according to a power law expression given by eq 3.10, where both the exponent P and the prefactor k are unconstrained fitting parameters. According to the nucleation theorem, the value of the exponent P indicates the number of H_2SO_4 molecules in a critical nucleus.[132,133]

Recently, Korhonen et al.[561] evaluated the performance of several mathematical tools developed previously for analysis of atmospheric new particle formation rates and estimation of nucleation rates and mechanisms. The accuracy of the estimates of particle

formation rate at both 3 and 1.5 nm sizes shows significant sensitivity to the form of the equations used and assumptions made about the initial size of nucleating clusters. The poor estimates of nucleation and growth rates can lead to large uncertainties in the nucleation prefactors and power exponents in eq 3.10. It is also suggested that combining data from several new particle formation events to scatter plots of H_2SO_4 versus formation rates and determining the slope of the regression line may not yield reliable information about the nucleation mechanism, and hence, caution needs to be excercised in interpreting the field results.

6. SUMMARY AND FUTURE RESEARCH NEEDS

Although new particle formation accounts for a major fraction of atmospheric aerosols in various environments, the fundamental chemical processes responsible for aerosol nucleation and growth remain poorly understood.[1] Available results on aerosol nucleation and growth from previous experimental, theoretical, and field studies are conflicting, hindering efforts to develop atmospheric models to simulate formation and growth of secondary aerosols on the regional and global scales. In particular, given the diversity of organic species produced from oxidation of biogenic and anthropogenic hydrocarbons in the atmosphere,[287] major challenges exist to model the sources and processes contributing to formation and growth of nanoparticles by organics.

Atmospheric new particle formation occurs in two distinct stages, i.e., nucleation of the critical nuclei and subsequent growth of the nuclei to larger particles. According to the classical nucleation theory, the critical nucleus corresponds to the free energy maximum of the nucleating system, resulting in a nucleation barrier beyond which the cluster grows spontaneously. A major limitation in the spontaneous growth of nanoparticles, particularly for freshly nucleated particles with a size of 1 to 2 nm, is due to the Kelvin effect. Also, growth competes with capture/removal of clusters by coagulation with pre-existing aerosols.[336] The rate at which nucleation occurs is related to the chemical composition of the critical nucleus and the gaseous concentrations of the nucleating species. The nucleation rate is an important variable in simulations of aerosol formation in regional and global atmospheric models.[392,483] Much of the previous research has focused on nucleation involving sulfuric acid, since sulfate represents an important component of the nucleation mode aerosols[308] and the presence of sulfuric acid in concentrations exceeding 10^5 molecules cm^{-3} has been shown as a necessary condition to observe new particle formation in the atmosphere.[11] Atmospheric measurements have revealed a weak dependence of the nucleation rate on sulfuric acid concentrations, implying that only 1−2 H_2SO_4 molecules may be present in the critical nucleus.[261] Available experimental results, however, show a large variability in the chemical composition of the critical nucleus, ranging from 1 to 10 sulfuric acid molecules, which is inferred indirectly from nucleation rate measurements. Those experimental and field findings raise an important question of whether one or two sulfuric acid molecules are sufficient to form a critical nucleus at the temperatures and concentrations of sulfuric acid corresponding to the lower troposphere.[1] Most recent laboratory experiments and field measurements suggest that this may be plausible only if other stabilizing species are involved in nucleation and present in the critical nucleus. For instance, organic compounds from anthropogenic and biogenic sources may assist the nucleation process either directly, e.g., by amines,[372,376] or following atmospheric photooxidation, such as by organic acids from aromatics[57] and monoterpenes.[58] The presence of amines and organic acids considerably enhances nucleation in the water−sulfuric acid system via formation of strongly hydrogen-bonded clusters containing these organic molecules in addition to sulfuric acid and water.[58,377,378]

Measurements of new particle formation in the free troposphere are mostly consistent with the binary water−sulfuric acid nucleation. In the boundary layer, however, binary nucleation is recognized as incapable of explaining atmospheric nucleation events and several alternative nucleation mechanisms may play a crucial role, including ternary nucleation of sulfuric acid with ammonia or organics and nucleation involving iodine species. The contribution from organics likely explains high aerosol concentrations observed in polluted environments,[264,392] where high concentrations of low-volatility organic species can be produced by direct emissions and by photochemical oxidation of hydrocarbons. Although each of these mechanisms may explain new particle formation in a specific environment, none of them provides a consistent explanation of particle nucleation under a wide range of environmental conditions. Although the activation and kinetic parametrizations of nucleation are suggested to represent a promising way to improve the performance of global models,[481−483] other model analyses indicate that only the ion-mediated nucleation can account for the measured particle number concentrations in the troposphere.[484,562] The relative role of ion-mediated nucleation in the atmospheric remains controversial.[61] Atmospherically measured growth rates of freshly nucleated particles cannot usually be explained solely by the condensation of sulfuric acid and associated water, ammonia, and amines. Low-volatility organic compounds are the most likely candidates for growth of nascent clusters and nanoparticles. The role of heterogeneous reactions of oxidized organics may become progressively important in growth of nanoparticles as their size increases beyond about 4−6 nm.[13]

To improve the understanding of atmospheric new particle formation, further field measurements and laboratory experiments are needed to monitor the gas-phase nucleating vapors and chemical compositions of neutral and ionic clusters and nanoparticles simultaneously. Advanced field measurements are crucial to providing information about the spatial distribution of the rate coefficient in the nucleation parametrizations. To achieve this level of chemical detail, development of more advanced analytical techniques is required, including identification and quantification of diverse gaseous nucleating precursors present in ambient air at the ppb and lower levels and detection and chemical analysis of critical nucleus to sub-10-nm diameter particles. Formation of clusters and their growth to nanoparticles in laboratory experiments needs to be investigated under conditions of atmospherically relevant vapor concentrations and time scales. Further developments in theoretical methods are required to corroborate and validate the results of laboratory experiments and ambient measurements. These include accurate quantum chemical calculations of free energies for formation of molecular clusters to calculate the cluster evaporation rates for use in dynamical atmospheric cluster models and also first-principle MD and MC simulations to investigate the dynamics, structures, and energetics of multicomponent clusters and the role of proton transfer in cluster stabilization.

Furthermore, improved physically based parametrizations of aerosol nucleation and growth developed on the basis of and validated against laboratory, field, and theoretical studies need to be implemented into regional and global atmospheric models to assess the impacts of aerosols on climate, weather, air quality, and human health.

AUTHOR INFORMATION

Corresponding Author

*E-mail: renyi-zhang@tamu.edu.

BIOGRAPHIES

Renyi Zhang received a B.S. degree in Atmospheric Science from Nanjing Institute of Meteorology, a M.S. in Physics from University of Nevada—Reno, and a Ph.D. in Atmospheric Chemistry from MIT (under the supervision of Mario J. Molina). After 3 years of postdoctoral research at NASA-JPL-Caltech, he spent 1 year as a Research Associate with Mario Molina at MIT, before he took on an Assistant Professor position at Texas A&M University in 1997. He was promoted to Associate Professor in 2002 and Professor in 2005. He has held a joint appointment as a professor in the Department of Chemistry at Texas A&M University since 2007. His research focuses on analytical/physical/environmental/atmospheric chemistry, including kinetics and mechanisms of gas-phase and heterogeneous reactions, laboratory studies of formation, growth, and chemical and physical properties of atmospheric aerosols, atmospheric measurements of trace gas species and aerosols, modeling of photochemistry and urban and regional air pollution, and assessment of the aerosol−cloud−climate interaction. He is an Editor of the *Journal of Geophysical Research−Atmospheres*, Director of the Center for Atmospheric Chemistry and Environment, and holder of Harold J. Haynes Endowed Chair at Texas A&M University. Currently, he chairs American Meteorological Society's Atmospheric Chemistry Committee and is a member of International Commission on Atmospheric Chemistry and Global Pollution.

Alexei Khalizov received his undergraduate degree in Chemistry in 1994 from Bashkir State University and a Ph.D. in Physical Chemistry in 1997 from the Ufa Research Center of the Russian Academy of Sciences (UFC RAS), under the supervision of Valery Shereshovets and Sergey Khursan. He then spent 2 years at the UFC RAS Institute of Organic Chemistry studying nonaqueous chemistry of chlorine dioxide. He joined the Atmospheric Chemistry field during his 2000−2002 NATO/NSERC Postdoctoral Fellowship at McGill University, where he investigated the reactions of atmospheric elemental mercury with Parisa Ariya. During 2003−2005, he studied the optical properties and homogeneous freezing of supercooled water aerosols as a Research Associate with Jim Sloan at the University of Waterloo. Since 2005, Alex is an Assistant Research Scientist at Texas A&M University, working with Renyi Zhang. His current research is focused on the chemical and physical transformations and impacts of atmospheric aerosols.

Lin Wang received a B.S. in Chemistry from Fudan University, China, in 1999, a M.S. in Environmental Sciences from Fudan University, China, in 2002, and a Ph.D. in Environmental Toxicology from the University of California, Riverside, in 2006. He is presently a Research Professor in the Department of Environmental Science & Engineering at Fudan University. From 2007 to 2010, he was an Assistant Research Scientist at Texas A&M University, working with Renyi Zhang. His research area is in atmospheric chemistry and physics with a focus on the evolution of atmospheric volatile organic compounds and aerosols in the atmosphere.

Min Hu is Professor and Director of State Key Joint Laboratory of Environmental Simulation and Pollution Control (Peking University), College of Environmental Sciences and Engineering,

Peking University, China. She received her Bachelor degree majoring in Applied Chemistry in 1987 and both Master and Doctorate degrees majoring in Environmental Chemistry in 1990 and 1993, respectively, from Peking University. She worked as a Lecturer and later an Associate Professor in Peking University, and was promoted to professor in the Center for Environmental Sciences (2001−2007) and College of Environmental Sciences and Engineering (June 2007−present) in Peking University. Her research interests span from aerosol characteristics and its impacts to biogenic sulfur emission from sea—dimethyl sulfide (DMS). Recently, her research mainly focuses on aerosol chemical and physical characteristics, source identification, secondary aerosol formation, and its impact on air quality, local visibility degradation, and health effects. She received support by China National Natural Science Foundation for Distinguished Young Scholars in 2010. She is a member of the Editorial Advisory Board of Atmospheric Environment, the Editorial Board of Acta Scientiae Circumstantiae (Chinese), China SOLAS (the Surface Ocean−Lower Atmosphere Study), and China ABC (the Atmospheric Brown Cloud).

Wen Xu is a Ph.D. candidate in the Department of Chemistry at Texas A&M University, College Station, Texas. His dissertation research seeks to elucidate the nucleation and growth mechanisms of atmospheric aerosols. He joined the Zhang's Laboratory in atmospheric chemistry research after receiving a B.S. in Chemical Physics at University of Science & Technology of China in 2008.

ACKNOWLEDGMENT

This work was supported by the Robert A. Welch Foundation (Grant A-1417) and National Science Foundation (AGS-0938352 and CBET-0932705). L.W. acknowledges financial support from the National Natural Science Foundation of China (21107015), Science & Technology Commission of Shanghai Municipality (11PJ1401100), and startup fund of Fudan University. M.H.'s work was supported by the National Natural Science Foundation of China (21025728, 20977001).

GLOSSARY OF ACRONYMS

AIS	air ion spectrometer
AMS	aerosol mass spectrometer
APi-TOF	atmospheric pressure interface time of flight
BCP	bond critical point
BSMA	balanced scanning mobility analyzer
CCN	cloud condensation nuclei
CIMS	chemical ionization mass spectrometry
CLOUD	cosmics leaving outdoor droplets
CN	condensation nuclei
CNT	classical nucleation theory
CPA	*cis*-pinonic acid
CPC	condensation particle counter
CVTST	canonical variational transition state theory
DEG	diethylene glycol
DFT	density functional theory
DMA	differential mobility analyzer
DMPS	differential mobility particle sizer
DNT	dynamical nucleation theory
EUCAARI	European Integrated project on Aerosol Cloud Climate and Air Quality Interactions
FT-ICR-MS	Fourier transform ion cyclotron resonance mass spectrometry
IN	ice nuclei
IMN	ion-mediated nucleation
LJ	Lennard−Jones
MC	Monte Carlo
MD	molecular dynamics
MS	mass spectrometry
NAIS	neutral cluster and air ion spectrometer
NAMS	nano aerosol mass spectrometer
NCCN	nucleation and cloud condensation nuclei
PBL	planetary boundary layer
PHA	pulse height analysis
PIMD	path-integral molecular dynamics
ppb	part per billion
ppm	part per million
ppt	part per trillion
PSI	Paul Scherrer Institute
PSM	particle size magnifier
QTAIM	quantum theory of atoms in molecules
RH	relative humidity
RI	resolution of identity
SMPS	scanning mobility particle sizer
TDCIMS	thermal desorption chemical ionization mass spectrometer
TD-ID-CIMS	thermal desorption−ion drift−chemical ionization mass spectrometer
TDMA	tandem differential mobility analyzer
TIP	transferable intermolecular potential
TMB	1,3,5-trimethylbenzene
UCPC	ultrafine condensation particle counter
VdW	van der Waals
VOCs	volatile organic compounds

REFERENCES

(1) Zhang, R. *Science* **2010**, *328*, 1366, DOI: 10.1126/science.1189732.
(2) Kulmala, M. *Science* **2003**, *302*, 1000.
(3) Vali, G. In *Nucleation and Atmospheric Aerosols*; Kulmala, M., Wagner, P. E., Eds.; 1996.
(4) Martin, S. T. *Chem. Rev.* **2000**, *100*, 3403, DOI: 10.1021/cr990034t.
(5) Jones, S. F.; Evans, G. M.; Galvin, K. P. *Adv. Colloid Interface Sci.* **1999**, *80*, 27.
(6) Kashchiev, D. *Nucleation: basic theory with applications*; Butterworth Heinemann: Oxford, Boston, 2000.
(7) Ford, I. *Proc. Inst. Mech. Eng. C: J. Mech. Eng. Sci.* **2004**, *218*, 883.

(8) Ayers, G. P.; Gillett, R. W.; Gras, J. L. *Geophys. Res. Lett.* **1980**, *7*, 433.
(9) Zhang, R.; Wooldridge, P. J.; Abbatt, J. P. D.; Molina, M. J. *J. Phys. Chem.* **1993**, *97*, 7351.
(10) Marti, J. J.; Jefferson, A.; Cai, X. P.; Richert, C.; McMurry, P. H.; Eisele, F. *J. Geophys. Res.* **1997**, *102*, 3725.
(11) Weber, R. J.; McMurry, P. H.; Mauldin, R. L.; Tanner, D. J.; Eisele, F. L.; Clarke, A. D.; Kapustin, V. N. *Geophys. Res. Lett.* **1999**, *26*, 307.
(12) Nieminen, T.; Manninen, H. E.; Sihto, S. L.; Yli-Juuti, T.; Mauldin, I. R. L.; Petaja, T.; Riipinen, I.; Kerminen, V. M.; Kulmala, M. *Environ. Sci. Technol.* **2009**, *43*, 4715.
(13) Wang, L.; Khalizov, A. F.; Zheng, J.; Xu, W.; Ma, Y.; Lal, V.; Zhang, R. *Nat. Geosci.* **2010**, *3*, 238.
(14) Yue, D. L.; Hu, M.; Zhang, R.; Wu, Z. J.; Sue, H.; Wang, Z. B.; Peng, J. F.; He, L. Y.; Huang, X. F.; Gong, Y. G.; Wiedensohler, A. *Atmos. Environ.* **2011**, *45*, 6070.
(15) IPCC "Intergovernmental Panel on Climate Change. Report. Solomon, S., et al. , Eds.; Cambridge University Press: Cambridge, U.K., 2007; http://www.ipcc.ch/ipccreports/ar4-wg1.htm,".
(16) Fan, J. W.; Zhang, R. Y.; Li, G. H.; Tao, W. K. *J. Geophys. Res.* **2007**, *112*, D14204–D14204, DOI: 10.1029/2006jd008136.
(17) Zhang, R. Y.; Li, G. H.; Fan, J. W.; Wu, D. L.; Molina, M. J. *Proc. Natl. Acad. Sci. U.S.A.* **2007**, *104*, 5295.
(18) Yuan, T. L.; Li, Z. Q.; Zhang, R. Y.; Fan, J. W. *J. Geophys. Res.* **2008**, *113*, D04201, DOI: 10.1029/2007jd008632.
(19) Li, G. H.; Wang, Y.; Lee, K. H.; Diao, Y. W.; Zhang, R. Y. *J. Geophys. Res.* **2009**, *114*, D17205, DOI: 10.1029/2008jd011581.
(20) Li, G. H.; Wang, Y.; Zhang, R. Y. *J. Geophys. Res.* **2008**, *113*, D15211, DOI: 10.1029/2007jd009361.
(21) Fan, J. W.; Zhang, R. Y.; Tao, W. K.; Mohr, K. I. *J. Geophys. Res.* **2008**, *113*, D08209.
(22) Haywood, J.; Boucher, O. *Rev. Geophys.* **2000**, *38*, 513.
(23) Molina, M. J.; Molina, L. T.; Kolb, C. E. *Annu. Rev. Phys. Chem.* **1996**, *47*, 327.
(24) Davidovits, P.; Kolb, C. E.; Williams, L. R.; Jayne, J. T.; Worsnop, D. R. *Chem. Rev.* **2006**, *106*, 1323.
(25) Solomon, S.; Garcia, R. R.; Rowland, F. S.; Wuebbles, D. J. *Nature* **1986**, *321*, 755.
(26) Lee, S. H.; Leard, D. C.; Zhang, R.; Molina, L. T.; Molina, M. J. *Chem. Phys. Lett.* **1999**, *315*, 7.
(27) Zhang, R. Y.; Jayne, J. T.; Molina, M. J. *J. Phys. Chem.* **1994**, *98*, 867.
(28) Molina, M. J.; Zhang, R.; Wooldridge, P. J.; McMahon, J. R.; Kim, J. E.; Chang, H. Y.; Beyer, K. D. *Science* **1993**, *261*, 1418.
(29) Zhang, R. Y.; Wooldridge, P. J.; Molina, M. J. *J. Phys. Chem.* **1993**, *97*, 8541.
(30) Zhang, R. Y.; Leu, M. T.; Keyser, L. F. *J. Phys. Chem.* **1994**, *98*, 13563.
(31) Wooldridge, P. J.; Zhang, R. Y.; Molina, M. J. *J. Geophys. Res.* **1995**, *100*, 1389.
(32) Zhang, R. Y.; Leu, M. T.; Molina, M. J. *Geophys. Res. Lett.* **1996**, *23*, 1669.
(33) Zhang, R.; Leu, M.-T.; Keyser, L. F. *J. Phys. Chem.* **1996**, *100*, 339, DOI: 10.1021/jp952060a.
(34) Zhang, R. Y.; Leu, M. T.; Keyser, L. F. *Geophys. Res. Lett.* **1995**, *22*, 1493.
(35) Molina, M. J.; Molina, L. T.; Zhang, R. Y.; Meads, R. F.; Spencer, D. D. *Geophys. Res. Lett.* **1997**, *24*, 1619.
(36) Lei, W. F.; Zhang, R. Y.; Tie, X. X.; Hess, P. *J. Geophys. Res.* **2004**, *109*, D12301–D12301, DOI: 10.1029/2003jd004219.
(37) Osthoff, H. D.; Roberts, J. M.; Ravishankara, A. R.; Williams, E. J.; Lerner, B. M.; Sommariva, R.; Bates, T. S.; Coffman, D.; Quinn, P. K.; Dibb, J. E.; Stark, H.; Burkholder, J. B.; Talukdar, R. K.; Meagher, J.; Fehsenfeld, F. C.; Brown, S. S. *Nat. Geosci.* **2008**, *1*, 324.
(38) Tie, X.; Madronich, S.; Walters, S.; Zhang, R.; Rasch, P.; Collins, W. *J. Geophys. Res.* **2003**, *108*, 4642, DOI: 10.1029/2003JD003659.
(39) Zhang, R. Y.; Lei, W. F.; Tie, X. X.; Hess, P. *Proc. Natl. Acad. Sci. U.S.A.* **2004**, *101*, 6346, DOI: 10.1073/pnas.0401484101.
(40) Li, G. H.; Zhang, R. Y.; Fan, J. W.; Tie, X. X. *J. Geophys. Res.* **2005**, *110*, D23206, DOI: 10.1029/2005JD005898.
(41) Zhang, R. Y.; Tie, X. X.; Bond, D. W. *Proc. Natl. Acad. Sci. U.S.A.* **2003**, *100*, 1505, DOI: 10.1073/pnas.252763799.
(42) EPA *Air quality criteria for particulate matter*; U.S. Environmental Protection Agency, 2004.
(43) NRC *Research priorities for airborne particulate matter, IV. Continuing research progress*; National Research Council, 2004.
(44) Kunzli, N.; Jerrett, M.; Mack, W. J.; Beckerman, B.; LaBree, L.; Gilliland, F.; Thomas, D.; Peters, J.; Hodis, H. N. *Environ. Health Perspect.* **2005**, *113*, 201, DOI: 10.1289/ehp.7523.
(45) Kimmel, T. A.; Chen, L. C.; Bosland, M. C.; Nadziejko, C. *Toxicol. Appl. Pharmacol.* **1997**, *144*, 348.
(46) Schlesinger, R. B.; Kunzli, N.; Hidy, G. M.; Gotschi, T.; Jerrett, M. *Inhal. Toxicol.* **2006**, *18*, 95, DOI: 10.1080/08958370500306016.
(47) Oberdorster, G.; Sharp, Z.; Atudorei, V.; Elder, A.; Gelein, R.; Kreyling, W.; Cox, C. *Inhal. Toxicol.* **2004**, *16*, 437.
(48) Araujo, J. A.; Barajas, B.; Kleinman, M.; Wang, X.; Bennett, B. J.; Gong, K. W.; Navab, M.; Harkema, J.; Sioutas, C.; Lusis, A. J.; Nel, A. E. *Circ. Res.* **2008**, *102*, 589, DOI: 10.1161/circresaha.107.164970.
(49) McMurry, P. H.; Woo, K. S.; Weber, R.; Chen, D. R.; Pui, D. Y. H. *Philos. Trans. R. Soc. London, Ser. a: Math. Phys. Eng. Sci.* **2000**, *358*, 2625.
(50) Kulmala, M.; Vehkamaki, H.; Petaja, T.; Dal Maso, M.; Lauri, A.; Kerminen, V. M.; Birmili, W.; McMurry, P. H. *J. Aerosol Sci* **2004**, *35*, 143, DOI: 10.1016/j.jaerosci.2003.10.003.
(51) Holmes, N. S. *Atmos. Environ.* **2007**, *41*, 2183, DOI: 10.1016/j.atmosenv.2006.10.058.
(52) O'Dowd, C. D.; Hoffmann, T. *Environ. Chem.* **2005**, *2*, 245, DOI: 10.1071/en05077.
(53) Curtius, J. *C. R. Phys.* **2006**, *7*, 1027.
(54) Kulmala, M.; Kerminen, V.-M. *Atmos. Res.* **2008**, *90*, 132.
(55) Hegg, D. A.; Baker, M. B. *Rep. Prog. Phys.* **2009**, *72*, 056801.
(56) Bzdek, B. R.; Johnston, M. V. *Anal. Chem.* **2010**, *82*, 7871, DOI: 10.1021/ac100856j.
(57) Zhang, R. Y.; Suh, I.; Zhao, J.; Zhang, D.; Fortner, E. C.; Tie, X. X.; Molina, L. T.; Molina, M. J. *Science* **2004**, *304*, 1487.
(58) Zhang, R.; Wang, L.; Khalizov, A. F.; Zhao, J.; Zheng, J.; McGraw, R. L.; Molina, L. T. *Proc. Natl. Acad. Sci. U.S.A.* **2009**, *106*, 17650, DOI: 10.1073/pnas.0910125106.
(59) Sipila, M.; Berndt, T.; Petaja, T.; Brus, D.; Vanhanen, J.; Stratmann, F.; Patokoski, J.; Mauldin, R. L.; Hyvarinen, A.-P.; Lihavainen, H.; Kulmala, M. *Science* **2010**, *327*, 1243, DOI: 10.1126/science.1180315.
(60) Smith, J. N.; Barsanti, K. C.; Friedli, H. R.; Ehn, M.; Kulmala, M.; Collins, D. R.; Scheckman, J. H.; Williams, B. J.; McMurry, P. H. *Proc. Natl. Acad. Sci. U.S.A.* **2010**, *107*, 6634, DOI: 10.1073/pnas.0912127107.
(61) Yu, F.; Turco, R. *Atmos. Chem. Phys. Discuss* **2011**, *11*, 11281, DOI: 10.5194/acpd-11-11281-2011.
(62) Truhlar, D. G.; Garrett, B. C.; Klippenstein, S. J. *J. Phys. Chem.* **1996**, *100*, 12771.
(63) Suh, I.; Lei, W. F.; Zhang, R. Y. *J. Phys. Chem. A* **2001**, *105*, 6471, DOI: 10.1021/jp0105950.
(64) Lei, W. F.; Zhang, R. Y.; McGivern, W. S.; Derecskei-Kovacs, A.; North, S. W. *Chem. Phys. Lett.* **2000**, *326*, 109.
(65) Zhang, D.; Zhang, R.; North, S. W. *J. Phys. Chem.* **2003**, *107*, 11013.
(66) Zhang, D.; Lei, W. F.; Zhang, R. Y. *Chem. Phys. Lett.* **2002**, *358*, 171.
(67) Zhang, D.; Zhang, R. Y.; Park, J.; North, S. W. *J. Am. Chem. Soc.* **2002**, *124*, 9600, DOI: 10.1021/ja0255195.
(68) Suh, I.; Zhang, D.; Zhang, R. Y.; Molina, L. T.; Molina, M. J. *Chem. Phys. Lett.* **2002**, *364*, 454.
(69) Lei, W. F.; Zhang, R. Y. *J. Phys. Chem. A* **2001**, *105*, 3808.
(70) Lei, W. F.; Zhang, R. Y.; McGivern, W. S.; Derecskei-Kovacs, A.; North, S. W. *J. Phys. Chem. A* **2001**, *105*, 471.
(71) Truhlar, D. G.; Garrett, B. C. *Annu. Rev. Phys. Chem.* **1984**, *35*, 159.

(72) Nadykto, A. B.; Al Natsheh, A.; Yu, F.; Mikkelsen, K. V.; Herb, J. In *Advances in Quantum Chemistry*; Michael, E. G., Matthew, S. J., Eds.; Academic Press: New York, 2008; Vol. 55.
(73) Kathmann, S. M.; Schenter, G. K.; Garrett, B. C. *J. Chem. Phys.* **2002**, *116*, 5046, DOI: 10.1063/1.1451059.
(74) Kathmann, S. M. *Theor. Chem. Acc.* **2006**, *116*, 169, DOI: 10.1007/s00214-005-0018-8.
(75) Kathmann, S. M.; Schenter, G. K.; Garrett, B. C.; Chen, B.; Siepmann, J. I. *J. Phys. Chem. C* **2009**, *113*, 10354, DOI: 10.1021/jp8092226.
(76) Becker, R.; Doring, W. *Ann. Phys.-Berlin* **1935**, *24*, 719.
(77) Frenkel, J. *J. Chem. Phys.* **1939**, *7*, 200.
(78) Volmer, M.; Weber, A. *Z. Phys. Chem., Stochiom. Verw.* **1926**, *119*, 277.
(79) Farkas, L. *Z. Phys. Chem., Stochiom. Verw.* **1927**, *125*, 236.
(80) Flood, H. *Z. Phys. Chem. A: Chem. Thermodyn. Kinet. Elektrochem. Eigensch.* **1934**, *170*, 286.
(81) Reiss, H. *J. Chem. Phys.* **1950**, *18*, 840.
(82) Seinfeld, J. H.; Pandis, S. N. *Atmospheric chemistry and physics: from air pollution to climate change*, 2nd ed.; John Wiley & Sons: Hoboken, NJ, 2006.
(83) McGraw, R. *J. Chem. Phys.* **1995**, *102*, 2098.
(84) Hung, C.-H.; Krasnopoler, M. J.; Katz, J. L. *J. Chem. Phys.* **1989**, *90*, 1856.
(85) Agarwal, G.; Heist, R. H. *J. Chem. Phys.* **1980**, *73*, 902.
(86) Thompson, S. M.; Gubbins, K. E.; Walton, J. P. R. B.; Chantry, R. A. R.; Rowlinson, J. S. *J. Chem. Phys.* **1984**, *81*, 530.
(87) Koga, K.; Zeng, X. C.; Shchekin, A. K. *J. Chem. Phys.* **1998**, *109*, 4063.
(88) Heath, C. H.; Streletzky, K. A.; Wyslouzil, B. E.; Wolk, J.; Strey, R. *J. Chem. Phys.* **2003**, *118*, 5465, DOI: 10.1063/1.1554736.
(89) Nadykto, A. B.; Al Natsheh, A.; Yu, F. Q.; Mikkelsen, K. V.; Ruuskanen, J. *Phys. Rev. Lett.* **2006**, *96*, 125701, DOI: 10.1103/PhysRevLett.96.125701.
(90) Merikanto, J.; Zapadinsky, E.; Lauri, A.; Vehkamaki, H. *Phys. Rev. Lett.* **2007**, *98*, 145702, DOI: 10.1103/PhysRevLett.98.145702.
(91) Du, H.; Nadykto, A. B.; Yu, F. Q. *Phys. Rev. E* **2009**, *79*, 021604, DOI: 10.1103/PhysRevE.79.021604.
(92) Courtney, W. G. *J. Chem. Phys.* **1961**, *35*, 2249.
(93) Shizgal, B.; Barrett, J. C. *J. Chem. Phys.* **1989**, *91*, 6505.
(94) Girshick, S. L.; Chiu, C. P. *J. Chem. Phys.* **1990**, *93*, 1273.
(95) Sorokin, A.; Vancassel, X.; Mirabel, P. *J. Chem. Phys.* **2005**, *123*, 244508, DOI: 10.1063/1.2141511.
(96) Kathmann, S. M.; Schenter, G. K.; Garrett, B. C. In *Advances in nQuantum Chemistry*; Michael, E. G., Matthew, S. J., Eds.; Academic Press: New York, 2008; Vol. 55.
(97) Ruckenstein, E.; Djikaev, Y. S. *Adv. Colloid Interface Sci.* **2005**, *118*, 51, DOI: 10.1016/j.cis.2005.06.001.
(98) Nowakowski, B.; Ruckenstein, E. *J. Chem. Phys.* **1991**, *94*, 1397.
(99) Nowakowski, B.; Ruckenstein, E. *J. Chem. Phys.* **1991**, *94*, 8487.
(100) Djikaev, Y. S.; Ruckenstein, E. *J. Chem. Phys.* **2005**, *123*, 214503, DOI: 10.1063/1.2135777.
(101) Schenter, G. K.; Kathmann, S. M.; Garrett, B. C. *Phys. Rev. Lett.* **1999**, *82*, 3484.
(102) Kathmann, S. M.; Schenter, G. K.; Garrett, B. C. *J. Chem. Phys.* **2004**, *120*, 9133, DOI: 10.1063/1.1695323.
(103) ten Wolde, P. R.; Oxtoby, D. W.; Frenkel, D. *J. Chem. Phys.* **1999**, *111*, 4762.
(104) Frenkel, D.; Smit, B. *Understanding molecular simulation: from algorithms to applications*, 2nd ed.; Academic: San Diego, CA, London, 2002.
(105) Reiss, H.; Katz, J. L.; Cohen, E. R. *J. Chem. Phys.* **1968**, *48*, 5553.
(106) Reiss, H.; Tabazadeh, A.; Talbot, J. *J. Chem. Phys.* **1990**, *92*, 1266.
(107) Laasonen, K.; Wonczak, S.; Strey, R.; Laaksonen, A. *J. Chem. Phys.* **2000**, *113*, 9741.
(108) Matsumoto, M.; Saito, S.; Ohmine, I. *Nature* **2002**, *416*, 409.
(109) Torrie, G. M.; Valleau, J. P. *Chem. Phys. Lett.* **1974**, *28*, 578.
(110) Vanduijneveldt, J. S.; Frenkel, D. *J. Chem. Phys.* **1992**, *96*, 4655.
(111) ten Wolde, P. R.; Frenkel, D. *J. Chem. Phys.* **1998**, *109*, 9901.
(112) Kusaka, I.; Wang, Z. G.; Seinfeld, J. H. *J. Chem. Phys.* **1998**, *108*, 6829.
(113) Tang, H. Y.; Ford, I. J. *J. Chem. Phys.* **2006**, *125*, 144316, DOI: 10.1063/1.2357147.
(114) Jorgensen, W. L.; Chandrasekhar, J.; Madura, J. D.; Impey, R. W.; Klein, M. L. *J. Chem. Phys.* **1983**, *79*, 926.
(115) Yasuoka, K.; Matsumoto, M. *J. Chem. Phys.* **1998**, *109*, 8463.
(116) Liu, J. Z.; Yang, L.; Doren, D. *J. Chem. Phys.* **2006**, *323*, 579, DOI: 10.1016/j.chemphys.2005.10.026.
(117) Merikanto, J.; Vehkamaki, H.; Zapadinsky, E. *J. Chem. Phys.* **2004**, *121*, 914, DOI: 10.1063/1.1740754.
(118) VandeVondele, J.; Krack, M.; Mohamed, F.; Parrinello, M.; Chassaing, T.; Hutter, J. *Comput. Phys. Commun.* **2005**, *167*, 103, DOI: 10.1016/j.cpc.2004.12.014.
(119) Kakizaki, A.; Motegi, H.; Yoshikawa, T.; Takayanagi, T.; Shiga, M.; Tachikawa, M. *J. Mol. Struct. THEOCHEM* **2009**, *901*, 1, DOI: 10.1016/j.theochem.2009.01.022.
(120) Ramakrishnan, T. V.; Yussouff, M. *Solid State Commun.* **1977**, *21*, 389.
(121) Lee, D. J.; Dagama, M. M. T.; Gubbins, K. E. *J. Chem. Phys.* **1986**, *85*, 490.
(122) Oxtoby, D. W.; Evans, R. *J. Chem. Phys.* **1988**, *89*, 7521.
(123) Oxtoby, D. W. *J. Phys.: Condens. Matter* **1992**, *4*, 7627.
(124) Evans, R. *Adv. Phys.* **1979**, *28*, 143.
(125) Granasy, L.; Jurek, Z.; Oxtoby, D. W. *Phys. Rev. E* **2000**, *62*, 7486.
(126) Obeidat, A.; Wilemski, G. *Atmos. Res.* **2006**, *82*, 481, DOI: 10.1016/j.atmosres.2006.02.005.
(127) Talanquer, V.; Oxtoby, D. W. *J. Chem. Phys.* **1996**, *104*, 1993.
(128) Laaksonen, A.; McGraw, R.; Vehkamaki, H. *J. Chem. Phys.* **1999**, *111*, 2019.
(129) Zeng, X. C.; Oxtoby, D. W. *J. Chem. Phys.* **1991**, *95*, 5940.
(130) Langer, J. S.; Turski, L. A. *Phys. Rev. A* **1973**, *8*, 3230.
(131) Talanquer, V.; Oxtoby, D. W. *J. Chem. Phys.* **1993**, *99*, 4670.
(132) Kashchiev, D. *J. Chem. Phys.* **1982**, *76*, 5098.
(133) Oxtoby, D. W.; Kashchiev, D. *J. Chem. Phys.* **1994**, *100*, 7665.
(134) Viisanen, Y.; Strey, R.; Reiss, H. *J. Chem. Phys.* **1993**, *99*, 4680.
(135) Ford, I. J. *Phys. Rev. E* **1997**, *56*, 5615.
(136) Strey, R.; Viisanen, Y. *J. Chem. Phys.* **1993**, *99*, 4693.
(137) Viisanen, Y.; Strey, R.; Laaksonen, A.; Kulmala, M. *J. Chem. Phys.* **1994**, *100*, 6062.
(138) McGraw, R.; Wu, D. T. *J. Chem. Phys.* **2003**, *118*, 9337, DOI: 10.1063/1.1565098.
(139) McGraw, R.; Zhang, R. Y. *J. Chem. Phys.* **2008**, *128*, 064508, DOI: 10.1063/1.2830030.
(140) Katz, J. L. *J. Chem. Phys.* **1970**, *52*, 4733.
(141) Schmitt, J. L. *Rev. Sci. Instrum.* **1981**, *52*, 1749.
(142) Wagner, P. E.; Strey, R. *J. Phys. Chem.* **1981**, *85*, 2694.
(143) Heist, R. H.; He, H. H. *J. Phys. Chem. Ref. Data* **1994**, *23*, 781.
(144) Miller, R. C.; Anderson, R. J.; Kassner, J. L.; Hagen, D. E. *J. Chem. Phys.* **1983**, *78*, 3204.
(145) Schmitt, J. L.; Adams, G. W.; Zalabsky, R. A. *J. Chem. Phys.* **1982**, *77*, 2089.
(146) Strey, R.; Wagner, P. E.; Schmeling, T. *J. Chem. Phys.* **1986**, *84*, 2325.
(147) Schmitt, J. L.; Zalabsky, R. A.; Adams, G. W. *J. Chem. Phys.* **1983**, *79*, 4496.
(148) Adams, G. W.; Schmitt, J. L.; Zalabsky, R. A. *J. Chem. Phys.* **1984**, *81*, 5074.
(149) Wagner, P. E.; Strey, R. *J. Chem. Phys.* **1984**, *80*, 5266.
(150) Fladerer, A.; Strey, R. *J. Chem. Phys.* **2006**, *124*, 164710.
(151) Iland, K.; Wolk, J.; Strey, R.; Kashchiev, D. *J. Chem. Phys.* **2007**, *127*, 154506.
(152) Iland, K.; Wedekind, J.; Wolk, J.; Strey, R. *J. Chem. Phys.* **2009**, *130*, 114508, DOI: 10.1063/1.3078246.
(153) Schmitt, J. L.; Whitten, J.; Adams, G. W.; Zalabsky, R. A. *J. Chem. Phys.* **1990**, *92*, 3693.

(154) Peters, F.; Paikert, B. *J. Chem. Phys.* **1989**, *91*, 5672.
(155) Looijmans, K. N. H.; Kriesels, P. C.; Vandongen, M. E. H. *Exp. Fluids* **1993**, *15*, 61.
(156) Looijmans, K. N. H.; vanDongen, M. E. H. *Exp. Fluids* **1997**, *23*, 54.
(157) Holten, V.; Labetski, D. G.; van Dongen, M. E. H. *J. Chem. Phys.* **2005**, *123*, 104505, DOI: 10.1063/1.2018638.
(158) Wyslouzil, B. E.; Heath, C. H.; Cheung, J. L.; Wilemski, G. *J. Chem. Phys.* **2000**, *113*, 7317.
(159) Kim, Y. J.; Wyslouzil, B. E.; Wilemski, G.; Wolk, J.; Strey, R. *J. Phys. Chem. A* **2004**, *108*, 4365, DOI: 10.1021/jp037030j.
(160) Ghosh, D.; Bergmann, D.; Schwering, R.; Wolk, J.; Strey, R.; Tanimura, S.; Wyslouzil, B. E. *J. Chem. Phys.* **2010**, *132*, 024307, DOI: 10.1063/1.3274629.
(161) Tanimura, S.; Wyslouzil, B. E.; Zahniser, M. S.; Shorter, J. H.; Nelson, D. D.; McManus, B. *J. Chem. Phys.* **2007**, *127*, 034305, DOI: 10.1063/1.2748397.
(162) Wyslouzil, B. E.; Wilemski, G.; Strey, R.; Seifert, S.; Winans, R. E. *Phys. Chem. Chem. Phys.* **2007**, *9*, 5353, DOI: 10.1039/b709363b.
(163) Tanimura, S.; Dieregsweiler, U. M.; Wyslouzil, B. E. *J. Chem. Phys.* **2010**, *133*, 174305, DOI: 10.1063/1.3493488.
(164) Matthew, M. W.; Steinwandel, J. *J. Aerosol Sci* **1983**, *14*, 755.
(165) Zahoransky, R. A.; Hoschele, J.; Steinwandel, J. *J. Chem. Phys.* **1995**, *103*, 9038.
(166) Sinha, S.; Bhabhe, A.; Laksmono, H.; Wolk, J.; Strey, R.; Wyslouzil, B. *J. Chem. Phys.* **2010**, *132*, 064304, DOI: 10.1063/1.3299273.
(167) Sinha, S.; Laksmono, H.; Wyslouzil, B. E. *Rev. Sci. Instrum.* **2008**, *79*, 114101, DOI: 10.1063/1.3006002.
(168) Anisimov, M. P.; Hämeri, K.; Kulmala, M. *J. Aerosol Sci* **1994**, *25*, 23.
(169) Vohra, V.; Heist, R. H. *J. Chem. Phys.* **1996**, *104*, 382.
(170) Hameri, K.; Kulmala, M.; Krissinel, E.; Kodenyov, G. *J. Chem. Phys.* **1996**, *105*, 7683.
(171) Nguyen, H. V.; Okuyama, K.; Mimura, T.; Kousaka, Y.; Flagan, R. C.; Seinfeld, J. H. *J. Colloid Interface Sci.* **1987**, *119*, 491.
(172) Mikheev, V. B.; Laulainen, N. S.; Barlow, S. E.; Knott, M.; Ford, I. J. *J. Chem. Phys.* **2000**, *113*, 3704.
(173) Hameri, K.; Kulmala, M. *J. Chem. Phys.* **1996**, *105*, 7696.
(174) Mikheev, V. B.; Irving, P. M.; Laulainen, N. S.; Barlow, S. E.; Pervukhin, V. V. *J. Chem. Phys.* **2002**, *116*, 10772, DOI: 10.1063/1.1480274.
(175) Pesthy, A. J.; Flagan, R. C.; Seinfeld, J. H. *J. Colloid Interface Sci.* **1983**, *91*, 525.
(176) Barrett, J. C.; Baldwin, T. J. *J. Aerosol Sci* **2000**, *31*, 633.
(177) Housiadas, C.; Papanicolaou, E.; Drossinos, Y. *J. Aerosol Sci* **2002**, *33*, 797.
(178) Okuyama, K.; Kousaka, Y.; Kreidenweis, S.; Flagan, R. C.; Seinfeld, J. H. *J. Chem. Phys.* **1988**, *89*, 6442.
(179) Wyslouzil, B. E.; Seinfeld, J. H.; Flagan, R. C.; Okuyama, K. *J. Chem. Phys.* **1991**, *94*, 6827.
(180) Viisanen, Y.; Kulmala, M.; Laaksonen, A. *J. Chem. Phys.* **1997**, *107*, 920.
(181) Ball, S. M.; Hanson, D. R.; Eisele, F. L.; McMurry, P. H. *J. Geophys. Res.* **1999**, *104*, 23709.
(182) Brus, D.; Hyvärinen, A. P.; Viisanen, Y.; Kulmala, M.; Lihavainen, H. *Atmos. Chem. Phys.* **2010**, *10*, 2631, DOI: 10.5194/acp-10-2631-2010.
(183) Boulaud, D.; Madelaine, G.; Vigla, D. *J. Chem. Phys.* **1977**, *66*, 4854.
(184) Young, L. H.; Benson, D. R.; Kameel, F. R.; Pierce, J. R.; Junninen, H.; Kulmala, M.; Lee, S. H. *Atmos. Chem. Phys.* **2008**, *8*, 4997.
(185) Berndt, T.; Boge, O.; Stratmann, F. *Atmos. Environ.* **2004**, *38*, 2145.
(186) Berndt, T.; Boge, O.; Stratmann, F.; Heintzenberg, J.; Kulmala, M. *Science* **2005**, *307*, 698.
(187) McMurry, P. H.; Friedlander, S. K. *Atmos. Environ.* **1979**, *13*, 1635.
(188) Metzger, A.; Verheggen, B.; Dommen, J.; Duplissy, J.; Prevot, A. S. H.; Weingartner, E.; Riipinen, I.; Kulmala, M.; Spracklen, D. V.; Carslaw, K. S.; Baltensperger, U. *Proc. Natl. Acad. Sci. U.S.A.* **2010**, *107*, 6646, DOI: 10.1073/pnas.0911330107.
(189) Strey, R.; Wagner, P. E.; Viisanen, Y. *J. Phys. Chem.* **1994**, *98*, 7748.
(190) McGraw, R. *J. Chem. Phys.* **1981**, *75*, 5514.
(191) Zahoransky, R. A.; Hoschele, J.; Steinwandel, J. *J. Chem. Phys.* **1999**, *110*, 8842.
(192) Reguera, D.; Reiss, H. *Phys. Rev. Lett.* **2004**, *93*, 165701, DOI: 10.1103/PhysRevLett.93.165701.
(193) Wolk, J.; Strey, R. *J. Phys. Chem. B* **2001**, *105*, 11683, DOI: 10.1021/jp0115805.
(194) Rudek, M. M.; Fisk, J. A.; Chakarov, V. M.; Katz, J. L. *J. Chem. Phys.* **1996**, *105*, 4707.
(195) Grassmann, A.; Peters, F. *J. Chem. Phys.* **2002**, *116*, 7617, DOI: 10.1063/1.1465400.
(196) Lihavainen, H.; Viisanen, Y.; Kulmala, M. *J. Chem. Phys.* **2001**, *114*, 10031.
(197) Rudek, M. M.; Katz, J. L.; Vidensky, I. V.; Zdimal, V.; Smolik, J. *J. Chem. Phys.* **1999**, *111*, 3623.
(198) Kane, D.; ElShall, M. S. *J. Chem. Phys.* **1996**, *105*, 7617.
(199) Ferguson, F. T.; Nuth, J. A. *J. Chem. Phys.* **2000**, *113*, 4093.
(200) Martinez, D. M.; Ferguson, F. T.; Heist, R. H.; Nuth, J. A. *J. Chem. Phys.* **2005**, *123*, 054323, DOI: 10.1063/1.1998834.
(201) Fisk, J. A.; Rudek, M. M.; Katz, J. L.; Beiersdof, D.; Uchtmann, H. *Atmos. Res.* **1998**, *46*, 211.
(202) Onischuk, A. A.; Purtov, P. A.; Baklanov, A. M.; Karasev, V. V.; Vosel, S. V. *J. Chem. Phys.* **2006**, *124*, 014506, DOI: 10.1063/1.2140268.
(203) Martens, J.; Uchtmann, H.; Hensel, F. *J. Phys. Chem.* **1987**, *91*, 2489.
(204) Uchtmann, H.; Dettmer, R.; Baranovskii, S. D.; Hensel, F. *J. Chem. Phys.* **1998**, *108*, 9775.
(205) Bahadur, R.; McClurg, R. B. *J. Chem. Phys.* **2004**, *121*, 12499, DOI: 10.1063/1.1804601.
(206) Knight, W. D.; Clemenger, K.; Deheer, W. A.; Saunders, W. A.; Chou, M. Y.; Cohen, M. L. *Phys. Rev. Lett.* **1984**, *52*, 2141.
(207) Develyn, M. P.; Rice, S. A. *J. Chem. Phys.* **1983**, *78*, 5081.
(208) Allen, L. B.; Kassner, J. L. *J. Colloid Interface Sci.* **1969**, *30*, 81.
(209) Heist, R. H.; Reiss, H. *J. Chem. Phys.* **1973**, *59*, 665.
(210) Maršík, F.; Němec, T.; Hrubý, J.; Demo, P.; Kožíšek, Z.; Petr, V.; Kolovratník, M. *J. Solution Chem.* **2008**, *37*, 1671.
(211) McGraw, R.; Laaksonen, A. *Phys. Rev. Lett.* **1996**, *76*, 2754.
(212) Rodemann, T.; Peters, F. *J. Chem. Phys.* **1996**, *105*, 5168.
(213) Tarek, M.; Klein, M. L. *J. Phys. Chem. A* **1997**, *101*, 8639.
(214) Viisanen, Y.; Wagner, P. E.; Strey, R. *J. Chem. Phys.* **1998**, *108*, 4257.
(215) Viisanen, Y.; Strey, R. *J. Chem. Phys.* **1996**, *105*, 8293.
(216) Doyle, G. J. *J. Chem. Phys.* **1961**, *35*, 795.
(217) Hanson, D. R.; Eisele, F. *J. Phys. Chem. A* **2000**, *104*, 1715.
(218) Giauque, W. F.; Hornung, E. W.; Kunzler, J. E.; Rubin, T. R. *J. Am. Chem. Soc.* **1960**, *82*, 62.
(219) Laaksonen, A.; Talanquer, V.; Oxtoby, D. W. *Annu. Rev. Phys. Chem.* **1995**, *46*, 489.
(220) Anisimov, M. P.; Fominykh, E. G.; Akimov, S. V.; Hopke, P. K. *J. Aerosol Sci* **2009**, *40*, 733, DOI: 10.1016/j.jaerosci.2009.06.002.
(221) Dunn, M. J.; Jimenez, J. L.; Baumgardner, D.; Castro, T.; McMurry, P. H.; Smith, J. N. *Geophys. Res. Lett.* **2004**, *31*, L10102, DOI: 10.1029/2004gl019483.
(222) Stolzenburg, M. R.; McMurry, P. H.; Sakurai, H.; Smith, J. N.; Mauldin, R. L.; Eisele, F. L.; Clement, C. F. *J. Geophys. Res.* **2005**, *110*, D22S05.
(223) Dal Maso, M.; Kulmala, M.; Riipinen, I.; Wagner, R.; Hussein, T.; Aalto, P. P.; Lehtinen, K. E. J. *Boreal Environ. Res.* **2005**, *10*, 323.
(224) Pryor, S. C.; Spaulding, A. M.; Barthelmie, R. J. *Atmos. Environ.* **2010**, *44*, 4413, DOI: 10.1016/j.atmosenv.2010.07.045.
(225) Wehner, B.; Petaja, T.; Boy, M.; Engler, C.; Birmili, W.; Tuch, T.; Wiedensohler, A.; Kulmala, M. *Geophys. Res. Lett.* **2005**, *32*, L17810, DOI: 10.1029/2005gl023827.
(226) O'Dowd, C. D.; Jimenez, J. L.; Bahreini, R.; Flagan, R. C.; Seinfeld, J. H.; Hameri, K.; Pirjola, L.; Kulmala, M.; Jennings, S. G.; Hoffmann, T. *Nature* **2002**, *417*, 632.

(227) Wen, J.; Zhao, Y. J.; Wexler, A. S. *J. Geophys. Res.* **2006**, *111*, D08207, DOI: 10.1029/2005jd006210.
(228) Komppula, M.; Lihavainen, H.; Hatakka, J.; Paatero, J.; Aalto, P.; Kulmala, M.; Viisanen, Y. *J. Geophys. Res.* **2003**, *108*, 4295, DOI: 10.1029/2002jd002939.
(229) Koponen, I. K.; Virkkula, A.; Hillamo, R.; Kerminen, V. M.; Kulmala, M. *J. Geophys. Res.* **2003**, *108*, 4587, DOI: 10.1029/2003jd003614.
(230) Asmi, E.; Frey, A.; Virkkula, A.; Ehn, M.; Manninen, H. E.; Timonen, H.; Tolonen-Kivimaki, O.; Aurela, M.; Hillamo, R.; Kulmala, M. *Atmos. Chem. Phys.* **2010**, *10*, 4253, DOI: 10.5194/acp-10-4253-2010.
(231) Brock, C. A.; Trainer, M.; Ryerson, T. B.; Neuman, J. A.; Parrish, D. D.; Holloway, J. S.; Nicks, D. K.; Frost, G. J.; Hubler, G.; Fehsenfeld, F. C.; Wilson, J. C.; Reeves, J. M.; Lafleur, B. G.; Hilbert, H.; Atlas, E. L.; Donnelly, S. G.; Schauffler, S. M.; Stroud, V. R.; Wiedinmyer, C. *J. Geophys. Res.* **2003**, *108*, 4111, DOI: 10.1029/2002jd002746.
(232) Kittelson, D. B.; Watts, W. F.; Johnson, J. P. *Atmos. Environ.* **2004**, *38*, 9, DOI: 10.1016/j.atmosenv.2003.09.037.
(233) Stolzenburg, M. R.; McMurry, P. H. *Aerosol Sci. Technol.* **1991**, *14*, 48.
(234) Winklmayr, W.; Reischl, G. P.; Lindner, A. O.; Berner, A. *J. Aerosol Sci* **1991**, *22*, 289.
(235) Chen, D. R.; Pui, D. Y. H.; Hummes, D.; Fissan, H.; Quant, F. R.; Sem, G. J. *J. Aerosol Sci* **1998**, *29*, 497.
(236) Eisele, F. L.; Tanner, D. J. *J. Geophys. Res.* **1993**, *98*, 9001.
(237) Birmili, W.; Berresheim, H.; Plass-Dülmer, C.; Elste, T.; Gilge, S.; Wiedensohler, A.; Uhrner, U. *Atmos. Chem. Phys.* **2003**, *3*, 361, DOI: 10.5194/acp-3-361-2003.
(238) Kazil, J.; Harrison, R. G.; Lovejoy, E. R. *Space Sci. Rev.* **2008**, *137*, 241, DOI: 10.1007/s11214-008-9388-2.
(239) Enghoff, M. B.; Svensmark, H. *Atmos. Chem. Phys.* **2008**, *8*, 4911.
(240) Hirsikko, A.; Nieminen, T.; Gagné, S.; Lehtipalo, K.; Manninen, H. E.; Ehn, M.; Hõrrak, U.; Kerminen, V. M.; Laakso, L.; McMurry, P. H.; Mirme, A.; Mirme, S.; Petäjä, T.; Tammet, H.; Vakkari, V.; Vana, M.; Kulmala, M. *Atmos. Chem. Phys.* **2011**, *11*, 767, DOI: 10.5194/acp-11-767-2011.
(241) O'Dowd, C. D.; De Leeuw, G. *Philos. Trans. R. Soc. a: Math. Phys. Eng. Sci.* **2007**, *365*, 1753, DOI: 10.1098/rsta.2007.2043.
(242) Kerminen, V. M.; Petäjä, T.; Manninen, H. E.; Paasonen, P.; Nieminen, T.; Sipilä, M.; Junninen, H.; Ehn, M.; Gagné, S.; Laakso, L.; Riipinen, I.; Vehkamäki, H.; Kurtén, T.; Ortega, I. K.; Dal Maso, M.; Brus, D.; Hyvärinen, A.; Lihavainen, H.; Leppä, J.; Lehtinen, K. E. J.; Mirme, A.; Mirme, S.; Hõrrak, U.; Berndt, T.; Stratmann, F.; Birmili, W.; Wiedensohler, A.; Metzger, A.; Dommen, J.; Baltensperger, U.; Kiendler-Scharr, A.; Mentel, T. F.; Wildt, J.; Winkler, P. M.; Wagner, P. E.; Petzold, A.; Minikin, A.; Plass-Dülmer, C.; Pöschl, U.; Laaksonen, A.; Kulmala, M. *Atmos. Chem. Phys.* **2010**, *10*, 10829, DOI: 10.5194/acp-10-10829-2010.
(243) McMurry, P. H. *Atmos. Environ.* **2000**, *34*, 1959.
(244) Agarwal, J. K.; Sem, G. J. *J. Aerosol Sci* **1980**, *11*, 343.
(245) Marti, J. J.; Weber, R. J.; Saros, M. T.; Vasiliou, J. G.; McMurry, P. H. *Aerosol Sci. Technol.* **1996**, *25*, 214.
(246) Saros, M. T.; Weber, R. J.; Marti, J. J.; McMurry, P. H. *Aerosol Sci. Technol.* **1996**, *25*, 200.
(247) Birmili, W.; Stratmann, F.; Wiedensohler, A. *J. Aerosol Sci* **1999**, *30*, 549.
(248) Wang, S. C.; Flagan, R. C. *Aerosol Sci. Technol.* **1990**, *13*, 230.
(249) Knutson, E. O.; Whitby, K. T. *J. Aerosol Sci* **1975**, *6*, 443.
(250) Yue, D. L.; Hu, M.; Zhang, R. Y.; Wang, Z. B.; Zheng, J.; Wu, Z. J.; Wiedensohler, A.; He, L. Y.; Huang, X. F.; Zhu, T. *Atmos. Chem. Phys.* **2010**, *10*, 4953, DOI: 10.5194/acp-10-4953-2010.
(251) Zheng, J.; Hu, M.; Zhang, R.; Yue, D.; Wang, Z.; Guo, S.; Li, X.; Bohn, B.; Shao, M.; He, L.; Huang, X.; Wiedensohler, A.; Zhu, T. *Atmos. Chem. Phys. Discuss.* **2011**, *11*, 5019, DOI: 10.5194/acpd-11-5019-2011.
(252) Heintzenberg, J.; Wehner, B.; Birmili, W. *Tellus B* **2007**, *59*, 273, DOI: 10.1111/j.1600-0889.2007.00249.x.
(253) Weber, R. J.; Marti, J. J.; McMurry, P. H.; Eisele, F. L.; Tanner, D. J.; Jefferson, A. *J. Geophys. Res.* **1997**, *102*, 4375.
(254) Stockwell, W. R.; Calvert, J. G. *Atmos. Environ.* **1983**, *17*, 2231.
(255) Calvert, J. G.; Lazrus, A.; Kok, G. L.; Heikes, B. G.; Walega, J. G.; Lind, J.; Cantrell, C. A. *Nature* **1985**, *317*, 27.
(256) Aalto, P.; Hameri, K.; Becker, E.; Weber, R.; Salm, J.; Makela, J. M.; Hoell, C.; O'Dowd, C. D.; Karlsson, H.; Hansson, H. C.; Vakeva, M.; Koponen, I. K.; Buzorius, G.; Kulmala, M. *Tellus Ser. B: Chem. Phys. Meteor.* **2001**, *53*, 344.
(257) O'Dowd, C. D.; Aalto, P.; Hameri, K.; Kulmala, M.; Hoffmann, T. *Nature* **2002**, *416*, 497.
(258) Laaksonen, A.; Kulmala, M.; O'Dowd, C. D.; Joutsensaari, J.; Vaattovaara, P.; Mikkonen, S.; Lehtinen, K. E. J.; Sogacheva, L.; Dal Maso, M.; Aalto, P.; Petaja, T.; Sogachev, A.; Yoon, Y. J.; Lihavainen, H.; Nilsson, D.; Facchini, M. C.; Cavalli, F.; Fuzzi, S.; Hoffmann, T.; Arnold, F.; Hanke, M.; Sellegri, K.; Umann, B.; Junkermann, W.; Coe, H.; Allan, J. D.; Alfarra, M. R.; Worsnop, D. R.; Riekkola, M. L.; Hyotylainen, T.; Viisanen, Y. *Atmos. Chem. Phys.* **2008**, *8*, 2657.
(259) Ristovski, Z. D.; Suni, T.; Kulmala, M.; Boy, M.; Meyer, N. K.; Duplissy, J.; Turnipseed, A.; Morawska, L.; Baltensperger, U. *Atmos. Chem. Phys.* **2010**, *10*, 2919, DOI: 10.5194/acp-10-2919-2010.
(260) O'Dowd, C. D.; Yoon, Y. J.; Junkermann, W.; Aalto, P.; Kulmala, M.; Lihavainen, H.; Viisanen, Y. *Atmos. Chem. Phys.* **2009**, *9*, 937, DOI: 10.5194/acp-9-937-2009.
(261) McMurry, P. H.; Fink, M.; Sakurai, H.; Stolzenburg, M. R.; Mauldin, R. L.; Smith, J.; Eisele, F.; Moore, K.; Sjostedt, S.; Tanner, D.; Huey, L. G.; Nowak, J. B.; Edgerton, E.; Voisin, D. *J. Geophys. Res.* **2005**, *110*, D22S02.
(262) Fortner, E. C.; Zheng, J.; Zhang, R.; Knighton, W. B.; Volkamer, R. M.; Sheehy, P.; Molina, L.; Andre, M. *Atmos. Chem. Phys.* **2009**, *9*, 467.
(263) Guenther, A.; Hewitt, C. N.; Erickson, D.; Fall, R.; Geron, C.; Graedel, T.; Harley, P.; Klinger, L.; Lerdau, M.; McKay, W. A.; Pierce, T.; Scholes, B.; Steinbrecher, R.; Tallamraju, R.; Taylor, J.; Zimmerman, P. *J. Geophys. Res.* **1995**, *100*, 8873.
(264) Paasonen, P.; Nieminen, T.; Asmi, E.; Manninen, H. E.; Petäjä, T.; Plass-Dülmer, C.; Flentje, H.; Birmili, W.; Wiedensohler, A.; Hõrrak, U.; Metzger, A.; Hamed, A.; Laaksonen, A.; Facchini, M. C.; Kerminen, V. M.; Kulmala, M. *Atmos. Chem. Phys.* **2010**, *10*, 11223, DOI: 10.5194/acp-10-11223-2010.
(265) Carpenter, L. J.; Sturges, W. T.; Penkett, S. A.; Liss, P. S.; Alicke, B.; Hebestreit, K.; Platt, U. *J. Geophys. Res.* **1999**, *104*, 1679.
(266) de Leeuw, G.; Kunz, G. J.; Buzorius, G.; O'Dowd, C. *J. Geophys. Res.* **2002**, *107*, 8102, DOI: 10.1029/2001jd001478.
(267) Hoffmann, T.; O'Dowd, C. D.; Seinfeld, J. H. *Geophys. Res. Lett.* **2001**, *28*, 1949.
(268) Makela, J. M.; Hoffmann, T.; Holzke, C.; Vakeva, M.; Suni, T.; Mattila, T.; Aalto, P. P.; Tapper, U.; Kauppinen, E. I.; O'Dowd, C. D. *J. Geophys. Res.* **2002**, *107*, 8110, DOI: 10.1029/2001jd000580.
(269) O'Dowd, C. D.; Hameri, K.; Makela, J.; Vakeva, M.; Aalto, P.; de Leeuw, G.; Kunz, G. J.; Becker, E.; Hansson, H. C.; Allen, A. G.; Harrison, R. M.; Berresheim, H.; Geever, M.; Jennings, S. G.; Kulmala, M. *J. Geophys. Res.* **2002**, *107*, 8107, DOI: 10.1029/2000jd000206.
(270) Stull, R. B. *An introduction to boundary layer meteorology*; Kluwer Academic Publishers: Dordrecht, Boston, 1988.
(271) Hermann, M.; Heintzenberg, J.; Wiedensohler, A.; Zahn, A.; Heinrich, G.; Brenninkmeijer, C. A. M. *J. Geophys. Res.* **2003**, *108*, 4114, DOI: 10.1029/2001jd001077.
(272) Khosrawi, F.; Ström, J.; Minikin, A.; Krejci, R. *Atmos. Chem. Phys.* **2010**, *10*, 1105, DOI: 10.5194/acp-10-1105-2010.
(273) de Reus, M.; Strom, J.; Kulmala, M.; Pirjola, L.; Lelieveld, J.; Schiller, C.; Zoger, M. *J. Geophys. Res.* **1998**, *103*, 31255.
(274) Khosrawi, F.; Konopka, P. *Atmos. Environ.* **2003**, *37*, 903, DOI: 10.1016/s1352-2310(02)00976-7.
(275) Young, L. H.; Benson, D. R.; Montanaro, W. M.; Lee, S. H.; Pan, L. L.; Rogers, D. C.; Jensen, J.; Stith, J. L.; Davis, C. A.; Campos, T. L.; Bowman, K. P.; Cooper, W. A.; Lait, L. R. *J. Geophys. Res.* **2007**, *112*, D10218, DOI: 10.1029/2006jd008109.
(276) de Reus, M.; Strom, J.; Hoor, P.; Lelieveld, J.; Schiller, C. *J. Geophys. Res.* **1999**, *104*, 23935.
(277) Twohy, C. H.; Clement, C. F.; Gandrud, B. W.; Weinheimer, A. J.; Campos, T. L.; Baumgardner, D.; Brune, W. H.; Faloona, I.; Sachse,

G. W.; Vay, S. A.; Tan, D. *J. Geophys. Res.* **2002**, *107*, 4560, DOI: 10.1029/2001jd000323.
(278) Benson, D. R.; Young, L. H.; Lee, S. H.; Campos, T. L.; Rogers, D. C.; Jensen, J. *Atmos. Chem. Phys.* **2008**, *8*, 3015.
(279) Clarke, A. D.; Kapustin, V. N.; Eisele, F. L.; Weber, R. J.; McMurry, P. H. *Geophys. Res. Lett.* **1999**, *26*, 2425.
(280) Clarke, A. D.; Varner, J. L.; Eisele, F.; Mauldin, R. L.; Tanner, D.; Litchy, M. *J. Geophys. Res.* **1998**, *103*, 16397.
(281) Wiedensohler, A.; Hansson, H. C.; Orsini, D.; Wendisch, M.; Wagner, F.; Bower, K. N.; Chourlarton, T. W.; Wells, M.; Parkin, M.; Acker, K.; Wieprecht, W.; Facchini, M. C.; Lind, J. A.; Fuzzi, S.; Arends, B. G.; Kulmalao, M. *Atmos. Environ.* **1997**, *31*, 2545.
(282) Mertes, S.; Galgon, D.; Schwirn, K.; Nowak, A.; Lehmann, K.; Massling, A.; Wiedensohler, A.; Wieprecht, W. *Atmos. Environ.* **2005**, *39*, 4233, DOI: 10.1016/j.atmosenv.2005.02.009.
(283) Lee, S. H.; Young, L. H.; Benson, D. R.; Suni, T.; Kulmala, M.; Junninen, H.; Campos, T. L.; Rogers, D. C.; Jensen, J. *J. Geophys. Res.* **2008**, *113*, D10210, DOI: 10.1029/2007jd009351.
(284) Russell, L. M.; Mensah, A. A.; Fischer, E. V.; Sive, B. C.; Varner, R. K.; Keene, W. C.; Stutz, J.; Pszenny, A. A. P. *J. Geophys. Res.* **2007**, *112*, , DOI: 10.1029/2006jd007736.
(285) Suni, T.; Kulmala, M.; Hirsikko, A.; Bergman, T.; Laakso, L.; Aalto, P. P.; Leuning, R.; Cleugh, H.; Zegelin, S.; Hughes, D.; van Gorsel, E.; Kitchen, M.; Vana, M.; Horrak, U.; Mirme, S.; Mirme, A.; Sevanto, S.; Twining, J.; Tadros, C. *Atmos. Chem. Phys.* **2008**, *8*, 129.
(286) Zheng, J.; Khalizov, A.; Wang, L.; Zhang, R. *Anal. Chem.* **2010**, *82*, 7302, DOI: 10.1021/ac101253n.
(287) Fan, J.; Zhang, R. *Environ. Chem.* **2004**, *1*, 140.
(288) Mauldin, R. L.; Cantrell, C. A.; Zondlo, M.; Kosciuch, E.; Eisele, F. L.; Chen, G.; Davis, D.; Weber, R.; Crawford, J.; Blake, D.; Bandy, A.; Thornton, D. *J. Geophys. Res.* **2003**, *108*, 8796, DOI: 10.1029/2003jd003410.
(289) Kavouras, I. G.; Mihalopoulos, N.; Stephanou, E. G. *Nature* **1998**, *395*, 683.
(290) Makela, J. M.; Yli-Koivisto, S.; Hiltunen, V.; Seidl, W.; Swietlicki, E.; Teinila, K.; Sillanpaa, M.; Koponen, I. K.; Paatero, J.; Rosman, K.; Hameri, K. *Tellus Ser. B: Chem. Phys. Meteor.* **2001**, *53*, 380.
(291) Pratt, K. A.; Mayer, J. E.; Holecek, J. C.; Moffet, R. C.; Sanchez, R. O.; Rebotier, T. P.; Furutani, H.; Gonin, M.; Fuhrer, K.; Su, Y.; Guazzotti, S.; Prather, K. A. *Anal. Chem.* **2009**, *81*, 1792, DOI: 10.1021/ac801942r.
(292) Gard, E.; Mayer, J. E.; Morrical, B. D.; Dienes, T.; Fergenson, D. P.; Prather, K. A. *Anal. Chem.* **1997**, *69*, 4083.
(293) Murphy, D. M.; Thomson, D. S. *Aerosol Sci. Technol.* **1995**, *22*, 237.
(294) Zelenyuk, A.; Imre, D. *Aerosol Sci. Technol.* **2005**, *39*, 554, DOI: 10.1080/027868291009242.
(295) Murphy, D. M. *Mass Spectrom. Rev.* **2007**, *26*, 150, DOI: 10.1002/mas.20113.
(296) Canagaratna, M. R.; Jayne, J. T.; Jimenez, J. L.; Allan, J. D.; Alfarra, M. R.; Zhang, Q.; Onasch, T. B.; Drewnick, F.; Coe, H.; Middlebrook, A.; Delia, A.; Williams, L. R.; Trimborn, A. M.; Northway, M. J.; DeCarlo, P. F.; Kolb, C. E.; Davidovits, P.; Worsnop, D. R. *Mass Spectrom. Rev.* **2007**, *26*, 185, DOI: 10.1002/mas.20115.
(297) Tobias, H. J.; Ziemann, P. J. *Anal. Chem.* **1999**, *71*, 3428.
(298) Hearn, J. D.; Smith, G. D. *Int. J. Mass Spectrom.* **2006**, *258*, 95, DOI: 10.1016/j.ijms.2006.05.017.
(299) Thornberry, T.; Murphy, D. M.; Thomson, D. S.; de Gouw, J.; Warneke, C.; Bates, T. S.; Quinn, P. K.; Coffman, D. *Aerosol Sci. Technol.* **2009**, *43*, 486.
(300) Holzinger, R.; Williams, J.; Herrmann, F.; Lelieveld, J.; Donahue, N. M.; Röckmann, T. *Atmos. Chem. Phys.* **2010**, *10*, 2257, DOI: 10.5194/acp-10-2257-2010.
(301) Yatavelli, R. L. N.; Thornton, J. A. *Aerosol Sci. Technol.* **2010**, *44*, 61.
(302) Voisin, D.; Smith, J. N.; Sakurai, H.; McMurry, P. H.; Eisele, F. L. *Aerosol Sci. Technol.* **2003**, *37*, 471.
(303) Smith, J. N.; Moore, K. F.; McMurry, P. H.; Eisele, F. L. *Aerosol Sci. Technol.* **2004**, *38*, 100.
(304) Held, A.; Rathbone, G. J.; Smith, J. N. *Aerosol Sci. Technol.* **2009**, *43*, 264, DOI: 10.1080/02786820802603792.
(305) Johnston, M. V.; Wang, S. Y.; Reinard, M. S. *Appl. Spectrosc.* **2006**, *60*, 264A.
(306) Zordan, C. A.; Pennington, M. R.; Johnston, M. V. *Anal. Chem.* **2010**, *82*, 8034, DOI: 10.1021/ac101700q.
(307) Wang, L.; Lal, V.; Khalizov, A. F.; Zhang, R. *Environ. Sci. Technol.* **2010**, *44*, 2461, DOI: 10.1021/es9036868.
(308) Smith, J. N.; Moore, K. F.; Eisele, F. L.; Voisin, D.; Ghimire, A. K.; Sakurai, H.; McMurry, P. H. *J. Geophys. Res.* **2005**, *110*, D22S03.
(309) Smith, J. N.; Dunn, M. J.; VanReken, T. M.; Iida, K.; Stolzenburg, M. R.; McMurry, P. H.; Huey, L. G. *Geophys. Res. Lett.* **2008**, *35*, L04808–L04808, DOI: 10.1029/2007gl032523.
(310) Bzdek, B. R.; Zordan, C. A.; Luther, G. W.; Johnston, M. V. *Aerosol Sci. Technol.* **2011**, *45*, 1041, DOI: 10.1080/02786826.2011.580392.
(311) Hirsikko, A.; Laakso, L.; Horrak, U.; Aalto, P. P.; Kerminen, V. M.; Kulmala, M. *Boreal Environ. Res.* **2005**, *10*, 357.
(312) Rader, D. J.; McMurry, P. H. *J. Aerosol Sci* **1986**, *17*, 771.
(313) Sakurai, H.; Fink, M. A.; McMurry, P. H.; Mauldin, L.; Moore, K. F.; Smith, J. N.; Eisele, F. L. *J. Geophys. Res.* **2005**, *110*, D22S04.
(314) Kulmala, M.; Mordas, G.; Petaja, T.; Gronholm, T.; Aalto, P. P.; Vehkamaki, H.; Hienola, A. I.; Herrmann, E.; Sipila, M.; Riipinen, I.; Manninen, H. E.; Hameri, K.; Stratmann, F.; Bilde, M.; Winkler, P. M.; Birmili, W.; Wagner, P. E. *J. Aerosol Sci* **2007**, *38*, 289, DOI: 10.1016/j.jaerosci.2006.11.008.
(315) Riipinen, I.; Manninen, H. E.; Yli-Juuti, T.; Boy, M.; Sipilä, M.; Ehn, M.; Junninen, H.; Petäjä, T.; Kulmala, M. *Atmos. Chem. Phys.* **2009**, *9*, 3317, DOI: 10.5194/acp-9-3317-2009.
(316) Ehn, M.; Petaja, T.; Birmili, W.; Junninen, H.; Aalto, P.; Kulmala, M. *Atmos. Chem. Phys.* **2007**, *7*, 677.
(317) Modini, R. L.; Ristovski, Z. D.; Johnson, G. R.; He, C.; Surawski, N.; Morawska, L.; Suni, T.; Kulmala, M. *Atmos. Chem. Phys.* **2009**, *9*, 7607.
(318) Joutsensaari, J.; Vaattovaara, P.; Vesterinen, M.; Hameri, K.; Laaksonen, A. *Atmos. Chem. Phys.* **2001**, *1*, 51.
(319) Vaattovaara, P.; Rasanen, M.; Kuhn, T.; Joutsensaari, J.; Laaksonen, A. *Atmos. Chem. Phys.* **2005**, *5*, 3277.
(320) Winkler, P. M.; Steiner, G.; Vrtala, A.; Vehkamaki, H.; Noppel, M.; Lehtinen, K. E. J.; Reischl, G. P.; Wagner, P. E.; Kulmala, M. *Science* **2008**, *319*, 1374, DOI: 10.1126/science.1149034.
(321) Winkler, P. M.; Vrtala, A.; Wagner, P. E. *Atmos. Res.* **2008**, *90*, 125.
(322) Sipila, M.; Lehtipalo, K.; Kulmala, M.; Petaja, T.; Junninen, H.; Aalto, P. P.; Manninen, H. E.; Kyro, E. M.; Asmi, E.; Riipinen, I.; Curtius, J.; Kurtén, A.; Borrmann, S.; O'Dowd, C. D. *Atmos. Chem. Phys.* **2008**, *8*, 4049.
(323) Sipila, M.; Lehtipalo, K.; Attoui, M.; Neitola, K.; Petaja, T.; Aalto, P. P.; O'Dowd, C. D.; Kulmala, M. *Aerosol Sci. Technol.* **2009**, *43*, 126, DOI: 10.1080/02786820802506227.
(324) Iida, K.; Stolzenburg, M. R.; McMurry, P. H. *Aerosol Sci. Technol.* **2009**, *43*, 81, DOI: 10.1080/02786820802488194.
(325) Jiang, J.; Chen, M.; Kuang, C.; Attoui, M.; McMurry, P. H. *Aerosol Sci. Technol.* **2011**, *45*, 510.
(326) Vanhanen, J.; Mikkilä, J.; Lehtipalo, K.; Sipilä, M.; Manninen, H. E.; Siivola, E.; Petäjä, T.; Kulmala, M. *Aerosol Sci. Technol.* **2011**, *45*, 533.
(327) Okuyama, K.; Kousaka, Y.; Motouchi, T. *Aerosol Sci. Technol.* **1984**, *3*, 353.
(328) Sgro, L. A.; Fernández de la Mora, J. *Aerosol Sci. Technol.* **2004**, *38*, 1, DOI: 10.1080/02786820490247560.
(329) Yu, F. Q.; Turco, R. P. *J. Geophys. Res.* **2001**, *106*, 4797.
(330) Kanawade, V.; Tripathi, S. N. *J. Geophys. Res.* **2006**, *111*, D02209, DOI: 10.1029/2005jd006366.
(331) Tammet, H. *Atmos. Res.* **2006**, *82*, 523.
(332) Mirme, A.; Tamm, E.; Mordas, G.; Vana, M.; Uin, J.; Mirme, S.; Bernotas, T.; Laakso, L.; Hirsikko, A.; Kulmala, M. *Boreal Environ. Res.* **2007**, *12*, 247.
(333) Kulmala, M.; Riipinen, I.; Sipila, M.; Manninen, H. E.; Petaja, T.; Junninen, H.; Dal Maso, M.; Mordas, G.; Mirme, A.; Vana, M.;

Hirsikko, A.; Laakso, L.; Harrison, R. M.; Hanson, I.; Leung, C.; Lehtinen, K. E. J.; Kerminen, V. M. *Science* **2007**, *318*, 89, DOI: 10.1126/science.1144124.
(334) Kulmala, M.; Lehtinen, K. E. J.; Laakso, L.; Mordas, G.; Hameri, K. *Boreal Environ. Res.* **2005**, *10*, 79.
(335) Lehtipalo, K.; Sipila, M.; Riipinen, I.; Nieminen, T.; Kulmala, M. *Atmos. Chem. Phys.* **2009**, *9*, 4177.
(336) Kulmala, M.; Pirjola, U.; Makela, J. M. *Nature* **2000**, *404*, 66.
(337) Mirme, S.; Mirme, A.; Minikin, A.; Petzold, A.; Hõrrak, U.; Kerminen, V. M.; Kulmala, M. *Atmos. Chem. Phys.* **2010**, *10*, 437, DOI: 10.5194/acp-10-437-2010.
(338) Manninen, H. E.; Nieminen, T.; Asmi, E.; Gagné, S.; Häkkinen, S.; Lehtipalo, K.; Aalto, P.; Vana, M.; Mirme, A.; Mirme, S.; Hõrrak, U.; Plass-Dülmer, C.; Stange, G.; Kiss, G.; Hoffer, A.; Töró, N.; Moerman, M.; Henzing, B.; de Leeuw, G.; Brinkenberg, M.; Kouvarakis, G. N.; Bougiatioti, A.; Mihalopoulos, N.; O'Dowd, C.; Ceburnis, D.; Arneth, A.; Svenningsson, B.; Swietlicki, E.; Tarozzi, L.; Decesari, S.; Facchini, M. C.; Birmili, W.; Sonntag, A.; Wiedensohler, A.; Boulon, J.; Sellegri, K.; Laj, P.; Gysel, M.; Bukowiecki, N.; Weingartner, E.; Wehrle, G.; Laaksonen, A.; Hamed, A.; Joutsensaari, J.; Petäjä, T.; Kerminen, V. M.; Kulmala, M. *Atmos. Chem. Phys.* **2010**, *10*, 7907, DOI: 10.5194/acp-10-7907-2010.
(339) Eisele, F. L.; Lovejoy, E. R.; Kosciuch, E.; Moore, K. F.; Mauldin, R. L.; Smith, J. N.; McMurry, P. H.; Iida, K. *J. Geophys. Res.* **2006**, *111*, D04305.
(340) Iida, K.; Stolzenburg, M.; McMurry, P.; Dunn, M. J.; Smith, J. N.; Eisele, F.; Keady, P. *J. Geophys. Res.* **2006**, *111*, D23201.
(341) Hirsikko, A.; Bergman, T.; Laakso, L.; Dal Maso, M.; Riipinen, I.; Horrak, U.; Kulmala, M. *Atmos. Chem. Phys.* **2007**, *7*, 201.
(342) Gagne, S.; Laakso, L.; Petaja, T.; Kerminen, V. M.; Kulmala, M. *Tellus Ser. B: Chem. Phys. Meteor.* **2008**, *60*, 318, DOI: 10.1111/j.1600-0889.2008.00347.x.
(343) Manninen, H. E.; Nieminen, T.; Riipinen, I.; Yli-Juuti, T.; Gagné, S.; Asmi, E.; Aalto, P. P.; Petäjä, T.; Kerminen, V. M.; Kulmala, M. *Atmos. Chem. Phys.* **2009**, *9*, 4077.
(344) Yu, F.; Turco, R. *Atmos. Chem. Phys.* **2008**, *8*, 6085.
(345) Yu, F.; Wang, Z.; Luo, G.; Turco, R. *Atmos. Chem. Phys.* **2008**, *8*, 2537, DOI: 10.5194/acp-8-2537-2008.
(346) Yu, F. Q. *J. Geophys. Res.* **2010**, *115*, D03206, DOI: 10.1029/2009jd012630.
(347) Junninen, H.; Ehn, M.; Petäjä, T.; Luosujärvi, L.; Kotiaho, T.; Kostiainen, R.; Rohner, U.; Gonin, M.; Fuhrer, K.; Kulmala, M.; Worsnop, D. R. *Atmos. Meas. Tech.* **2010**, *3*, 1039, DOI: 10.5194/amt-3-1039-2010.
(348) Ehn, M.; Junninen, H.; Petäjä, T.; Kurtén, T.; Kerminen, V. M.; Schobesberger, S.; Manninen, H. E.; Ortega, I. K.; Vehkamäki, H.; Kulmala, M.; Worsnop, D. R. *Atmos. Chem. Phys.* **2010**, *10*, 8513, DOI: 10.5194/acp-10-8513-2010.
(349) Ehn, M.; Junninen, H.; Schobesberger, S.; Manninen, H. E.; Franchin, A.; Sipilä, M.; Petäjä, T.; Kerminen, V.-M.; Tammet, H.; Mirme, A.; Mirme, S.; Hõrrak, U.; Kulmala, M.; Worsnop, D. R. *Aerosol Sci. Technol.* **2011**, *45*, 522.
(350) Zhao, J.; Eisele, F. L.; Titcombe, M.; Kuang, C. G.; McMurry, P. H. *J. Geophys. Res.* **2010**, *115*, D08205, DOI: 10.1029/2009jd012606.
(351) Eisele, F. L.; Hanson, D. R. *J. Phys. Chem. A* **2000**, *104*, 830.
(352) Hanson, D. R.; Eisele, F. L. *J. Geophys. Res.* **2002**, *107*, 4158, DOI: 10.1029/2001jd001100.
(353) Hanson, D. R.; Lovejoy, E. R. *J. Phys. Chem. A* **2006**, *110*, 9525, DOI: 10.1021/jp062844w.
(354) Jiang, J.; Zhao, J.; Chen, M.; Eisele, F. L.; Scheckman, J.; Williams, B. J.; Kuang, C.; McMurry, P. H. *Aerosol Sci. Technol.* **2011**, *45*, 2.
(355) Mirabel, P.; Katz, J. L. *J. Chem. Phys.* **1974**, *60*, 1138.
(356) Shugard, W. J.; Heist, R. H.; Reiss, H. *J. Chem. Phys.* **1974**, *61*, 5298.
(357) Vehkamaki, H.; Kulmala, M.; Napari, I.; Lehtinen, K. E. J.; Timmreck, C.; Noppel, M.; Laaksonen, A. *J. Geophys. Res.* **2002**, *107*, 4622, DOI: 10.1029/2002jd002184.
(358) Reiss, H.; Margolese, D. I.; Schelling, F. J. *J. Colloid Interface Sci.* **1976**, *56*, 511.
(359) Schelling, F. J.; Reiss, H. *J. Colloid Interface Sci.* **1981**, *83*, 246.
(360) Mirabel, P.; Clavelin, J. L. *J. Chem. Phys.* **1978**, *68*, 5020.
(361) Wyslouzil, B. E.; Seinfeld, J. H.; Flagan, R. C.; Okuyama, K. *J. Chem. Phys.* **1991**, *94*, 6842.
(362) Yu, F. Q. *J. Chem. Phys.* **2007**, *127*, 054301.
(363) Weber, R. J.; Marti, J. J.; McMurry, P. H.; Eisele, F. L.; Tanner, D. J.; Jefferson, A. *Chem. Eng. Commun.* **1996**, *151*, 53.
(364) Sihto, S. L.; Kulmala, M.; Kerminen, V. M.; Dal Maso, M.; Petäjä, T.; Riipinen, I.; Korhonen, H.; Arnold, F.; Janson, R.; Boy, M.; Laaksonen, A.; Lehtinen, K. E. J. *Atmos. Chem. Phys.* **2006**, *6*, 4079, DOI: 10.5194/acp-6-4079-2006.
(365) Berndt, T.; Boge, O.; Stratmann, F. *Geophys. Res. Lett.* **2006**, *33*, L15817.
(366) Benson, D. R.; Young, L. H.; Kameel, F. R.; Lee, S. H. *Geophys. Res. Lett.* **2008**, *35*, L11801–L11801, DOI: 10.1029/2008gl033387.
(367) Berndt, T.; Stratmann, F.; Brasel, S.; Heintzenberg, J.; Laaksonen, A.; Kulmala, M. *Atmos. Chem. Phys.* **2008**, *8*, 6365.
(368) Laaksonen, A.; Kulmala, M.; Berndt, T.; Stratmann, F.; Mikkonen, S.; Ruuskanen, A.; Lehtinen, K. E. J.; Dal Maso, M.; Aalto, P.; Petaja, T.; Riipinen, I.; Sihto, S. L.; Janson, R.; Arnold, F.; Hanke, M.; Ucker, J.; Umann, B.; Sellegri, K.; O'Dowd, C. D.; Viisanen, Y. *Atmos. Chem. Phys.* **2008**, *8*, 7255.
(369) Sorokin, A. *Atmos. Chem. Phys.* **2010**, *10*, 3141.
(370) Sorokin, A.; Arnold, F. *Atmos. Environ.* **2007**, *41*, 3740, DOI: 10.1016/j.atmosenv.2007.01.017.
(371) Du, H.; Yu, F. *Atmos. Chem. Phys.* **2009**, *9*, 7913, DOI: 10.5194/acp-9-7913-2009.
(372) Berndt, T.; Stratmann, F.; Sipilä, M.; Vanhanen, J.; Petäjä, T.; Mikkilä, J.; Grüner, A.; Spindler, G.; Lee Mauldin, R.; Curtius, J.; Kulmala, M.; Heintzenberg, J. *Atmos. Chem. Phys.* **2010**, *10*, 7101, DOI: 10.5194/acp-10-7101-2010.
(373) Brus, D.; Neitola, K.; Hyvärinen, A. P.; Petäjä, T.; Vanhanen, J.; Sipilä, M.; Paasonen, P.; Kulmala, M.; Lihavainen, H. *Atmos. Chem. Phys.* **2011**, *11*, 5277, DOI: 10.5194/acp-11-5277-2011.
(374) Kuang, C.; McMurry, P. H.; McCormick, A. V.; Eisele, F. L. *J. Geophys. Res.* **2008**, *113*, D10209–D10209, DOI: 10.1029/2007jd009253.
(375) Paasonen, P.; Nieminen, T.; Asmi, E.; Manninen, H. E.; Petäjä, T.; Plass-Dülmer, C.; Flentje, H.; Birmili, W.; Wiedensohler, A.; Hõrrak, U.; Metzger, A.; Hamed, A.; Laaksonen, A.; Facchini, M. C.; Kerminen, V. M.; Kulmala, M. *Atmos. Chem. Phys. Discuss.* **2010**, *10*, 11795, DOI: 10.5194/acpd-10-11795-2010.
(376) Erupe, M. E.; Viggiano, A. A.; Lee, S. H. *Atmos. Chem. Phys.* **2011**, *11*, 4767, DOI: 10.5194/acp-11-4767-2011.
(377) Zhao, J.; Khalizov, A.; Zhang, R.; McGraw, R. *J. Phys. Chem. A* **2009**, *113*, 680, doi: 10.1021/jp806693r.
(378) Kurtén, T.; Loukonen, V.; Vehkamäki, H.; Kulmala, M. *Atmos. Chem. Phys.* **2008**, *8*, 4095.
(379) Coffman, D. J.; Hegg, D. A. *J. Geophys. Res.* **1995**, *100*, 7147.
(380) Korhonen, P.; Kulmala, M.; Laaksonen, A.; Viisanen, Y.; McGraw, R.; Seinfeld, J. H. *J. Geophys. Res.* **1999**, *104*, 26349, DOI: 10.1029/1999jd900784.
(381) Kim, T. O.; Ishida, T.; Adachi, M.; Okuyama, K.; Seinfeld, J. H. *Aerosol Sci. Technol.* **1998**, *29*, 111.
(382) Merikanto, J.; Napari, I.; Vehkamaki, H.; Anttila, T.; Kulmala, M. *J. Geophys. Res.* **2007**, *112*, D15207, DOI: 10.1029/2006jd007977.
(383) Napari, I.; Noppel, M.; Vehkamaki, H.; Kulmala, M. *J. Chem. Phys.* **2002**, *116*, 4221, DOI: 10.1063/1.1450557.
(384) Benson, D. R.; Erupe, M. E.; Lee, S. H. *Geophys. Res. Lett.* **2009**, *36*, L15818–L15818, DOI: 10.1029/2009gl038728.
(385) Benson, D. R.; Yu, J. H.; Markovich, A.; Lee, S. H. *Atmos. Chem. Phys.* **2011**, *11*, 4755, DOI: 10.5194/acp-11-4755-2011.
(386) Ge, X. L.; Wexler, A. S.; Clegg, S. L. *Atmos. Environ.* **2011**, *45*, 524, DOI: 10.1016/j.atmosenv.2010.10.012.
(387) Barsanti, K. C.; McMurry, P. H.; Smith, J. N. *Atmos. Chem. Phys.* **2009**, *9*, 2949.

(388) Loukonen, V.; Kurtén, T.; Ortega, I. K.; Vehkamaki, H.; Padua, A. A. H.; Sellegri, K.; Kulmala, M. *Atmos. Chem. Phys.* **2010**, *10*, 4961, DOI: 10.5194/acp-10-4961-2010.
(389) Kanakidou, M.; Seinfeld, J. H.; Pandis, S. N.; Barnes, I.; Dentener, F. J.; Facchini, M. C.; Van Dingenen, R.; Ervens, B.; Nenes, A.; Nielsen, C. J.; Swietlicki, E.; Putaud, J. P.; Balkanski, Y.; Fuzzi, S.; Horth, J.; Moortgat, G. K.; Winterhalter, R.; Myhre, C. E. L.; Tsigaridis, K.; Vignati, E.; Stephanou, E. G.; Wilson, J. *Atmos. Chem. Phys.* **2005**, *5*, 1053.
(390) Hoffmann, T.; Bandur, R.; Marggraf, U.; Linscheid, M. *J. Geophys. Res.* **1998**, *103*, 25569.
(391) Nadykto, A. B.; Yu, F. Q. *Chem. Phys. Lett.* **2007**, *435*, 14, DOI: 10.1016/j.cplett.2006.12.050.
(392) Fan, J. W.; Zhang, R. Y.; Collins, D.; Li, G. H. *Geophys. Res. Lett.* **2006**, *33*, , DOI: 10.1029/2006gl026295.
(393) Forstner, H. J. L.; Flagan, R. C.; Seinfeld, J. H. *Environ. Sci. Technol.* **1997**, *31*, 1345.
(394) Jang, M. S.; Kamens, R. M. *Environ. Sci. Technol.* **2001**, *35*, 3626, DOI: 10.1021/es010676+.
(395) Jimenez, J. L.; Bahreini, R.; Cocker, D. R.; Zhuang, H.; Varutbangkul, V.; Flagan, R. C.; Seinfeld, J. H.; O'Dowd, C. D.; Hoffmann, T. *J. Geophys. Res.* **2003**, *108*, 4318, DOI: 10.1029/2002jd002452.
(396) Saunders, R. W.; Plane, J. M. C. *Environ. Chem.* **2005**, *2*, 299, DOI: 10.1071/en05079.
(397) Burkholder, J. B.; Curtius, J.; Ravishankara, A. R.; Lovejoy, E. R. *Atmos. Chem. Phys.* **2004**, *4*, 19.
(398) Allan, B. J.; McFiggans, G.; Plane, J. M. C.; Coe, H. *J. Geophys. Res.* **2000**, *105*, 14363.
(399) Allan, B. J.; Plane, J. M. C.; McFiggans, G. *Geophys. Res. Lett.* **2001**, *28*, 1945.
(400) Saiz-Lopez, A.; Plane, J. M. C. *Geophys. Res. Lett.* **2004**, *31*, L04112, DOI: 10.1029/2003gl019215.
(401) McFiggans, G.; Coe, H.; Burgess, R.; Allan, J.; Cubison, M.; Alfarra, M. R.; Saunders, R.; Saiz-Lopez, A.; Plane, J. M. C.; Wevill, D. J.; Carpenter, L. J.; Rickard, A. R.; Monks, P. S. *Atmos. Chem. Phys.* **2004**, *4*, 701.
(402) Saunders, R. W.; Plane, J. M. C. *J. Phys. IV Fr.* **2006**, *139*, 239.
(403) Sellegri, K.; Loon, Y. J.; Jennings, S. G.; O'Dowd, C. D.; Pirjola, L.; Cautenet, S.; Chen, H. W.; Hoffmann, T. *Environ. Chem.* **2005**, *2*, 260, DOI: 10.1071/en05074.
(404) Vohra, K. G.; Ramu, M. C. S.; Muraleedharan, T. S. *Atmos. Environ.* **1984**, *18*, 1653.
(405) Raes, F.; Janssens, A.; Eggermont, G. *Atmos. Environ.* **1985**, *19*, 1069.
(406) Kim, T. O.; Adachi, M.; Okuyama, K.; Seinfeld, J. H. *Aerosol Sci. Technol.* **1997**, *26*, 527.
(407) Svensmark, H.; Pedersen, J. O. P.; Marsh, N. D.; Enghoff, M. B.; Uggerhøj, U. I. *Proc. R. Soc. A: Math. Phys. Eng. Sci.* **2007**, *463*, 385, DOI: 10.1098/rspa.2006.1773.
(408) Duplissy, J.; Enghoff, M. B.; Aplin, K. L.; Arnold, F.; Aufmhoff, H.; Avngaard, M.; Baltensperger, U.; Bondo, T.; Bingham, R.; Carslaw, K.; Curtius, J.; David, A.; Fastrup, B.; Gagné, S.; Hahn, F.; Harrison, R. G.; Kellett, B.; Kirkby, J.; Kulmala, M.; Laakso, L.; Laaksonen, A.; Lillestol, E.; Lockwood, M.; Mäkelä, J.; Makhmutov, V.; Marsh, N. D.; Nieminen, T.; Onnela, A.; Pedersen, E.; Pedersen, J. O. P.; Polny, J.; Reichl, U.; Seinfeld, J. H.; Sipilä, M.; Stozhkov, Y.; Stratmann, F.; Svensmark, H.; Svensmark, J.; Veenhof, R.; Verheggen, B.; Viisanen, Y.; Wagner, P. E.; Wehrle, G.; Weingartner, E.; Wex, H.; Wilhelmsson, M.; Winkler, P. M. *Atmos. Chem. Phys.* **2010**, *10*, 1635, DOI: 10.5194/acp-10-1635-2010.
(409) Enghoff, M. B.; Pedersen, J. O. P.; Uggerhøj, U. I.; Paling, S. M.; Svensmark, H. *Geophys. Res. Lett.* **2011**, *38*, L09805, DOI: 10.1029/2011gl047036.
(410) Castleman, A. W.; Keesee, R. G. *Chem. Rev.* **1986**, *86*, 589.
(411) Goken, E. G.; Castleman, A. W., Jr. *J. Geophys. Res.* **2010**, *115*, D16203, DOI: 10.1029/2009jd013249.
(412) Lovejoy, E. R. *Int. J. Mass Spectrom.* **1999**, *191*, 231.
(413) Froyd, K. D.; Lovejoy, E. R. *J. Phys. Chem. A* **2003**, *107*, 9800, DOI: 10.1021/jp027803o.
(414) Froyd, K. D.; Lovejoy, E. R. *J. Phys. Chem. A* **2003**, *107*, 9812, DOI: 10.1021/jp0278059.
(415) Curtius, J.; Froyd, K. D.; Lovejoy, E. R. *J. Phys. Chem. A* **2001**, *105*, 10867, DOI: 10.1021/jp0124950.
(416) Lovejoy, E. R.; Curtius, J. *J. Phys. Chem. A* **2001**, *105*, 10874, DOI: 10.1021/jp012496s.
(417) Lovejoy, E. R.; Curtius, J.; Froyd, K. D. *J. Geophys. Res.* **2004**, *109*, D08204, DOI: 10.1029/2003jd004460.
(418) Wilhelm, S.; Eichkorn, S.; Wiedner, D.; Pirjola, L.; Arnold, F. *Atmos. Environ.* **2004**, *38*, 1735, DOI: 10.1016/j.atmosenv.2003.12.025.
(419) Sorokin, A.; Arnold, F.; Wiedner, D. *Atmos. Environ.* **2006**, *40*, 2030, DOI: 10.1016/j.atmosenv.2005.11.053.
(420) Bzdek, B. R.; Ridge, D. P.; Johnston, M. V. *Atmos. Chem. Phys.* **2010**, *10*, 3495.
(421) Bzdek, B. R.; Ridge, D. P.; Johnston, M. V. *J. Geophys. Res.* **2011**, *116*, D03301–D03301, DOI: 10.1029/2010jd015217.
(422) Bzdek, B. R.; Ridge, D. P.; Johnston, M. V. *J. Phys. Chem. A* **2010**, *114*, 11638, DOI: 10.1021/jp106363m.
(423) Bzdek, B. R.; Ridge, D. P.; Johnston, M. V. *Atmos. Chem. Phys. Discuss.* **2011**, *11*, 14637, DOI: 10.5194/acpd-11-14637-2011.
(424) Ortega, I. K.; Kurtén, T.; Vehkamäki, H.; Kulmala, M. *Atmos. Chem. Phys.* **2008**, *8*, 2859.
(425) Nadykto, A.; Yu, F.; Herb, J. *Int. J. Mol. Sci.* **2008**, *9*, 2184.
(426) Nadykto, A. B.; Yu, F.; Herb, J. *Atmos. Chem. Phys.* **2009**, *9*, 4031, DOI: 10.5194/acp-9-4031-2009.
(427) Jaecker-Voirol, A.; Mirabel, P. *J. Phys. Chem.* **1988**, *92*, 3518.
(428) Kulmala, M.; Lazaridis, M.; Laaksonen, A.; Vesala, T. *J. Chem. Phys.* **1991**, *94*, 7411.
(429) Noppel, M.; Vehkamaki, H.; Kulmala, M. *J. Chem. Phys.* **2002**, *116*, 218.
(430) Kurtén, T.; Berndt, T.; Stratmann, F. *Atmos. Chem. Phys.* **2009**, *9*, 3357.
(431) Salonen, M.; Kurtén, T.; Vehkamaki, H.; Berndt, T.; Kulmala, M. *Atmos. Res.* **2009**, *91*, 47, DOI: 10.1016/j.atmosres.2008.05.008.
(432) Miller, C. E.; Francisco, J. S. *J. Am. Chem. Soc.* **2001**, *123*, 10387.
(433) Kurtén, T.; Bonn, B.; Vehkamaki, H.; Kulmala, M. *J. Phys. Chem. A* **2007**, *111*, 3394.
(434) Kurdi, L.; Kochanski, E. *Chem. Phys. Lett.* **1989**, *158*, 111.
(435) Arstila, H.; Laasonen, K.; Laaksonen, A. *J. Chem. Phys.* **1998**, *108*, 1031.
(436) Bandy, A. R.; Ianni, J. C. *J. Phys. Chem. A* **1998**, *102*, 6533.
(437) Ianni, J. C.; Bandy, A. R. *J. Phys. Chem. A* **1999**, *103*, 2801.
(438) Re, S.; Osamura, Y.; Morokuma, K. *J. Phys. Chem. A* **1999**, *103*, 3535.
(439) Ding, C. G.; Laasonen, K. *Chem. Phys. Lett.* **2004**, *390*, 307, DOI: 10.1016/j.cplett.2004.02.112.
(440) Ding, C. G.; Laasonen, K.; Laaksonen, A. *J. Phys. Chem. A* **2003**, *107*, 8648, DOI: 10.1021/jp022575j.
(441) Al Natsheh, A.; Nadykto, A. B.; Mikkelsen, K. V.; Yu, F. Q.; Ruuskanen, J. *J. Phys. Chem. A* **2004**, *108*, 8914, DOI: 10.1021/jp048858o.
(442) Kurtén, T.; Sundberg, M. R.; Vehkamaki, H.; Noppel, M.; Blomqvist, J.; Kulmala, M. *J. Phys. Chem. A* **2006**, *110*, 7178, DOI: 10.1021/jp0613081.
(443) Kurtén, T.; Noppel, M.; Vehkamaki, H.; Salonen, M.; Kulmala, M. *Boreal Environ. Res.* **2007**, *12*, 431.
(444) Kurtén, T.; Vehkamäki, H. In *Advances in Quantum Chemistry*; Michael, E. G., Matthew, S. J., Eds.; Academic Press: New York, 2008; Vol. 55.
(445) Zhao, Y.; Truhlar, D. G. *J. Phys. Chem. A* **2004**, *108*, 6908, DOI: 10.1021/jp048147q.
(446) Torpo, L.; Kurtén, T.; Vehkamaki, H.; Laasonen, K.; Sundberg, M. R.; Kulmala, M. *J. Phys. Chem. A* **2007**, *111*, 10671, DOI: 10.1021/jp0741307.
(447) Larson, L. J.; Largent, A.; Tao, F. M. *J. Phys. Chem. A* **1999**, *103*, 6786.
(448) Kurtén, T.; Torpo, L.; Ding, C. G.; Vehkamaki, H.; Sundberg, M. R.; Laasonen, K.; Kulmala, M. *J. Geophys. Res.* **2007**, *112*, D04210, DOI: 10.1029/2006jd007391.

(449) Kurtén, T.; Torpo, L.; Sundberg, M. R.; Kerminen, V. M.; Vehkamäki, H.; Kulmala, M. *Atmos. Chem. Phys.* **2007**, *7*, 2765, DOI: 10.5194/acp-7-2765-2007.
(450) Hunter, E. P. L.; Lias, S. G. *J. Phys. Chem. Ref. Data* **1998**, *27*, 413.
(451) Nadykto, A.; Yu, F.; Jakovleva, M.; Herb, J.; Xu, Y. *Entropy* **2011**, *13*, 554.
(452) Kurtén, T. *Entropy* **2011**, *13*, 915.
(453) Xu, Y. S.; Nadykto, A. B.; Yu, F. Q.; Jiang, L.; Wang, W. *J. Mol. Struct. THEOCHEM* **2010**, *951*, 28, DOI: 10.1016/j.theochem.2010.04.004.
(454) Xu, Y. S.; Nadykto, A. B.; Yu, F. Q.; Herb, J.; Wang, W. *J. Phys. Chem. A* **2010**, *114*, 387, DOI: 10.1021/jp9068575.
(455) Rosen, S.; Froyd, K. D.; Curtius, J.; Lovejoy, E. R. *Int. J. Mass Spectrom.* **2004**, *232*, 9, DOI: 10.1016/j.ijms.2003.10004.
(456) Nadykto, A. B.; Yu, F. Q.; Al Natsheh, A. *Int. J. Mol. Sci.* **2009**, *10*, 507, DOI: 10.3390/ijms10020507.
(457) Kathmann, S. M.; Hale, B. N. *J. Phys. Chem. B* **2001**, *105*, 11719, DOI: 10.1021/jp0116499.
(458) Ding, C. G.; Taskila, T.; Laasonen, K.; Laaksonen, A. *Chem. Phys.* **2003**, *287*, 7.
(459) Matsubara, H.; Ebisuzaki, T.; Yasuoka, K. *J. Chem. Phys.* **2009**, *130*, 104705, DOI: 10.1063/1.3082079.
(460) Toivola, M.; Napari, I.; Vehkamaki, H. *Boreal Environ. Res.* **2009**, *14*, 654.
(461) Choe, Y. K.; Tsuchida, E.; Ikeshoji, T. *J. Chem. Phys.* **2007**, *126*, 154510, DOI: 10.1063/1.2718526.
(462) Anderson, K. E.; Siepmann, J. I.; McMurry, P. H.; VandeVondele, J. *J. Am. Chem. Soc.* **2008**, *130*, 14144, DOI: 10.1021/ja8019774.
(463) Yu, F. Q. *J. Chem. Phys.* **2005**, *122*, 074501, DOI: 10.1063/1.1850472.
(464) Kulmala, M.; Toivonen, A.; Makela, J. M.; Laaksonen, A. *Tellus Ser. B: Chem. Phys. Meteor.* **1998**, *50*, 449.
(465) Wilemski, G. *J. Chem. Phys.* **1984**, *80*, 1370.
(466) Yu, F. Q. *J. Geophys. Res.* **2006**, *111*, D04201, DOI: 10.1029/2005jd006358.
(467) Yu, F. Q. *J. Geophys. Res.* **2008**, *113*, D24201–D24201, DOI: 10.1029/2008jd010527.
(468) Vehkamaki, H.; Napari, I.; Kulmala, M.; Noppel, M. *Phys. Rev. Lett.* **2004**, *93*, 148501, DOI: 10.1103/PhysRevLett.93.148501.
(469) Anttila, T.; Vehkamaki, H.; Napari, I.; Kulmala, M. *Boreal Environ. Res.* **2005**, *10*, 511.
(470) Yu, F. Q. *J. Geophys. Res.* **2006**, *111*, D01204, DOI: 10.1029/2005jd005968.
(471) Yu, F. *Atmos. Chem. Phys.* **2006**, *6*, 5193.
(472) Nadykto, A. B.; Yu, F. Q. *J. Geophys. Res.* **2003**, *108*, 4717, DOI: 10.1029/2003jd003664.
(473) Yu, F. Q. *J. Chem. Phys.* **2005**, *122*, 084503, DOI: 10.1063/1.1845395.
(474) Laakso, L.; Makela, J. M.; Pirjola, L.; Kulmala, M. *J. Geophys. Res.* **2002**, *107*, 4427, DOI: 10.1029/2002jd002140.
(475) Lucas, D. D.; Akimoto, H. *Geophys. Res. Lett.* **2006**, *33*, L10808, DOI: 10.1029/2006gl025672.
(476) McMurry, P. H. *J. Colloid Interface Sci.* **1983**, *95*, 72.
(477) Kulmala, M. *Atmos. Res.* **2010**, *98*, 201, DOI: 10.1016/j.atmosres.2010.03.022.
(478) Kulmala, M.; Lehtinen, K. E. J.; Laaksonen, A. *Atmos. Chem. Phys.* **2006**, *6*, 787.
(479) Pirjola, L.; O'Dowd, C. D.; Yoon, Y. J.; Sellegri, K. *Environ. Chem.* **2005**, *2*, 271, DOI: 10.1071/en05075.
(480) Vuollekoski, H.; Kerminen, V. M.; Anttila, T.; Sihto, S. L.; Vana, M.; Ehn, M.; Korhonen, H.; McFiggans, G.; O'Dowd, C. D.; Kulmala, M. *J. Geophys. Res.* **2009**, *114*, D02206, DOI: 10.1029/2008jd010713.
(481) Wang, M.; Penner, J. E. *Atmos. Chem. Phys.* **2009**, *9*, 239.
(482) Makkonen, R.; Asmi, A.; Korhonen, H.; Kokkola, H.; Jarvenoja, S.; Raisanen, P.; Lehtinen, K. E. J.; Laaksonen, A.; Kerminen, V. M.; Jarvinen, H.; Lohmann, U.; Bennartz, R.; Feichter, J.; Kulmala, M. *Atmos. Chem. Phys.* **2009**, *9*, 1747.
(483) Spracklen, D. V.; Carslaw, K. S.; Merikanto, J.; Mann, G. W.; Reddington, C. L.; Pickering, S.; Ogren, J. A.; Andrews, E.; Baltensperger, U.; Weingartner, E.; Boy, M.; Kulmala, M.; Laakso, L.; Lihavainen, H.; Kivekas, N.; Komppula, M.; Mihalopoulos, N.; Kouvarakis, G.; Jennings, S. G.; O'Dowd, C.; Birmili, W.; Wiedensohler, A.; Weller, R.; Gras, J.; Laj, P.; Sellegri, K.; Bonn, B.; Krejci, R.; Laaksonen, A.; Hamed, A.; Minikin, A.; Harrison, R. M.; Talbot, R.; Sun, J. *Atmos. Chem. Phys.* **2010**, *10*, 4775, DOI: 10.5194/acp-10-4775-2010.
(484) Yu, F. Q.; Luo, G.; Bates, T. S.; Anderson, B.; Clarke, A.; Kapustin, V.; Yantosca, R. M.; Wang, Y. X.; Wu, S. L. *J. Geophys. Res.* **2010**, *115*, D17205, DOI: 10.1029/2009jd013473.
(485) Fuchs, N. A. *The mechanics of aerosols*; Pergamon Press: London, 1964.
(486) Zhang, K. M.; Wexler, A. S. *J. Geophys. Res.* **2002**, *107*, , DOI: 10.1029/2002jd002180.
(487) Kroll, J. H.; Seinfeld, J. H. *Atmos. Environ.* **2008**, *42*, 3593, DOI: 10.1016/j.atmosenv.2008.01.003.
(488) Pruppacher, J. H.; Klett, J. D. *Microphysics of clouds and precipitation*; Kluwer Academics: Norwell, MA, 1997.
(489) Kulmala, M.; Kerminen, V. M.; Anttila, T.; Laaksonen, A.; O'Dowd, C. D. *J. Geophys. Res.* **2004**, *109*, D04205.
(490) Pirjola, L.; Kulmala, M.; Wilck, M.; Bischoff, A.; Stratmann, F.; Otto, E. *J. Aerosol Sci* **1999**, *30*, 1079.
(491) Fuchs, N. A.; Sutugin, A. G. In *Topics in current aerosol research*; Hidy, G. M., Brock, J. R., Eds.; Pergamon Press: New York, 1971.
(492) Shi, Q.; Davidovits, P.; Jayne, J. T.; Worsnop, D. R.; Kolb, C. E. *J. Phys. Chem. A* **1999**, *103*, 8812.
(493) Swartz, E.; Shi, Q.; Davidovits, P.; Jayne, J. T.; Worsnop, D. R.; Kolb, C. E. *J. Phys. Chem. A* **1999**, *103*, 8824.
(494) Arnold, F.; Fabian, R. *Nature* **1980**, *283*, 55.
(495) Kurtén, T.; Petäjä, T.; Smith, J.; Ortega, I. K.; Sipilä, M.; Junninen, H.; Ehn, M.; Vehkamäki, H.; Mauldin, L.; Worsnop, D. R.; Kulmala, M. *Atmos. Chem. Phys.* **2011**, *11*, 3007, DOI: 10.5194/acp-11-3007-2011.
(496) Boy, M.; Kulmala, M.; Ruuskanen, T. M.; Pihlatie, M.; Reissell, A.; Aalto, P. P.; Keronen, P.; Dal Maso, M.; Hellen, H.; Hakola, H.; Jansson, R.; Hanke, M.; Arnold, F. *Atmos. Chem. Phys.* **2005**, *5*, 863.
(497) Fiedler, V.; Dal Maso, M.; Boy, M.; Aufmhoff, H.; Hoffmann, J.; Schuck, T.; Birmili, W.; Hanke, M.; Uecker, J.; Arnold, F.; Kulmala, M. *Atmos. Chem. Phys.* **2005**, *5*, 1773.
(498) Ravishankara, A. R. *Science* **1997**, *276*, 1058.
(499) Kolb, C. E.; Cox, R. A.; Abbatt, J. P. D.; Ammann, M.; Davis, E. J.; Donaldson, D. J.; Garrett, B. C.; George, C.; Griffiths, P. T.; Hanson, D. R.; Kulmala, M.; McFiggans, G.; Pöschl, U.; Riipinen, I.; Rossi, M. J.; Rudich, Y.; Wagner, P. E.; Winkler, P. M.; Worsnop, D. R.; O' Dowd, C. D. *Atmos. Chem. Phys.* **2010**, *10*, 10561, DOI: 10.5194/acp-10-10561-2010.
(500) Vaden, T. D.; Song, C.; Zaveri, R. A.; Imre, D.; Zelenyuk, A. *Proc. Natl. Acad. Sci. U.S.A.* **2010**, *107*, 6658, DOI: 10.1073/pnas.0911206107.
(501) Wang, L.; Xu, W.; Khalizov, A. F.; Zheng, J.; Zhang, R. Y. *J. Phys. Chem. A* **2011**, , .
(502) Biskos, G.; Buseck, P. R.; Martin, S. T. *J. Aerosol Sci* **2009**, *40*, 338.
(503) Ge, X.; Wexler, A. S.; Clegg, S. L. *Atmos. Environ.* **2011**, *45*, 561.
(504) Van Neste, A.; Duce, R. A.; Lee, C. *Geophys. Res. Lett.* **1987**, *14*, 711.
(505) Rabaud, N. E.; Ebeler, S. E.; Ashbaugh, L. L.; Flocchini, R. G. *Atmos. Environ.* **2003**, *37*, 933, DOI: 10.1016/s1352-2310(02)00970-6.
(506) Murphy, S. M.; Sorooshian, A.; Kroll, J. H.; Ng, N. L.; Chhabra, P.; Tong, C.; Surratt, J. D.; Knipping, E.; Flagan, R. C.; Seinfeld, J. H. *Atmos. Chem. Phys.* **2007**, *7*, 2313.
(507) Angelino, S.; Suess, D. T.; Prather, K. A. *Environ. Sci. Technol.* **2001**, *35*, 3130.
(508) Weng, J. Y.; Wang, C. M.; Li, H. R.; Wang, Y. *Green Chem.* **2006**, *8*, 96, DOI: 10.1039/b508325g.
(509) Lloyd, J. A.; Heaton, K. J.; Johnston, M. V. *J. Phys. Chem. A* **2009**, *113*, 4840, DOI: 10.1021/jp900634d.
(510) Qiu, C.; Wang, L.; Lal, V.; Khalizov, A. F.; Zhang, R. *Environ. Sci. Technol.* **2011**, *45*, 4748, DOI: 10.1021/es1043112.

(511) Finlayson-Pitts, B. J.; Pitts, J. N. *Chemistry of the upper and lower atmosphere: theory, experiments, and applications*; Academic Press: San Diego, CA, 2000.
(512) Barton, D.; Ollis, W. D. *Comprehensive organic chemistry: the synthesis and reactions of organic compounds*, 1st ed.; Pergamon Press: Oxford, New York, 1979.
(513) Carey, F. A.; Sundberg, R. J. *Advanced organic chemistry*, 4th ed.; Kluwer Academic/Plenum Publishers: New York, 2000.
(514) Jayne, J. T.; Worsnop, D. R.; Kolb, C. E.; Swartz, E.; Davidovits, P. *J. Phys. Chem.* **1996**, *100*, 8015.
(515) Zhao, J.; Levitt, N. P.; Zhang, R. Y. *Geophys. Res. Lett.* **2005**, *32*, L09802.
(516) Jang, M.; Kamens, R. M. *Environ. Sci. Technol.* **2001**, *35*, 4758.
(517) Jang, M. S.; Czoschke, N. M.; Lee, S.; Kamens, R. M. *Science* **2002**, *298*, 814.
(518) Jang, M.; Lee, S.; Kamens, R. M. *Atmos. Environ.* **2003**, *37*, 2125, DOI: 10.1016/s1352-2310(03)00077-3.
(519) Jang, M. S.; Carroll, B.; Chandramouli, B.; Kamens, R. M. *Environ. Sci. Technol.* **2003**, *37*, 3828, DOI: 10.1021/es021006u.
(520) Jang, M. S.; Czoschke, N. M.; Northcross, A. L. *Environ. Sci. Technol.* **2005**, *39*, 164, DOI: 10.1021/es048977h.
(521) Kroll, J. H.; Ng, N. L.; Murphy, S. M.; Varutbangkul, V.; Flagan, R. C.; Seinfeld, J. H. *J. Geophys. Res.* **2005**, *110*, D23207–D23207, DOI: 10.1029/2005jd006004.
(522) Garland, R. M.; Elrod, M. J.; Kincaid, K.; Beaver, M. R.; Jimenez, J. L.; Tolbert, M. A. *Atmos. Environ.* **2006**, *40*, 6863.
(523) Lee, A. K. Y.; Li, Y. J.; Lau, A. P. S.; Chan, C. K. *Aerosol Sci. Technol.* **2008**, *42*, 992, DOI: 10.1080/02786820802382736.
(524) Atkinson, R.; Arey, J. *Chem. Rev.* **2003**, *103*, 4605, DOI: 10.1021/cr0206420.
(525) Suh, I.; Zhang, R. Y.; Molina, L. T.; Molina, M. J. *J. Am. Chem. Soc.* **2003**, *125*, 12655, DOI: 10.1021/ja0350280.
(526) Zhao, J.; Zhang, R. Y.; Misawa, K.; Shibuya, K. *J. Photochem. Photobiol., A* **2005**, *176*, 199, DOI: 10.1016/j.jphotochem.2005.07.013.
(527) Lee, Y. N.; Zhou, X.; Kleinman, L. I.; Nunnermacker, L. J.; Springston, S. R.; Daum, P. H.; Newman, L.; Keigley, W. G.; Holdren, M. W.; Spicer, C. W.; Young, V.; Fu, B.; Parrish, D. D.; Holloway, J.; Williams, J.; Roberts, J. M.; Ryerson, T. B.; Fehsenfeld, F. C. *J. Geophys. Res.* **1998**, *103*, 22449.
(528) Kawamura, K.; Steinberg, S.; Kaplan, I. R. *Atmos. Environ.* **2000**, *34*, 4175.
(529) Grosjean, D.; Grosjean, E.; Moreira, L. F. R. *Environ. Sci. Technol.* **2002**, *36*, 1389, DOI: 10.1021/es0111232.
(530) Ho, S. S. H.; Yu, J. Z. *Environ. Sci. Technol.* **2004**, *38*, 862, DOI: 10.1021/es034784w.
(531) Volkamer, R.; Molina, L. T.; Molina, M. J.; Shirley, T.; Brune, W. H. *Geophys. Res. Lett.* **2005**, *32*, L08806–L08806, DOI: 10.1029/2005gl022616.
(532) Kalberer, M.; Paulsen, D.; Sax, M.; Steinbacher, M.; Dommen, J.; Prevot, A. S. H.; Fisseha, R.; Weingartner, E.; Frankevich, V.; Zenobi, R.; Baltensperger, U. *Science* **2004**, *303*, 1659.
(533) Lim, Y. B.; Tan, Y.; Perri, M. J.; Seitzinger, S. P.; Turpin, B. J. *Atmos. Chem. Phys.* **2010**, *10*, 10521, DOI: 10.5194/acp-10-10521-2010.
(534) Liggio, J.; Li, S. M.; McLaren, R. *Environ. Sci. Technol.* **2005**, *39*, 1532.
(535) Liggio, J.; Li, S. M.; McLaren, R. *J. Geophys. Res.* **2005**, *110*, D10304.
(536) Loeffler, K. W.; Koehler, C. A.; Paul, N. M.; De Haan, D. O. *Environ. Sci. Technol.* **2006**, *40*, 6318.
(537) Zhao, J.; Zhang, R. Y. *Atmos. Environ.* **2004**, *38*, 2177.
(538) Shapiro, E. L.; Szprengiel, J.; Sareen, N.; Jen, C. N.; Giordano, M. R.; McNeill, V. F. *Atmos. Chem. Phys.* **2009**, *9*, 2289, DOI: 10.5194/acp-9-2289-2009.
(539) Surratt, J. D.; Kroll, J. H.; Kleindienst, T. E.; Edney, E. O.; Claeys, M.; Sorooshian, A.; Ng, N. L.; Offenberg, J. H.; Lewandowski, M.; Jaoui, M.; Flagan, R. C.; Seinfeld, J. H. *Environ. Sci. Technol.* **2007**, *41*, 517.
(540) Galloway, M. M.; Chhabra, P. S.; Chan, A. W. H.; Surratt, J. D.; Flagan, R. C.; Seinfeld, J. H.; Keutsch, F. N. *Atmos. Chem. Phys.* **2009**, *9*, 3331.
(541) Zhao, J.; Levitt, N. P.; Zhang, R. Y.; Chen, J. M. *Environ. Sci. Technol.* **2006**, *40*, 7682.
(542) Yasmeen, F.; Sauret, N.; Gal, J. F.; Maria, P. C.; Massi, L.; Maenhaut, W.; Claeys, M. *Atmos. Chem. Phys.* **2010**, *10*, 3803, DOI: 10.5194/acp-10-3803-2010.
(543) De Haan, D. O.; Corrigan, A. L.; Tolbert, M. A.; Jimenez, J. L.; Wood, S. E.; Turley, J. J. *Environ. Sci. Technol.* **2009**, *43*, 8184, DOI: 10.1021/es902152t.
(544) Kane, S. M.; Leu, M. T. *J. Phys. Chem. A* **2001**, *105*, 1411.
(545) Iraci, L. T.; Essin, A. M.; Golden, D. M. *J. Phys. Chem. A* **2002**, *106*, 4054, DOI: 10.1021/jp012332b.
(546) Levitt, N. P.; Zhao, J.; Zhang, R. Y. *J. Phys. Chem. A* **2006**, *110*, 13215.
(547) Timonen, R. S.; Leu, M. T. *J. Phys. Chem. A* **2006**, *110*, 6660.
(548) Michelsen, R. R.; Staton, S. J. R.; Iraci, L. T. *J. Phys. Chem. A* **2006**, *110*, 6711.
(549) Minerath, E. C.; Casale, M. T.; Elrod, M. J. *Environ. Sci. Technol.* **2008**, *42*, 4410, doi: 10.1021/es8004333.
(550) Cole-Filipiak, N. C.; O'Connor, A. E.; Elrod, M. J. *Environ. Sci. Technol.* **2010**, *44*, 6718, DOI: 10.1021/es1019228.
(551) Paulot, F.; Crounse, J. D.; Kjaergaard, H. G.; Kurten, A.; St. Clair, J. M.; Seinfeld, J. H.; Wennberg, P. O. *Science* **2009**, *325*, 730, DOI: 10.1126/science.1172910.
(552) Surratt, J. D.; Chan, A. W. H.; Eddingsaas, N. C.; Chan, M.; Loza, C. L.; Kwan, A. J.; Hersey, S. P.; Flagan, R. C.; Wennberg, P. O.; Seinfeld, J. H. *Proc. Natl. Acad. Sci. U.S.A.* **2010**, *107*, 6640, DOI: 10.1073/pnas.0911114107.
(553) Minerath, E. C.; Elrod, M. J. *Environ. Sci. Technol.* **2009**, *43*, 1386, DOI: 10.1021/es8029076.
(554) Minerath, E. C.; Schultz, M. P.; Elrod, M. J. *Environ. Sci. Technol.* **2009**, *43*, 8133, DOI: 10.1021/es902304p.
(555) Kulmala, M. Univeristy of Helsinki, 1988.
(556) Kulmala, M.; Dal Maso, M.; Makela, J. M.; Pirjola, L.; Vakeva, M.; Aalto, P.; Miikkulainen, P.; Hameri, K.; O'Dowd, C. D. *Tellus Ser. B-Chem. Phys. Meteor.* **2001**, *53*, 479.
(557) Dal Maso, M.; Kulmala, M.; Lehtinen, K. E. J.; Makela, J. M.; Aalto, P.; O'Dowd, C. D. *J. Geophys. Res.* **2002**, *107*, 8097, DOI: 10.1029/2001jd001053.
(558) Lehtinen, K. E. J.; Kulmala, M. *Atmos. Chem. Phys.* **2003**, *3*, 251.
(559) Nieminen, T.; Lehtinen, K. E. J.; Kulmala, M. *Atmos. Chem. Phys.* **2010**, *10*, 9773, DOI: 10.5194/acp-10-9773-2010.
(560) Kerminen, V.-M.; Kulmala, M. *J. Aerosol Sci.* **2002**, *33*, 609.
(561) Korhonen, H.; Sihto, S. L.; Kerminen, V. M.; Lehtinen, K. E. J. *Atmos. Chem. Phys.* **2011**, *11*, 3051, DOI: 10.5194/acp-11-3051-2011.
(562) Yu, F.; Luo, G. *Atmos. Chem. Phys.* **2009**, *9*, 7691, DOI: 10.5194/acp-9-7691-2009.